UNIVERSITÀ
DEGLI STUDI
DI BRESCIA

Università degli Studi di Brescia

DOTTORATO DI RICERCA IN *Technology for Health*

Settore scientifico disciplinare CHIM/07

CICLO XXXV

Design of porous materials derived from industrial non-hazardous waste powder for air particulate matter entrapment

SUPERVISOR: Prof. Elza Bontempi

DOTTORANDA: Antonella Cornelio

A Lolo

Sommario

Tra le sfide più importanti che l'uomo sta affrontando negli ultimi anni, sicuramente, l'inquinamento ambientale (in particolare quello dell'aria) è una delle più difficili; per questo motivo è al centro di numerosi studi al fine di trovare soluzioni efficaci a contrastarlo. L'inquinante più presente nelle aree urbane, e che desta la maggiore preoccupazione a causa della sua capacità di penetrare nel sistema respiratorio con gravi danni per la salute, è il particolato atmosferico (PM). Le concentrazioni di PM spesso superano i limiti imposti dalla normativa; nel 2021 l'Organizzazione Mondiale della Sanità (OMS) ha imposto nuovi e più restrittivi limiti alle concentrazioni di PM al fine di ridurne le concentrazioni in atmosfera. Fra le diverse soluzioni proposte per intrappolare il PM si distingue un nuovo e sostenibile materiale, chiamato SUNSPACE (*SUstaiNable materials Synthesized from by-Products and Alginates for Clean air and better Environment*), e realizzato a partire da uno scarto industriale, la silica fume (SF), con processi a basse emissioni di CO_2. La sua capacità di catturare il PM è stata valutata effettuando numerosi test e ottenendo buoni risultati ma il suo colore scuro rappresenta un limite ad un suo possibile sviluppo commerciale. In questa tesi di dottorato sono state proposte delle soluzioni alternative al fine di ottenere un materiale dal colore chiaro e per eliminare il trattamento termico, semplificando la fase di realizzazione del materiale. Il primo punto è stato ottenuto utilizzando la *bottom ash* (BA), cenere proveniente dalla combustione dei rifiuti municipali negli inceneritori, mentre la sostituzione del bicarbonato di sodio (utilizzato la formazione dei pori) con il perossido d'idrogeno ha permesso di eliminare il trattamento termico. I campioni, caratterizzati, sono stati testati per valutarne la capacità di intrappolare il PM utilizzando un generatore di aerosol e TiO_2 per simulare una fonte di PM. Buoni risultati sono stati ottenuti per i campioni realizzati con SF e per SUNSPACE BA mentre quelli realizzati con BA e perossido d'idrogeno hanno mostrato un comportamento idrorepellente che è stato studiato con delle prove di bagnabilità. I risultati hanno dimostrato che questi materiali presentano un angolo di contatto al di sopra del limite di idrofobicità.

I campioni sono stati anche testati per fotodegradare inquinanti organici ottenendo buoni risultati per i campioni realizzati con BA, perossido di idrogeno e TiO_2 (ottimo fotocatalizzatore, aggiunto durante la preparazione dei campioni). Infine, il trattamento termico di SUNSPACE è stato sostituito con un trattamento a microonde che permette di ridurre i tempi necessari alla preparazione del campione e di migliorare la sua sostenibilità. I campioni sono stati caratterizzati e testati utilizzando il generatore di aerosol, con lo stesso set-up sperimentale dei precedenti campioni. Si tratta però di test preliminari volti a proporre nuove possibili applicazioni del materiale, ad esempio per realizzare vasi da esterno che aiutino a intrappolare il PM.

Nell'ultimo capitolo sono stati riportati alcuni lavori, realizzati durante la COVID-19, e incentrati sulle sue conseguenze su vari aspetti ambientali e sull'estrazione di materie prime.

Abstract

Environmental pollution is one of the biggest issue in modern society. In particular, the most present pollutant in urban areas is particulate matter (PM) that is cause of concern as it can easily penetrate the respiratory system causing severe health problems. As PM concentrations often exceed limits established by legislation, in 2021 World Health Organization (WHO) imposed new and stricter limits to PM_{10} and $PM_{2.5}$ concentrations. Several solutions have been proposed to reduce PM concentrations in cities, including the realization of a new and sustainable material, SUNSPACE (SUstaiNable materials Synthesized from by-Products and Alginates for Clean air and better Environment), realized with silica fume (SF) and low CO_2 emissions processes. Its adsorption capacity was tested obtaining good results but, from a commercial development perspective, its dark color represents a limit. In this Ph.D. work, new SUNSPACE modification have been proposed to obtain a lighter colored material and to simplify the synthesis process by the elimination of the thermal treatment. The color change was obtained using another industrial by-product, the bottom ash (BA), residue of municipal waste combustion while the substitution of sodium bicarbonate (used as pore former in SUNSPACE synthesis) with hydrogen peroxide allowed to avoid the thermal treatment. Samples were fully characterized and tested to evaluate the adsorption capacity using for the first time an aerosol nanoparticle generator and a TiO_2 suspension as PM source. The results obtained are encouraging for samples realized with SF and for SUNSPACE BA. On the contrary, samples realized with BA and hydrogen peroxide showed a water repellent behavior, studied with wettability tests. Results showed that the contact angle of these materials is above the hydrophobicity limit. Moreover, samples were also tested to photodegrade organic pollutants obtaining the best results for samples realized with BA, hydrogen peroxide and TiO_2 (added during the samples' preparation due to its good photocatalytic activity). Finally, the thermal treatment of SUNSPACE was changed with a microwave treatment that allowed to improve the material sustainability and to speed up the treatment. Samples were characterized and tested

using the aerosol nanoparticles generator, with the same experimental set-up defined for previous samples. However, these are preliminary tests aimed at thinking about new possible applications of the material, for example to make outdoor vases that help trap the PM.

In the last chapter, some works, carried out during COVID-19, were reported focusing on its consequences on various environmental aspects and on the extraction of raw materials.

Index

1. Introduction

1.1 Scope of the thesis

Environmental pollution is one of the biggest challenges to be faced because of its serious global consequences. For years, the impact of the indiscriminate use of resources, the generation of waste and the release into the atmosphere of potentially harmful substances has been neglected. The effects caused by these actions led to a greater awareness, over the past 30 years, of the importance of preserving the environment and promoting new policies aimed at reducing environmental pollution, also promoting the reduction of social disparities [1][2][3]. Focusing on air pollution, it is estimated more than 90% of humans live in areas subjected to air pollution [4][5]. Among air pollutants, particulate matter (PM) is the one that causes the great concern due to high risks related to human health as it can easily penetrate the respiratory system [6][7]. It is therefore important to define the correct solutions to address the problem and reduce PM emissions. At this purpose, the main aim of my Ph.D. project was improving people's quality of life and air quality reducing the risks to human health due to environmental pollution. In this perspective, the research activity was focused on:

- reducing PM concentration in urban areas;
- recycling industrial by-products following the "Azure Chemistry" principles [8].

There are several ways to entrap airborne PM like cyclones, fabric filter (bag-house), transparent air filter and leaves [9][10][11][12]. Most of them are used at the industrial level. Recently household filters are being developed to improve the indoor air quality [13][14]. Unfortunately, despite their efficiency, the main problem is that the materials used for filters' production are petroleum based, such as polystyrene (PS) or polypropylene (PP), having a bad impact on environment. On the contrary, leaves, whose adsorption capacity of the PM has been proven, are the most natural and sustainable way to trap the PM [12]. However, leaves alone are not able to reduce PM

concentrations significantly; moreover, large spaces are needed which very often are not available in cities. Given the current environmental situation and the large waste production, the idea is to propose a more sustainable and eco-friendly material following the Azure Chemistry principles, a new sustainable approach which aims at restore or reconstruct the ecosystems by sustainable solutions in terms of energy, materials and emissions [8]. Inspired by the natural ability of the leaves to trap the PM and following the Azure Chemistry principles, in the Chemical for Technologies Laboratory (Chem4Tech), of the University of Brescia (Italy), a new, porous and sustainable material, called SUNSPACE (SUstaiNable materials Synthesized from by-Products and Alginates for Clean air and better Environment), has been developed [15]. SUNSPACE is synthetized using silica fume, a by-product derived from ferrosilicon or silicon metal production. The synthesis process uses non-toxic, economical and eco-friendly reagents and low emission processes. Several tests have been conducted on SUNSPACE to define its possible application and its adsorption capacity, obtaining good results, but its dark color represents a limit to its application as highlighted by a survey conducted [8][15][16][17][18].

1.2 Objectives of the thesis

The experimental activity of my Ph.D. project was based primarily on the improvement of SUNSPACE characteristics that can be achieved through different steps:

- color change, implementing SUNSPACE characteristics to obtain a lighter colored material;
- elimination of the thermal treatment;
- evaluation of other application possibilities.

The color change can be achieved using another industrial by-product, the bottom ash, residue of municipal solid waste incineration. In this thesis work, bottom ash is provided by the A2A waste incineration plant of Brescia (Italy), a new generation plant that allows to recover the heat produced by the combustion phase and reuse it for domestic

heating; in fact, it produces every year over 70% of the energy distributed by the district heating network [19]. Since about 25 - 30% of bottom ash is produced per ton of waste burned, it is necessary to think about its possible alternative reuses because they do not end up in landfills. The reuse of bottom ash to realize sustainable porous materials could be a valid alternative. Moreover, the addition of calcium hydroxide favors the pozzolanic reaction in order to increase the material strength.

The second goal can be accomplished changing the pore former. In SUNSPACE synthesis the pore former is the sodium bicarbonate, the thermal process allows its decomposition and the consequent release of CO_2 leading to pore formation. The need for heat treatment can cause problems in the application of SUNSPACE, the substitution of sodium bicarbonate with hydrogen peroxide allows the elimination of thermal treatment.

Finally, the last objective can be pursued for example: using these materials to photodegrade organic pollutants or using instead of the heating plate the microwave oven to reduce emissions associated to the drying process with the purpose of producing furniture.

1.3 Organization of the thesis

After this brief introduction on the scope and objectives of the project, the thesis will be so articulated:

- Chapter 2. State of the art will be devoted to an overview of atmospheric particulate matter describing its origin, human health problems and regulatory limits with a brief digression of the situation of the city of Brescia. Then the focus will be on SUNSPACE, the starting material from which my Ph.D. project has developed, describing the synthesis process, its characterization, the tests carried out and its possible applications. From the results, SUNSPACE showed good adsorption capacity, however it has limitations that have been investigated

in this thesis. Since the key word of this Ph.D. project is definitely the sustainability, the last part of the chapter is dedicated to the Sustainable Development Goals (SDGs), reported in the 2030 Agenda, considering those that have the greatest influence on the project: 3, 7, 11 and 13.

- In Chapter 3. Materials, the materials used in the synthesis process of SUNSPACE and its modification will be described. First of all, the industrial by-products, silica fume and bottom ash, and then the commercial chemicals used.
- Chapter 4. Materials synthesis and nanoparticles entrapment concerns the synthesis and characterizations of samples. Adsorption tests will be performed, for the first time, using an aerosol nanoparticles generator, which allows the flow of aerosols generated to be controlled, and a titanium dioxide suspension will be used as particulate matter source.
- Chapter 5. Photodegradation of organic pollutants, other applicative solutions of these materials will be presented using them to eliminate organic pollutants from water through photodegradation processes given the increasing levels of pollution of groundwater and watercourses. In addition to those made in Chapter 4, other samples will be synthetized with the addition of titanium dioxide, well known for its photocatalytic activity.
- In Chapter 6. Wettability, some samples realized with hydrogen peroxide will be better characterized as they showed a water repellent behavior that will be investigated by wettability tests to measure the contact angle.
- Chapter 7. Future perspective concerns the change of thermal treatment of SUNSPACE to speed out the synthesis process. Moreover, as the CO_2 emissions related to production processes are increasing, it is necessary to develop methods that allow to reduce them as much as possible. At this purpose, the heating plate treatment previously used will be substituted with a microwave treatment. Lastly, the sustainability analysis of all samples will be performed thanks to the software Ces Selector as a pillar of the work is the sustainability of the materials with the aim of having the least possible impact on the environment. The evaluation will be performed considering the values of

Embodied Energy and Carbon Footprint associated with the reagents used and the processes carried out.

- Chapter 8. SDGs activity and PM will cover works performed during the lockdown period. During my first year of Ph.D., the COVID-19 epidemic spread worldwide. Italy was one of the most affected nations and severe prevention measures were taken making any laboratory activity impossible. For this reason, in this Chapter, other works, carried out during COVID-19 first wave, are reported to assess the pandemic consequences due to the use of face masks, on pollutants concentrations in the city of Brescia and on raw materials extraction.
- Chapter 9. Conclusions will be dedicated to the conclusions of this Ph.D. thesis and the future perspective of this work.

2. State of the art

The introduction in 2015 of the Sustainable Development Goals (SDGs), with the emphasis of reaching the targets by 2030, stressed how environmental pollution is one of the biggest problems to be addressed [20][21]. The impact of pollutants on the environment has been neglected for years causing great concern in new generations. In this situation, the control of air quality has become a very current topic as it is estimated more than 90% of humans live in areas subjected to air pollution [4][5]. Awareness of this situation has led to the development of new environmental policies [22] aimed at reducing pollution levels, especially atmospheric pollution. Nevertheless, the situation is still very critical in several areas of Europe, including certainly Northern Italy [23][24]. Among pollutants, particulate matter (PM) is the one that causes the greatest concern.

2.1 Particulate matter

PM is composed of a complex mixture of solid and liquid particles of organic and inorganic substances suspended in the air [25]. PM is characterized by a complex mix of mineral dust, sulfates, ammonium, nitrates, organic compounds, pollens, spores, elemental and organic carbon and trace elements. It is, therefore, a pollutant very different from all the others, presenting itself not as a specific chemical entity but as a mixture of particles with various properties.

PM can be classified in different ways, according to sources, origin and size dimension. One of the most used classification is based on natural and anthropogenic sources. PM can be produce from natural sources, deriving from soil erosion or volcanic eruptions or it can also be produced from anthropogenic sources, such as domestic heating and household tasks, industrial processes and traffic (abrasion of road pavement, tires and brakes) [26]. Moreover, its composition depends on the geographical area (city, sea, rural area) and the season [27]. For example, vehicles and domestic heating are the most important sources of PM in cities. It is composed by organic compound such as polycyclic

aromatic hydrocarbons (PAHs) from vehicular emissions [28] and levoglucosan, a reliable tracer of biomass burning [27]. In addition, these components are present especially in winter due to the greater atmospheric stability that limits the dispersion of pollutants and the necessity to turn on heating in homes.

Another distinction is between primary and secondary aerosol:

- Primary aerosol is directly emitted into the atmosphere from natural or anthropogenic sources. Primary aerosol sources can be the mechanical action of the wind, marine aerosols and powders produced by resuspension of fine material deposited on the ground, ash produced by combustion processes, vehicle exhaust, industrial processing, cement and fertilizer production.

- Secondary aerosol is almost characterized by fine particles with a diameter of less than 1 μm, formed by chemical reactions with substances present in the atmosphere or conversion processes of the gas into solid particles, like sulphates, nitrates, some organic compounds.

PM can be also classified according to its aerodynamic diameter[1] in:

- Coarse fraction (aerodynamic diameter > 2.5 μm) produced by mechanical process, like erosion, grinding and wind resuspension; this fraction contains elements present in the soil and in the sea salts.

- Fine fraction (0.1 μm < aerodynamic diameter < 2.5 μm) constituted by sulphates, nitrates, ammonium ion, elemental carbon and organic especially in urban areas.

- Ultrafine fraction (aerodynamic diameter < 0.1 μm) constituted by SO_2, NH_3, NO_x and combustion products.

PM is characterized by long persistence times in the atmosphere that is strongly influenced by its particle size, weather conditions (wind, precipitations) and urban

[1] The diameter of a spherical particle having unit density and aerodynamic behavior equal to the considered particle.

canopy. Meteorology plays significant roles in air pollution formation, transport, deposition and transformation. Unfavorable meteorological conditions could bring severe pollution days even if the total emission is reduced [29]. In fact, changes in weather conditions have a greater influence on the time variability in PM concentrations. Wind speed was identified as an important factor influencing atmospheric levels of ultrafine, fine, and coarse particles concentrations, especially in winter [30]. Moreover, the alternation of the seasons also favors or hinders the dispersion of pollutants. In winter, due to the low temperatures and temperature inversion of mass air, the atmospheric stability favors the accumulation of pollutants, hindering their dispersion. In addition, low temperature involves the greater use of the heating systems and power production. This situation is particularly exacerbated in areas characterized by low ventilation, like the Po Valley (Northern Italy) [31]. On the contrary, in summer, the high temperatures promote not only the photochemical reactions between PM and precursor leading to the formation of secondary PM, but also convection of air, causing the dilution and dispersion of pollutants [32]. Since it can be transported even at a great distance from the emission point, this increases its impact in a large part of the population. Moreover, the urban canopy also greatly influences the dispersion of pollutants, in particular, the presence of street canyons, characterized by a ratio between height of buildings (H) and width of the road (W) greater than 0.65 [33][34]. The street canyon is characterized by a very limited dispersion of pollutants due to the buildings that delimit the street and that act as a screen for the wind: this is reflected in an increase in concentrations close to the soil as recirculation phenomena that lead to a stagnation of pollutants are determined. This phenomenon can have serious repercussions on air quality and also on human health.

Health risks due to PM are related to the particle size. Due to its small size dimension, PM can easily penetrate the respiratory system. According to the ability to penetrate more or less deeply the respiratory tract, can be defined three different fractions:

- inhalable fraction with an aerodynamic diameter > 10 μm;
- thoracic fraction (PM_{10}) can penetrate the upper part of the respiratory system up to the bronchi;

- respirable fraction ($PM_{2.5}$) that can reach the lungs [6][35][36].

Due to its capability to penetrate the respiratory system, the correlation between the mortality for respiratory and cardiovascular diseases and the ultrafine PM has been widely studied [6][7][12]. High concentrations of PM cause concern not only for human health but also for energy production. Nowadays, energy production is moving towards renewable energy sources with a large development of solar and photovoltaic systems. $PM_{2.5}$ is responsible for the formation of urban haze [37] leading to a reduced visibility in cities. The reduced visibility leads to a decrease of solar intensity and the alteration of the spectrum reaching the ground [38] reducing the transmittance of solar energy to photovoltaics [39][40][41].

Lot of cities all over the world are facing with this problem from Lahore (Pakistan) which is one of the most polluted city in the World [42] to New York (USA), including Brescia (Italy).

Brescia is located in the Po Valley, one of the most industrialized and polluted areas in Europe. Its geographical position and morphological conformation favor the accumulation and stagnation of pollutants [43]. The strong industrialization, the high traffic flows and the large presence of farms contribute negatively to the air quality in this area [43][44]. Over the last 20 years, the annual average PM_{10} concentrations have often exceeded the limits imposed by guidelines (with a decrease in last years) [44][45] including the maximum number of daily exceedances during the year (35 days/year) of the regulatory limits (50 $\mu g/m^3$) [44], as reported in Figure 1.

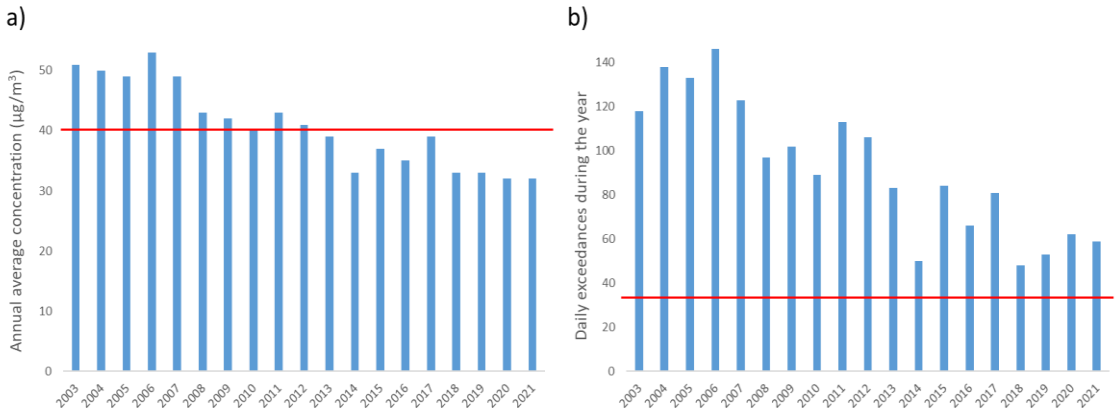

Figure 1. a) Annual average concentrations of PM_{10} in Brescia from 2003 to 2021, the red line represents the annual average concentration limit imposed by legislation 40 µg/m³; b) Daily exceedances of the limit value (50 µg/m³) imposed by legislation, the red represents the limit value of 35 exceedances/year.

Despite the decrease of PM_{10} concentrations during last years, the number of exceedances always overcomes the limit imposed by legislation [44].

In 2021 World Health Organization (WHO) imposed new and stricter limits to PM_{10} and $PM_{2.5}$ concentration [46] leading them to 15 µg/m³ and 5 µg/m³ respectively. In accordance with the new guidelines established by the WHO [46], it is increasingly necessary to implement concrete solutions to reduce PM concentrations, especially in urban areas. This can be done both with new policies that provide for a reduction in concentrations of pollutants, and with the use of materials that can help entrap the PM.

2.1.1 Conventional methods to remove airborne PM

As mentioned in Paragraph 2.1, PM, in addition to being of natural origin, can also originate from anthropogenic sources such as industries, traffic and domestic activities (for example, sweeping and dusting). It becomes therefore necessary to define methods that allow to reduce the concentrations of PM emitted by industries, vehicles, domestic activities as well as to reduce as much as possible the exposure of people both inside and outside the home. Different solutions, discussed in this Paragraph, have been implemented to try to trap the PM: cyclones, electrostatic precipitator (ESP), fabric filter (bag-house), particulate filters for internal combustion engines (gasoline particulate

filters and diesel particulate filters, GPF and DPF respectively), High-Efficiency Particulate Air (HEPA) filter, transparent air filter and leaves.

Mechanical collectors, like cyclones, are mostly used as preliminary separation devices of PM (diameter > 10 μm) from flue gas, to avoid the abrasion in the finer filtration methods. Once the contaminated air enters into the chamber, thanks to the centrifugal force, the particles separate from the flue gas and slam against the wall of the cyclone. Then, they are dragged by gravity force in the bottom part of the device and removed. While, the treated air comes out from the upper part of the cyclone. Despite some indisputable advantages due to low maintenance and management costs, however, they have some limitations related to the impossibility of retaining particles with a diameter of less than 10 μm and not being able to treat sticky materials [10].

ESP is a dust collector that can separate PM suspended within the gaseous stream using electrostatic forces. Three-steps process characterize wet and dry ESP: particle charging, particle collection on the oppositely charged surface, and the cleaning of the collection surface [47]. The system is composed of negative (metal wires, bars or plates) and positive electrodes through which the gas flow passes. A high voltage (10000 - 70000 V/m) is applied to the discharge wires to form an electrical field between the wires and the collecting plates, and also ionizes the gas around the discharge wires to supply ions. Therefore, negatively charged particles are attracted to the positive plates [11]. This process can operate in low-temperature and high-moisture conditions and can handle multi-pollutant control (SO_3, $PM_{2.5}$, aerosols, metals, mercury) [48][49]. There are different methods to remove the collected particles like by craping off with a brush (for dry ESP) or washing off with water (for wet ESP). Unlike cyclones, EPS allows to eliminate even the finest fraction but among the disadvantages there are high costs and that the removal efficiency depends on the gas flow [10].

With fabric filters, the filtration process of PM is achieved by passing the contaminated airflow through filters made by different types of textile fibers. At first, these filters were produced using natural products such as wool or cotton but they had low efficiency and resistance. Nowadays, the development of synthetic fibers, like nylon, polypropylene

(PP), polyamide (PA) and polyethylene (PE) allows to obtain more resistant materials to heat, erosion and attack of corrosive substances and with a higher removal efficiency [47]. The most common type requires that the filter elements are structured as a cylindrical shape with bags or sleeves structure. The contaminated air flows through the bags and then the purified air exits from the top of the bags as the dust is blocked on the surface of the filter bag by the combined effects of screening, adhesion, inertia, diffusion, and static electricity [50]. PM accumulates on the filter can be removed by reverse air, shake deflate and pulse jet. The fiber filters are extremely widespread due to their high efficiency (99.9 %) with a purification action generally independent of the chemical composition of the PM. The deposition of the PM on the filtering material favors the further capture of other airborne particles, increasing the efficiency of PM capture. The disadvantages are the high maintenance costs as it is necessary, in order to maintain a certain gas pressure, that the filters are periodically cleaned; problems with potentially explosive dusts and gases and limited operating temperatures (maximum about 300 °C) [10].

GPF and DPF [51][52] are ceramic based filters, characterized by a honeycomb structure, installed at the beginning of the exhaust system for internal combustion engines (generally immediately after the turbo charger). The exhaust gas passes through the filter and the bigger particles get trapped. Normally, 2 pressure sensors are installed before and after the filter and are linked directly to the electronic control unit (ECU) which, using a physical model, is able to calculate the amount of soot trapped into the filter. With a regular use of the engine, filter regenerates automatically (the soot gets burned degrading in smaller particles able to pass through the filters and be emitted in the atmosphere). It is evident that the great advantage of these filters is to remove the bigger PM particles (> 10 µm) that otherwise would be emitted in the atmosphere. On the other hand, the great disadvantage is the emission of PM with size dimension much smaller and certainly more dangerous for human health.

Unlike the first methods, more widespread in industry and in the automotive sector, the latter are also designed for domestic use.

HEPA is a type of pleated mechanical air filter that can theoretically remove at least 99.97% of dust, pollen, mold, bacteria, and any airborne particles with a size of 0.3 µm [9][53]. They are composed of microfiber filter sheets, usually borosilicate, assembled in several layers and separated by aluminum septa. The gas flow to be treated passes through the microfiber filter sheets that block the polluting solid particles. These types of filters have a large application in laboratories, chemical and pharmaceutical fields, air conditioners, air purification systems or masks protections. The main advantage is the high filter efficiency but on the contrary HEPA filters are not regenerable so it is necessary to replace them periodically [10].

Having regard to the high levels of PM in many cities, in recent years, researchers are trying to develop new transparent filters [13][14] to be applied for example to windows and able to trap the PM, using natural passive ventilation, ensuring a better air quality inside houses. This is possible thanks to new polymer nanofiber filter technologies. The material used in the air filter can be significantly reduced to a transparent level to allow both transparency in sunlight and sufficient airflow. Moreover, by reducing the fiber diameter to the nanometer scale, with the same packing density, the possibility of particle capture increases greatly due to the large surface area, ensuring effective capture of PM with a much thinner air filter [13][14]. These filters can be produced in different polymers such as polyacrylonitrile (PAN), polystyrene (PS), polyvinylpyrrolidone (PVP), polyvinyl alcohol (PVA) and PP. Despite their good removal efficiency, these filters are still under study and not commercially available.

The last analyzed method for the removal of PM is also the most natural one, based on the ability of the leaves to trap the PM. Plants play an important role in filtering ambient air by adsorbing PM onto leaves surfaces. Leaves currently represent the most sustainable and low-cost material for PM reduction. Trees, with their large total leaf area, are considered the most effective type of vegetation for this purpose [54]. The airborne PM entrapment by vegetation is due to the interactions between particles and plant surfaces. It is influenced by particles size and by plants morphology such as roughness, hair, and wax cover [55]. Literature reports many works about the PM capture by plants. Generally, the species used are: Field maple such as *Acer campestre*,

European ash such as *Fraxinus*, London plane such as *Platanus*, and Common Ivy such as *Hedera Helix*, the widely used evergreen [12]. All of them accumulated large quantities of PM, particles of each size fraction were found in the epicuticular wax layer [12]. The leaves therefore certainly play a very important role in trapping the PM, but unfortunately in big cities the green spaces are always insufficient, as only in recent years we have realized their importance. Moreover, trees occupy very high surfaces not always available in cities, therefore new and alternative solutions must be proposed.

2.2 SUNSPACE

In order to try to reduce emissions related to traffic, heating systems and industry, several materials have been discussed to trap PM in Paragraph 2.1.1, such as filters [13][14] and leaves. Despite their efficiency, the main problem is that the materials used for filters' production are petroleum based, such as PS or polypropylene (PP). This makes the filter expensive and not competitive on the market. In addition, these materials have bad impacts on environment.

Given the current environmental situation, the idea is to propose a more sustainable and eco-friendly material. Inspired by the natural ability of the leaves to trap the PM, in the Chemical for Technologies Laboratory (Chem4Tech), of the University of Brescia, a new, porous and sustainable material, called SUNSPACE (SUstaiNable materials Synthesized from by-Products and Alginates for Clean air and better Environment), has been developed [8][15][16][17][18]. SUNSPACE is synthetized using silica fume, a by-product derived from ferrosilicon or silicon metal alloy processing (with particles dimensions of about 20 - 500 nm), and sodium alginate, a natural polysaccharide readily extracted from various species of algae and seaweeds [56], following the Azure Chemistry principles [8]. Azure Chemistry is a new sustainable approach, developed by Prof. Elza Bontempi (University of Brescia, Italy), aimed at restore or reconstruct the ecosystems by sustainable solutions in terms of energy, materials and emissions and based on the following principles:

- use low-energy materials by selecting nontoxic low-cost materials and by-products;
- use low-energy processes;
- make long-lasting and excellent products that can be easily regenerated;
- design products with a minimum amount of material;
- quantify the sustainability of the new proposed material, in terms of materials, energy, and emissions [8].

SUNSPACE is obtained by mixing 25 mL of MilliQ water with 0.6 g of sodium alginate and 1 g of calcium iodate (as cross-linker). Once the gel is formed, 17.88 g of silica fume and 5 g of sodium bicarbonate are added. The slurry obtained is put on aluminum molds and placed on a heating plate for 1 h at low temperature (70 - 80 °C). The temperature increase favors the decomposition of sodium bicarbonate and the release of CO_2 allowing the pores' formation [16]. In Figure 2 an example of SUNSPACE sample.

Figure 2. SUNSPACE sample.

SUNSPACE material was fully characterized by structural, morphological and sustainability analysis [8][15][16]. In Figure 3, the X-ray diffraction (XRD) patterns of SUNSPACE and silica fume revealed the presence of a large halo due to the amorphous

phase, typical of silica fume, and some crystalline peaks attributable to sodium iodate hydrate and cristobalite [15] due to the synthesis process of SUNSPACE.

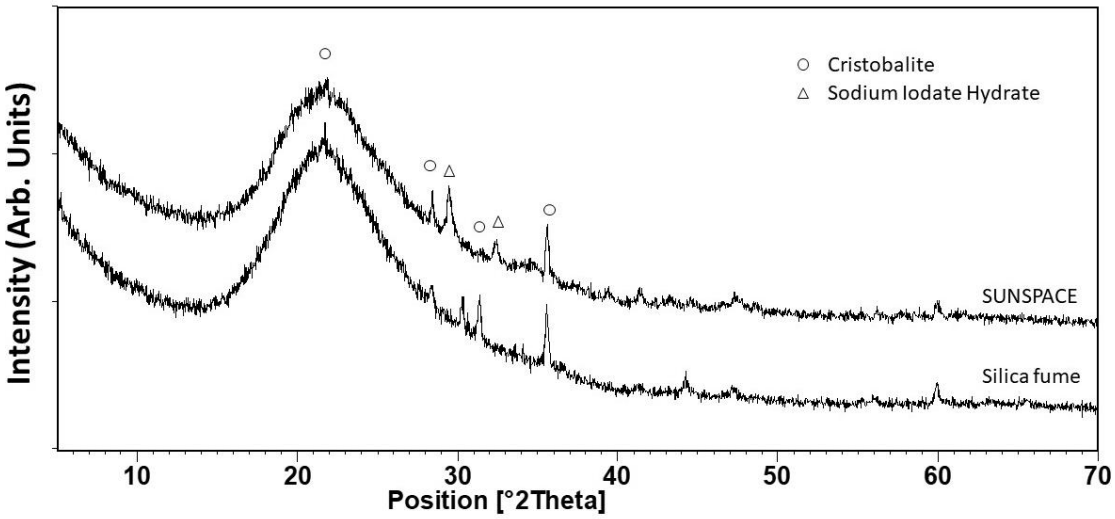

Figure 3. XRD pattern of SUNSPACE and silica fume.

SEM (Scanning Electron Microscope) analysis revealed that the structure of the SUNSPACE is porous, similar to a sponge with pores, which seem to be interconnected [15]. This was confirmed by the N_2 physisorption measurements that allowed to investigate the presence and dimension of pores highlighting that the material contains both mesopores and macropores [15]. Moreover, SEM, TEM (Transmission Electron Microscope) and physisorption analyses carried out allowed to establish that the material presents ink-bottle shaped pores, with large cavities (about 200 − 300 nm) and narrow constriction (about 70 − 100 nm) [15][17]. This particular shape of the pores can help the entrapment of the PM that once entered the pore cannot get out.

Finally, the sustainability analysis of SUNSPACE was performed through the software Ces Selector [57] considering the Embodied Energy (EE) and Carbon Footprint (CF) values (that will be discussed in more detail in Paragraph 4.3) associated to reagents and process. It results that the material is more sustainable compared to other materials used in the field of construction and those used for the filters realization, as described in Paragraph 2.1.1 (Figure 4).

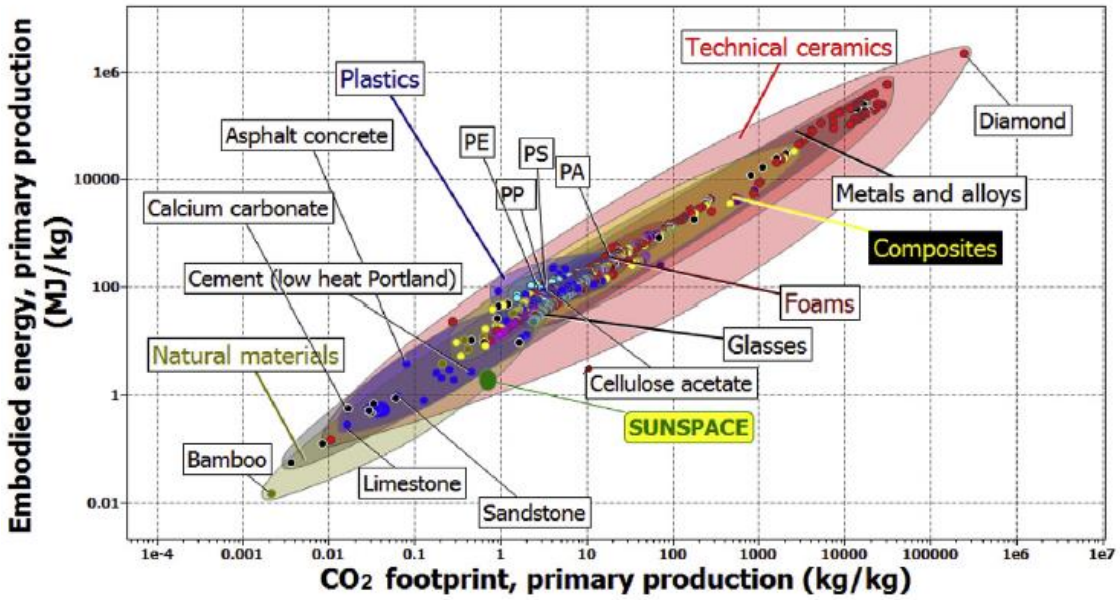

Figure 4. Embodied energy (EE) in respect to CO2 footprint (CF) of the synthesized material [8].

According to the presence of pores, the idea is to use SUNSPACE providing spatial confinement to trap small PM sizes [16]. At this purpose, several tests were carried out in order to evaluate its entrapment capacity. Preliminary tests were conducted in controlled conditions (exposure to TiO_2 and Fe particles) [16][17] and in not controlled conditions, exposing SUNSPACE to candles and car exhaust smoke, steel industry, highway, and in the courtyard area of Brescia [8][15][18]. Results showed an adsorption capacity of 30 g/m^2, encouraging in developing the potentialities of the new material to reduce air pollution.

Once evaluated the adsorption capacity of SUNSPACE, other tests were conducted to define the possible ways of application of the material as the slurry appeared to be very versatile and well-suited for direct foaming, extrusion, 3D printing or coatings [15], as seen in Figure 5.

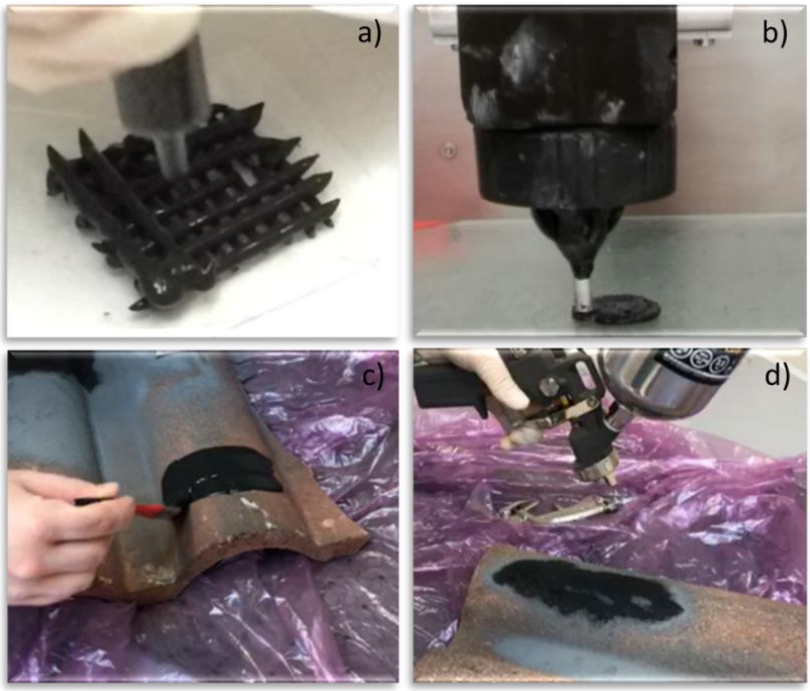

Figure 5. Different ways of SUNSPACE application: a) by extrusion, b) 3D printing, c) deposited by brush, d) or by spray [15].

Due to its versatility, it was also applied on a wall [58] of a structure of the Department of Civil Engineering of the University of Brescia, in collaboration with the company Delta Phoenix, as shown in Figure 6.

Figure 6. Application by spray of SUNSPACE on a wall of a structure of the Department of Civil Engineering of the University of Brescia [58].

SUNSPACE is a dark grey material, due to the use of silica fume. Different surveys have been conducted to evaluate the opinion of the population on the possibility of using such a dark material as plaster for indoor or outdoor [58]. Surveys have shown that, despite the idea of using a durable material that helps improve air quality is appreciated by many, its dark color is definitely a limitation to its application.

My Ph.D. project starts from this limitation with the aim of finding other waste materials that can be used to make sustainable and lighter-colored materials that can help reduce PM and investigate other solution to simplify the synthesis process and reduce the associated emissions.

2.3 Sustainable Development Goals

Key word of this Ph.D. project is definitely sustainability. Sustainable development is based on the principle of being able to meet the needs of the present without compromising the possibility of future generations to satisfy their [59][60]. For decades the effects of uncontrolled use of resources, waste generation and emissions of polluting gases into the environment have been neglected as well as a heavy exploitation of populations in developing countries. Nowadays, the awareness of the serious climate situation and social disparities have led the countries of the World to propose initiatives to mitigate the effects of pollution, through the reduction of pollutants' emissions, recycling, a more conscious use of resources and reducing disparities. There have been many initiatives during the last decades, one of the most important is definitely the 2030 Agenda, an action program for people, planet and prosperity signed by the governments of 193 UN member countries in 2015 [3]. Program foundation are 17 objectives, articulated in 169 target and over 200 indicators , called Sustainable Development Goals (SDGs) [61], reported in Figure 7.

Figure 7. Sustainable Development Goals (SDGs) according to 2030 Agenda.

SDGs are a universal call to action to end poverty, ensure that all people enjoy peace and prosperity and protect the planet by reducing emissions, using sustainable technologies and responsible use of resources. The aim is to achieve the 17 objectives by 2030.

According to the object of this Ph.D. thesis, we focused the attention on goals 3, 7, 11 and 13.

Goal 3 concerns good health and well-being, ensuring healthy lives. Good health is essential to sustainable development. It takes into account economic and social inequalities, rapid urbanization, the continuing burden of infectious diseases, like COVID-19 pandemic, and not least the effects of environmental pollution. WHO report reveals that air pollution is associated with 7 million premature deaths annually [62]. SDG target 3.9 concerns the mortality from environmental pollution. The aim is reduce the number of deaths and illnesses from hazardous chemicals and air, water and soil pollution and contamination as healthier environments could prevent almost one quarter of the global burden of disease [63]. When applied, for example, as plaster on facades or tiles of buildings, SUNSPACE could help reduce PM concentrations in cities, making air cleaner and reducing people's exposure to pollution.

Affordable and clean energy is the purpose of Goal 7, ensuring access to affordable, reliable, sustainable and modern energy for all. Energy efficiency is key. Investing in sustainable energy and promoting low-energy processes would help reduce greenhouse gas (GHG) emissions in the environment by improving air quality. The processes took into account in this thesis are low energy consuming, following the Azure Chemistry [8].

Goal 11 concerns making cities and human settlements inclusive, safe, resilient and sustainable. The rapid growth of cities led to a boom in mega-cities, especially in the developing world. Making cities sustainable means creating career and business opportunities, safe and affordable housing, and building resilient societies and economies. It involves investment in public transport, creating green public spaces, improving urban planning and management in participatory and inclusive ways [64]. SUNSPACE can help improve the air quality in cities by making it more salubrious and helping to achieve the goal of more sustainable cities.

Goal 13 concerns climate action. Global warming is causing long-lasting changes to climate system. GHG emissions are a major problem for the environment, in 2021 energy related CO_2 emissions increased 6%, reaching highest level ever [65]. Recycling of waste materials and the use of low-emission processes can help reduce GHG emissions in the environment to limit the global warming. The synthesis process of SUNSPACE uses low energy processes, pursuing the objective proposed by SDG 13.

COVID-19 pandemic has certainly slowed down the pursuit of the objectives proposed by the 2030 Agenda because of the associated social and economic crisis. It is certainly necessary to reschedule some actions taking into account the new needs that the pandemic has brought to light, identifying new strategies and attitudes to be implemented in order to achieve the objectives of sustainable development.

3. Materials

3.1 Industrial by-products

3.1.1 Silica fume

Silica fume is by-product of elemental silicon or alloys containing silicon, like ferrochromium, ferromanganese, ferromagnesium and calcium silicon, in electric arc furnaces. At high temperature (approximately 2000 °C) the reduction of high-purity quartz to silicon produces silicon dioxide vapor, which oxidizes and then condenses at low temperatures producing silica fume. Silica fume particles are spherically shaped and very fine, with a mean size of 20 nm to 500 nm, and a specific area around 20 m^2/g [66]. Several studies analyzed its chemical properties. As shown in Table 1, silica fume is characterized by a high content of amorphous silicon dioxide. Moreover, small amounts of iron, magnesium, and alkali oxides are also found.

Table 1. Chemical composition of silica fume according to different works. LOI = Limit Of Identification.

Compositon (%)	**Guneyisi et al. 2012** [67]	**Haruehansapong et al. 2014** [68]	**Lilkov et al. 2014** [69]	**Mardani-Aghabaglou et al. 2014** [70]
SiO_2	90.36	88.3	89.5	87.29
Al_2O_3	0.71	1.17	1.13	0.47
Fe_2O_3	1.31	4.76	2.31	0.63
CaO	0.45	0.48	0.98	0.81
MgO	-	2.14	1.55	4.47
K_2O	1.52	-	0.6	1.28
Na_2O	0.45	-	0.42	1.25
SO_3	0.41	1.05	0.4	0.22
LOI	3.11	2.1	2.4	2.7

Given the increasing industrial production, it is necessary to think about a reuse of this waste, in the perspective of a circular economy. Silica fume has been recognized as a pozzolanic material, due to its high silica content and extreme fineness. Conforming to specifications of ASTM C1240 [71], silica fume can be used as supplementary

cementitious material in cement mortar and concrete to enhance mechanical and durability properties [72]. In this regard many studies have been conducted to reuse the silica fume inside the cement [72][73][74][75] obtaining beneficial effects on durability and strength properties of mortar and concrete.

The silica fume used for the realization of SUNSPACE was provided by Metalleghe spa (Brescia, Italy), specifically by the B.S.I group which produces silicon metal alloys. The silica fume supplied has a SiO_2 content of 94% (composition provided by B.S.I. group).

3.1.2 Bottom ash

Incineration is a thermal process at high temperature that allows to burn the waste in order to reduce its size. In Italy, 37 incineration plants are active [76], the new generation plants allow to recover the heat produced by the combustion phase and reuse it for domestic heating. One of these new generation plants is located in Brescia (Lombardy, Italy). In operation since 1998, the plant received the prestigious "Wtert Industry Award" of Columbia University in New York as best plant in the world in 2006. The Brescia waste incinerator plant, managed by A2A spa, is the first source of heat generation for the city of Brescia; it produces every year over 70% of the energy distributed by the district heating network, producing electricity equal to the needs of 200,000 households [19].

The plant consists of three interdependent combustion units fed by unsorted municipal waste and sewage sludge. The waste is transported to the incinerator and discharged into the collection and mixing tank. Through cranes, the waste is loaded into the hoppers that feed the grids on which combustion takes place. The combustion lines consist of steam generators, with combustion chambers whose temperature is constantly regulated over 1000 °C, for the complete oxidation of waste and to avoid the formation of dioxins. The heat produced by combustion generates high pressure steam, which is fed into a turbine for the production of electricity and, subsequently, used to heat the

water supplying the district heating network in the city [19]. The plant diagram is shown in Figure 8.

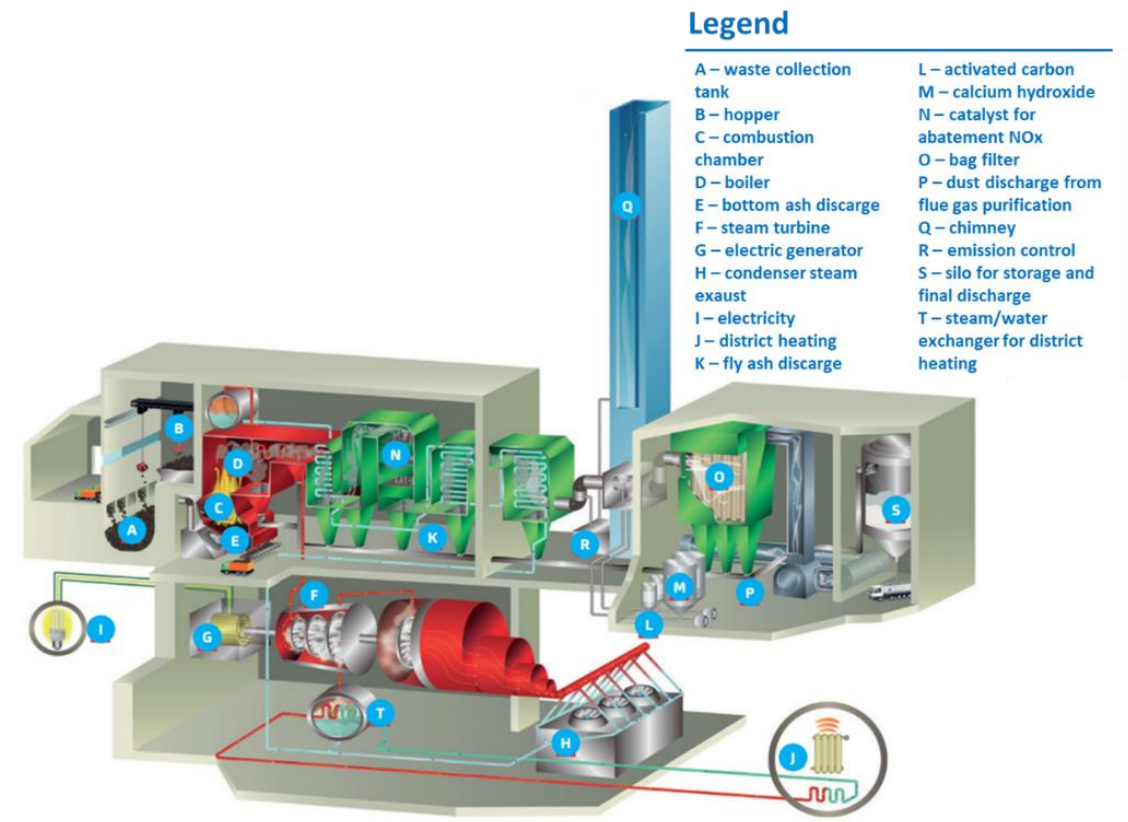

Figure 8. Scheme of Brescia waste incineration plant [19].

Waste incineration produces gaseous emissions that are treated to reduce the emission levels of the plant below the regulatory limits [77][78] and solid residues. The latter are divided into fly ash (FA) and bottom ash (BA). FA, resulting from the treatment of waste gas, consists of the salts of metals condensed on the walls of the boiler energy recovery. About 1 – 3% of FA are produced per ton of waste burned [79]. They are classified as hazardous waste [80] and must first be stabilized in order to be reused [81]. BA consists of the non-combustible residue of waste, metallic and non-metallic residues and unburned organic material; BA represents the most significant fraction of the waste produced by the incineration process, about 25 – 30% per ton of waste burned [79]. The Brescia incinerator plant supplies the BA used in the Chemistry for Technologies Laboratory of the University of Brescia (Figure 9).

Figure 9. Bottom ash supplied by Brescia incinerator plant.

As shown in Figure 9, the BA are characterized by a very coarse grain size mainly represented by sand and gravel; from a mineralogical point of view, the BA composition, although variable in relation to the characteristics of incinerated waste, can be traced back to a matrix consisting mainly of calcium oxide, aluminum and silicon[82]. According to leaching tests performed, bottom ashes are not toxic [81] and therefore can be recovered.

BA recovery is a common practice in many nations, such as Italy, Spain, Germany, Denmark, China, USA [82]. This is possible thanks to the chemical composition of BA and their remarkable hydraulic and lithoid properties. Considering the composition of this by-product, the main recycling applications concern the construction sector in the formation of bituminous conglomerates or in the cement industry as an alternative to common fillers and aggregates [83].

The idea of this work is to use BA instead of silica fume to obtain a lighter material, with the addition of calcium hydroxide to obtain a resistant material.

3.2 Commercial chemicals

In order to realize the porous samples covered by this Ph.D. thesis, in addition to the just described by-products, some commercial reagents will also be needed: sodium alginate, calcium iodate, calcium hydroxide, sodium bicarbonate and hydrogen peroxide.

3.2.1 Sodium alginate

Sodium alginate is a natural polysaccharide that can be extracted from various species of algae and seaweeds [56]. Its function is to give strength and flexibility to the tissue of the algae, playing a role similar to that of cellulose in plants. Sodium alginate is a linear polymer consisting of D-mannuronic and L-glucuronic acid units. Sodium alginate, like all alginates, forms physical hydrogels in which polymer chains have electrostatic interactions or hydrogen bonds. The physical crosslink gives the hydrogel a reticular structure particularly used in the biomedical or pharmaceutical field.

Due to its biocompatibility, biodegradability, immunogenicity and non-toxicity properties, sodium alginate is widely used in different applications. Sodium alginate is used as a gelling and viscosity agent in cosmetics, inks, and as a food additive. It is also used in the paper industry, in that of artificial fibers and colors.

3.2.2 Calcium iodate

Calcium iodate is an inorganic salt composed of calcium and iodate anions. Two forms of calcium iodate are known, $Ca(IO_3)_2$ anhydrous and $Ca(IO_3)_2(H_2O)$ hexahydrate. Both are colorless salts that are naturally generated in the form of minerals, called lautarite and brüggenite respectively. Calcium iodate is one of the main chemical forms in which iodine is present in animal feed [84]. It is also used in the pharmaceutical industry in the production process of antiseptics, disinfectants and deodorants [85].

3.2.3 Calcium hydroxide

Calcium hydroxide is an inorganic compound which is usually found in the form of a colorless crystal or white powder, produced by thermal decomposition of limestone and subsequent exothermic reaction of calcium oxide with water. Calcium hydroxide is produced on a large scale and is generally economical, making it ideal for different applications.

Calcium hydroxide is widely used in the construction industry as part of the mortar, since its reaction with air carbon dioxide binds particles of sand and gravel to form calcium carbonate. In this thesis it was decided to use calcium hydroxide in combination with BA in order to promote the pozzolanic reaction to give resistance to the material. In fact, the reaction between calcium hydroxide and pozzolanic materials (like BA) favors the formation of binder material known as calcium silicate hydrate.

Other important applications are the use of calcium hydroxide:

- as flocculants in water and wastewater treatment: it forms a soft solid that helps to remove particles that are difficult to filter. This application is possible given the low cost and low toxicity of calcium hydroxide;
- treatment of potable water to increase the pH of the water and prevent corrosion of the pipes.

3.2.4 Sodium bicarbonate

Sodium bicarbonate is a sodium salt of carbonic acid. Sodium bicarbonate is present in nature but can also be reproduced industrially. In the latter case, its production takes place through the Solvay method, an industrial chemical process for the synthesis of sodium carbonate using sodium chloride, calcium carbonate and ammonia. The Solvay method is cheap, not very dangerous and also does not produce toxic residues.

Sodium bicarbonate is a very versatile product. It is used for food and medicine purposes. The different uses of sodium bicarbonate are related to its ability to neutralize the pH of an excessively alkaline or acidic substance.

In this work sodium bicarbonate was used as pore former because with temperature tends to decompose releasing CO_2 and allowing the formation of pores.

3.2.5 Hydrogen peroxide

Hydrogen peroxide is a chemical containing peroxide ions $(O\text{-}O)^{2-}$ characterized by strong oxidizing power. The peroxide bond between the two oxygen atoms breaks down when two •OH radicals form, which react quickly with other substances to form new radicals and initiate a chain reaction.

It is a very versatile substance that finds its main application in the chemical, medical and health fields. From 1920 to 1950 hydrogen peroxide was produced by electrolysis from pure hydrogen, while today processes of self-ossidation, always from hydrogen, are used. It must be transported, usually in diluted form, in containers made of polyethylene, stainless steel or aluminum, particularly protected as hydrogen peroxide is a highly flammable substance and if in contact with flammable substances (wood, paper, oil, cellulose) may give rise to spontaneous ignition. Commercially available hydrogen peroxide is present only in dilution in aqueous solution.

It is widely used in environmental sanitization (for example potable water sanitization) thanks to its many advantages, it is in fact particularly effective (it guarantees a decontamination to 99%), environmentally friendly and safe [86].

In this work, hydrogen peroxide was used as an alternative to sodium bicarbonate as pore former to avoid heat treatment otherwise needed with SUNSPACE.

4. Materials synthesis and nanoparticles entrapment

4.1 Synthesis of samples for nanoparticles capture

Different porous samples were synthetized by using two industrial by-products: silica fume (SF) and BA. Two different typologies of samples were realized: with and without thermal treatment.

Sample 1 (SUNSPACE) synthesis process was described in Paragraph 2.2. Samples 2 and 3 synthesis process is quite similar to sample 1 but sodium bicarbonate was substituted by 5.4 mL and 7.2 mL of hydrogen peroxide, respectively, and only 20 mL of MilliQ water were added.

The use of BA in the materials' synthesis required some pre-treatments. After manually separating the fraction greater than 2 cm, the BA was dried at 100 °C for 1 h. Then, BA was manually sieved to obtain a fraction lower than 300 µm. This fraction was chosen because it is the most reactive and can better react with calcium hydroxide favoring the pozzolanic reaction. SUNSPACE BA (sample 4) sample was made by mixing 32 mL of MilliQ water with 0.6 g of sodium alginate and 1 g of calcium iodate. Then, 9 g of BA and 9 g of calcium hydroxide were added, and finally 5 g of sodium bicarbonate were mixed with the compound. Instead, samples 5 and 6 were synthetized without thermal treatment: 9 g of BA, 9 g of calcium hydroxide were mixed with 9 mL of MilliQ water, finally 5.4 mL or 7.2 mL of hydrogen peroxide were added, respectively.

For all samples, the slurry was put in circular aluminum mold, (2.73 ± 0.21) cm of diameter. Samples 1 and 4 were put on a heating plate for 1 h at low temperature (70 – 80 °C) while samples 2, 3, 5 and 6 were left at room temperature for 1 week to reach the final consolidation. Table 2 reports porous materials composition, while Figure 10 reports the images of all six samples.

Table 2. Porous materials composition synthetized by two different industrial by-products: silica fume (1, 2 and 3) and bottom ash (4, 5 and 6).

	Silica fume (g)	Bottom ash (g)	Calcium hydroxide (g)	Sodium alginate (g)	Calcium iodate (g)	Sodium bicarbonate (g)	Hydrogen peroxide (mL)	Thermal treatment
Sample 1	17.88			0.6	1	5		Yes
Sample 2	17.88			0.6	1		5.4	No
Sample 3	17.88			0.6	1		7.2	No
Sample 4		9	9	0.6	1	5		Yes
Sample 5		9	9				5.4	No
Sample 6		9	9				7.2	No

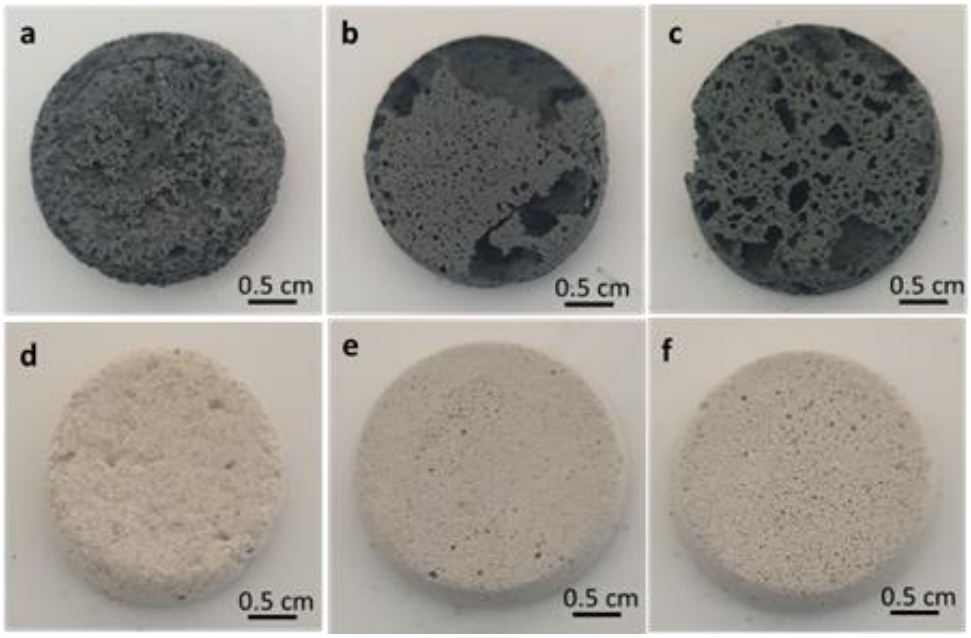

Figure 10. Porous materials synthetized with silica fume and bottom ash: sample 1 (a), sample 2 (b), sample 3 (c), sample 4 (d), sample 5 (e) and sample 6 (f).

In addition, *Hedera Helix* leaf and cement were used as reference materials, Figure 11. As already said in Paragraph 2.1.1, *Hedera Helix* has shown relatively high PM densities in all size fractions due to the important role of leaf surface wax in removing particles [12]. *Hedera Helix* leaves were collected before carrying out the experiments in a town near Brescia (Italy). To have the same exposed surface, (5.9 ± 0.5) cm^2, the leaves of *Hedera Helix* were cut to obtain samples with a diameter of about 2.7 cm. Before PM exposure, leaves samples were carefully washed with MilliQ water to eliminate any impurities present. Cement is the most used material in the field of construction. Cement (TECNOCEM- 42.5 class) was crumbled into a ball vibratory mill (MM400 Retsch)

for 3 minutes at a frequency of 25 Hz with one zirconium sphere (20 mm of diameter), obtaining a fine powder with particle size in a range from 106 to 300 µm. 17 g of cement were mixed with 6.8 mL of MilliQ water, (water/cement ratio 0.4). The slurry obtained was inserted in circular aluminum molds (2.73 ± 0.21) cm of diameter and put on a heating plate for 1 h at a low temperature (70 - 80°C).

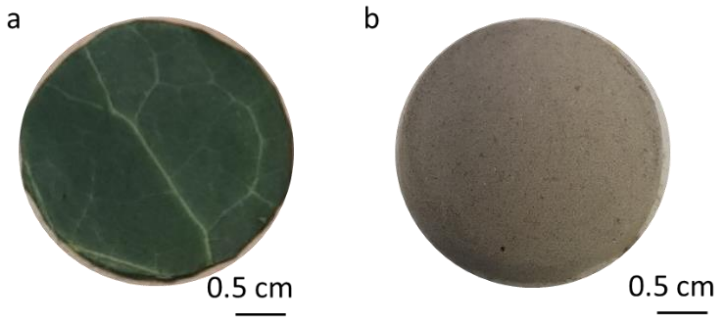

Figure 11. Hedera Helix leaf (a) and cement sample (b) used as reference materials.

4.2 Samples characterization

Samples were characterized through different colorimetric, structural, morphological analysis.

Colorimetric analysis was performed by UV-Vis Spectroscopy-Color Measurement Minolta CM 2600d. This technique allows to define an accurate color through a color space defined by Luminance (L, lightness) and two-color channels (a and b). L changes from 0 (black) to 100 (white), while a and b can range from positive and negative values. Negative values represent green and blue colors for a and b, respectively. Instead, positive values correspond to red and yellow colors for a and b, respectively. The analysis allows to evaluate SCI (including specular component) and SCE (excluding specular component) values. As data obtained are very similar for the two components, Table 3 reports only SCI component for all porous samples.

Table 3. Colorimetric analysis of six porous samples. Measurements are reported in SCI modality.

Samples	L	a	b
Sample 1	38.83 ± 0.01	-0.92 ± 0.01	2.33 ± 0.01
Sample 2	47.46 ± 0.52	0.81 ± 0.02	1.46 ± 0.06
Sample 3	46.69 ± 0.39	0.63 ± 0.02	0.76 ± 0.24
Sample 4	81.97 ± 0.01	0.77 ± 0.01	6.34 ± 0.01
Sample 5	86.01 ± 0.01	0.21 ± 0.01	3.41 ± 0.01
Sample 6	86.32 ± 0.01	0.16 ± 0.01	3.13 ± 0.01

According to the results, the use of BA allows to obtain a lighter color material. Taking the average of the 3 L values for the samples with SF (samples 1, 2 and 3) and the average of the 3 L values for the samples with BA (samples 4, 5 and 6), by replacing the SF with BA, L increases from about 44 to about 84, changing from dark grey to light grey.

The structural characterization was performed by XRD analysis by mean with Panalytical diffractometer (Netherlands), using Cu Ka (1.5406 Å) radiation and operating at 40 kV and 40 mA. About 1 g of each sample was crushed in a mortar to obtain a fine powder that can be analyzed by the instrument.

Figure 12 reports the XRD patterns for SF samples (1, 2 and 3), moreover the SF pattern is reported as reference.

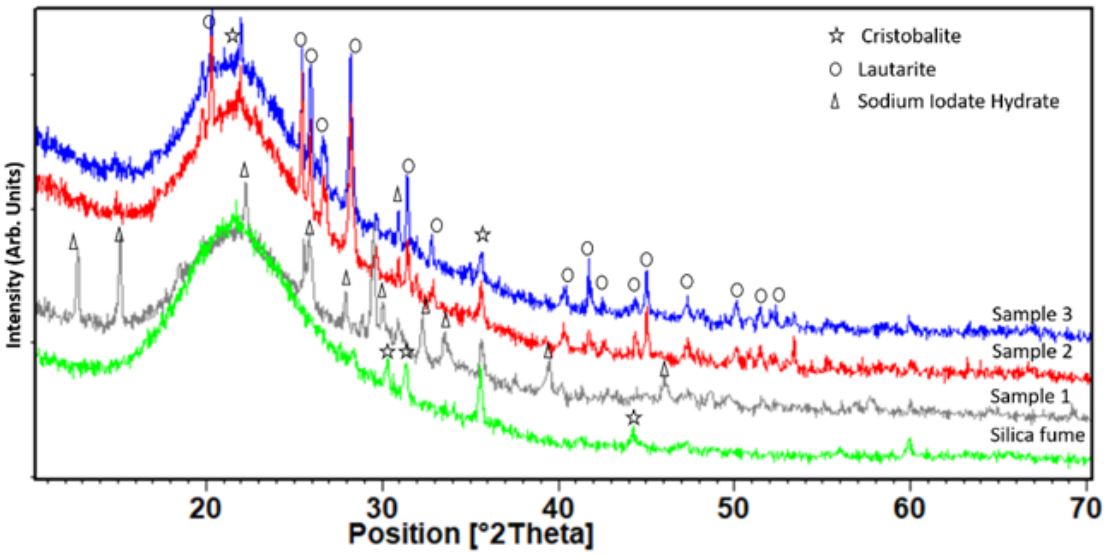

Figure 12. XRD patterns of silica fume and samples synthetized with silica fume (sample 1, sample 2, and sample 3).

All samples present a large halo in a range between 15° and 30° (2θ) and cristobalite (SiO_2) peaks, due to the amorphous phase of silica fume powder. Sample 1 is characterized by several diffraction peaks identified by sodium iodate hydrate ($Na(IO_3)!H_2O$) generated during the synthesis of the material [15]. Sample 2 and sample 3 show similar patterns. This reveals that the different concentrations of hydrogen peroxide, used as pore former, do not change the structure of the sample. These two samples are mainly characterized by peaks of lautarite $Ca(IO_3)_2$, used in the sample realization. The lack of sodium iodate hydrate phase is probably related to the absence of sodium bicarbonate.

Figure 13 reports the XRD patterns for BA samples (4, 5 and 6), moreover the BA pattern is reported as reference.

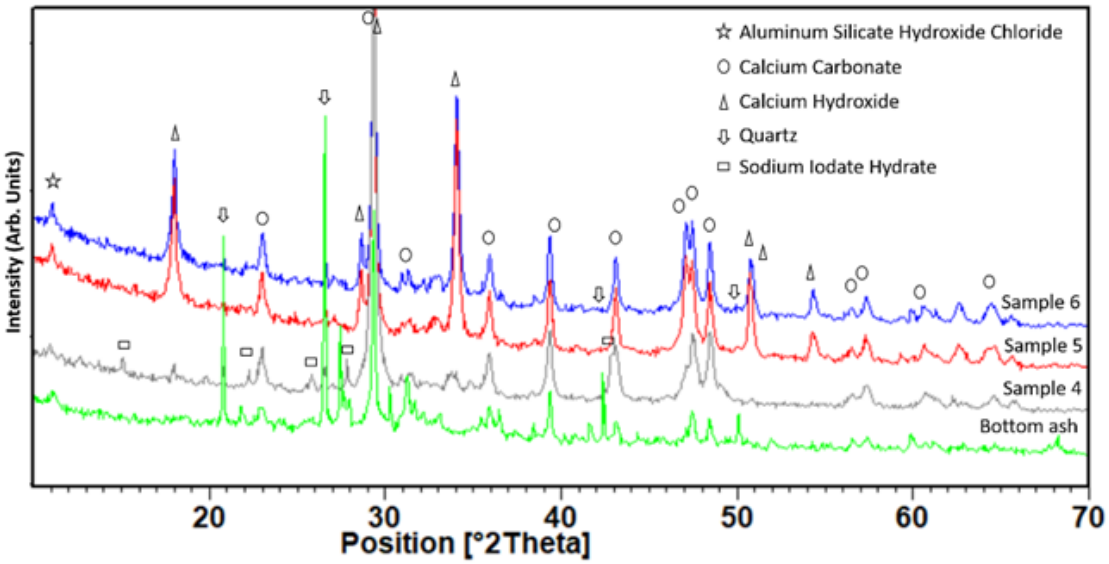

Figure 13. XRD patterns of bottom ash and samples synthetized with bottom ash (sample 4, sample 5, and sample 6).

Sample 4 is characterized mainly by sodium iodate hydrate ($Na(IO_3)!H_2O$), generated during the material synthesis, quartz (SiO_2) and calcium carbonate ($CaCO_3$), derived from BA powder. Calcium carbonate is probably generated also during the carbonation process between calcium hydroxide and carbon dioxide. Some peaks of aluminum silicate hydroxide chloride ($Al_3(SiO_4)_5(OH)_{18}Cl$) are also identified. Samples 5 and 6 show similar patterns. The crystalline phases identified are calcium carbonate ($CaCO_3$),

calcium hydroxide ($Ca(OH)_2$), and quartz (SiO_2). Also, aluminum silicate hydroxide chloride ($Al_3(SiO_4)_5(OH)_{18}Cl$) peaks are detected. Instead, sodium iodate hydrate is not identified, probably due to the absence of sodium bicarbonate.

In Figure 14 the optical microscopy images of the 6 porous samples are reported. All samples are characterized by porous surfaces. The shape and size of pores are the main differences of samples obtained by using SF or BA. Samples 1 and 3 show pores with irregular shapes and sizes in order to 100 – 200 µm. Pores with higher dimensions (up to about 1 mm), were identified in sample 2. Samples with BA are characterized by pores with more regular shape. Sample 4 shows pores with a diameter up to 1 mm, instead samples 5 and 6 present pores of smaller size and well distributed over the entire surface. Some pores with a diameter of about 300 µm of size were identified in sample 5. Instead, pores of that size are much more widespread in sample 6, probably due to the greater amount of hydrogen peroxide used in the sample synthesis.

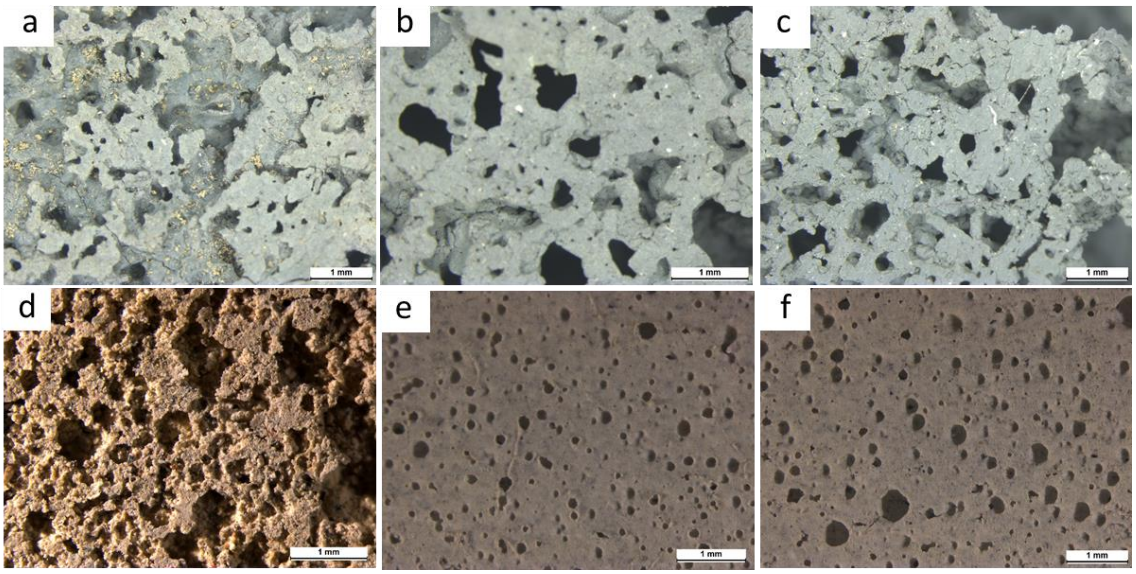

Figure 14. Optical microscopy images of sample 1 (a), 2 (b), 3 (c), 4 (d), 5 (e), 6 (f).

The accessible porosity and pore size distribution of the 6 samples were quantified using a Pascal 240 Mercury Porosimeter from Thermo Scientific, capable of intruding mercury by a stepwise increase of pressure from vacuum to 200 MPa. After drying at 60 °C for 12 h, a broken piece of each sample of about 1 cm^2 size was tested. The volume change of mercury between each pressure step allows to define different parameters, of which

the pore size distribution, the accessible porosity, the mode, mean and median pore size values were evaluated from the results. Figure 15 reports the pore size distributions of samples, while Table 4 reports the basic descriptive statistics.

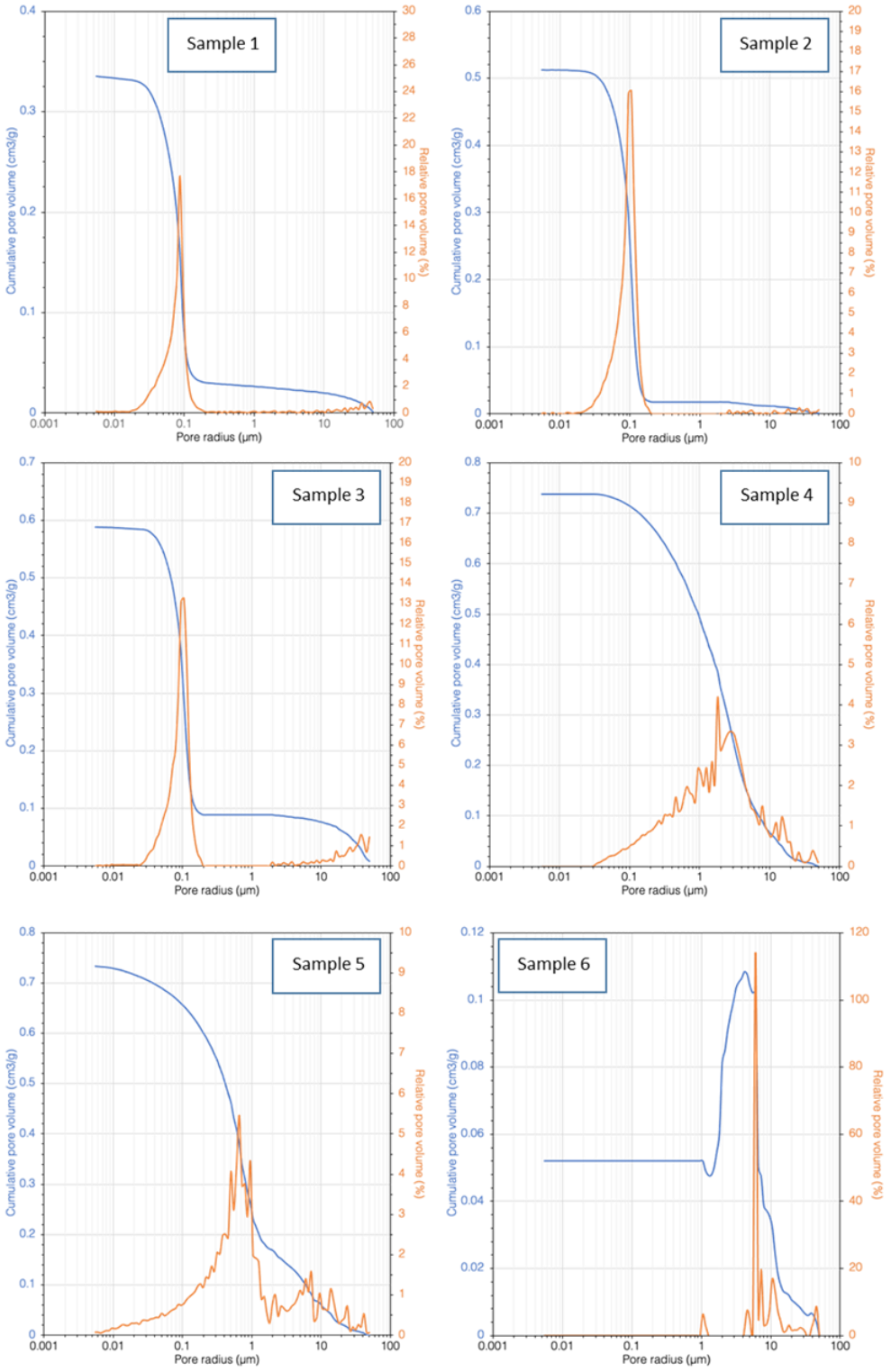

Figure 15. Pore size distributions of all six samples quantified by mercury porosimetry analysis.

Table 4. Results from mercury intrusion porosimetry.

Samples	Accessible Porosity (%)	Average Pore Radius (µm)	Median Pore Radius (µm)	Modal Pore Radius (µm)
Sample 1	41	0.0356	0.0777	0.0849
Sample 2	49	0.0455	0.0911	0.1063
Sample 3	52	0.0418	0.0954	0.1058
Sample 4	63	0.0282	1.7808	1.7938
Sample 5	58	0.0387	0.6153	0.6127
Sample 6	3	0.0141	9.6896	5.6504

The accessible porosity by intrusion is always above 41%, with a maximum of 63% for the sample 4. The anomalously low value for sample 6 (about 3% accessible porosity), which is clearly at odds with the morphological observations, indicates sample deformation and porosity collapse during the test. The sample 6 is therefore not considered in the mercury porosimetry results. The pore sizes of the samples prepared with SF (1, 2 and 3) follow a unimodal distribution with a pore radius mode of 0.08 – 0.1 µm. The sample 5 shows a bimodal pore size distribution, with a main peak at about 0.65 µm and a secondary peak related to larger pores with a radius of about 7 – 8 µm. Finally, the pore size distribution of sample 4 spans about an order of magnitude, with a mode of 1.79 µm. The porosimetric analysis confirmed that samples with BA show pores with higher dimensions compared to those with SF.

Scanning electron microscopy (SEM, LEO EVO 40, Zeiss) analysis was performed to evaluate the morphology of samples. As reported by XRD analysis the different concentrations of hydrogen peroxide do not influence the structure of the samples. Therefore, only samples 1, 2, 4 and 5 were analyzed. Figure 16 shows SEM images of samples synthetized with SF and different pore formers: sodium bicarbonate (a and b) and hydrogen peroxide (c and d). Sample 1 is characterized by spherical particles, typical of silica fume powder, with size dimension about 20 - 700 nm, agglomerated together [15][80]. Figure 16a reveals the presence of some macro-pores with dimensions in order to µm. Some needle-shaped structures appeared on sample 1 surface (as reported in Figure 16b), probably they can be attributed to sodium iodate peaks, as confirmed by

XRD analysis reported in Figure 12. The use of hydrogen peroxide instead of sodium bicarbonate changes the morphology of the sample. Sample 2 is characterized by spherical particles very compact with them (Figure 16c). In addition, some lamellae appear on the sample surface (Figure 16d).

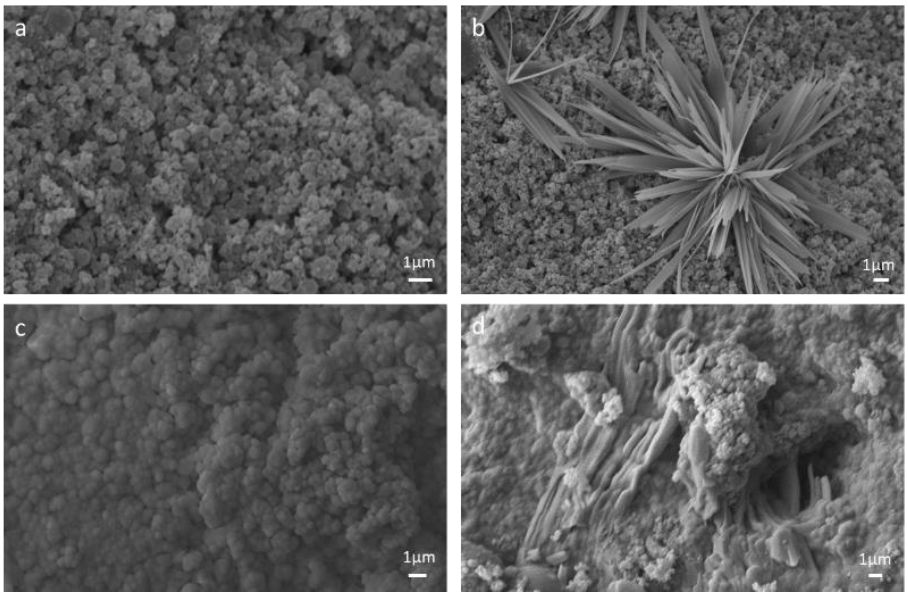

Figure 16. SEM images of samples synthetized with silica fume and different pore former: sodium bicarbonate (a and b) and hydrogen peroxide (c and d)

Figure 17 shows SEM images of samples synthetized with BA and different pore formers: sodium bicarbonate and hydrogen peroxide. Unlike samples synthetized with SF, those with BA are characterized by particles with different forms and irregular morphologies. This is attributed to the BA powder [87]. Sample 4 (Figure 17a and Figure 17b) shows a fibrillar matrix, clearly visible in Figure 17b. It is probably related to the C-S-H formation, typical of pozzolanic reaction [81].

As reported in Figure 13, XRD spectrum of sample 5 is characterized mainly by calcium hydroxide peaks. This means that probably this phase did not react with the amorphous phase of BA, so the fibrillar matrix typical of C-S-H formation is not present (as reported in Figure 17c and Figure 17d).

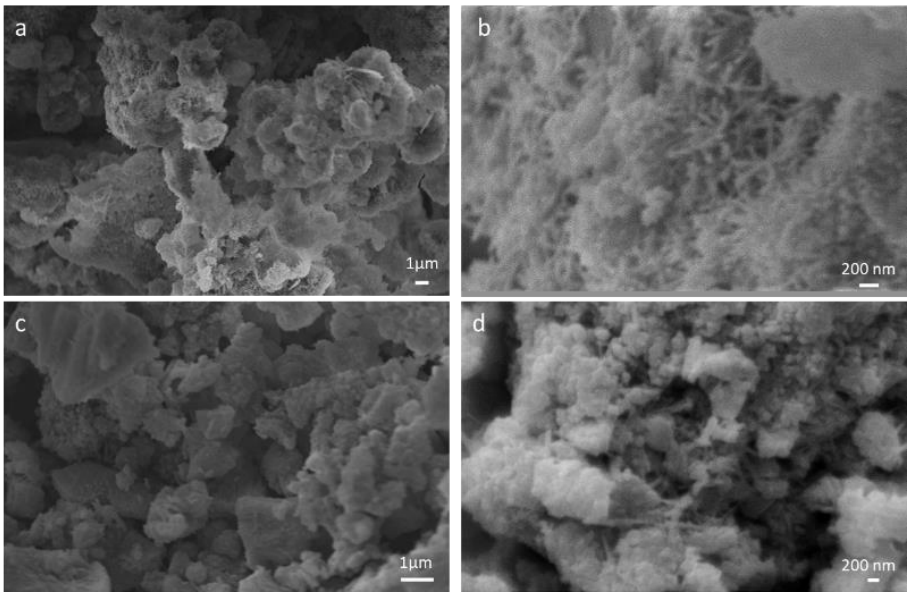

Figure 17. SEM images of samples synthetized with bottom ash and different pore former: sodium bicarbonate (a and b) and hydrogen peroxide (c and d).

4.3 Sustainability analysis

The environmental impact of these samples was performed in terms of Embodied Energy (EE) and Carbon Footprint (CF). As reported by [88], EE includes all the energies (direct and indirect) consumed during the production of 1 kg of material. CF is related to the GHG generated during the production of 1 kg of material [88] and reported as CO_2 equivalent. This approach allows to have a preliminary estimate of the impacts related to the energy and emissions necessary to the production of the material. It is a simplified approach compared to LCA (Life Cycle Assessment) that definitely requires more data for the evaluation, it can be considered as a preliminary assessment [89]. The evaluation was carried out with the software Ces selector [57]. Figure 18 shows the EE versus CF of six porous samples synthetized by SF (samples 1, 2 and 3) and by BA (samples 4, 5 and 6). The sustainability evaluation takes into account the use of chemicals and thermal treatment performed during the synthesis of the material.

As reported in Figure 18, all samples are more sustainable compared to materials frequently used in the production of air filters such as PS, PE, PP and polyamide (PA). The idea is to use these porous materials in building construction. Therefore, a

comparison was performed with brick, Portland cement, plaster of Paris, and concrete. Figure 18 shows that sample 1 has lower EE, while samples 2 and 3 synthetized with SF and hydrogen peroxide (used as pore former instead of sodium bicarbonate) are more sustainable in terms of CO_2 emission compared to other samples. The elimination of thermal treatment allows for improving material sustainability in terms of carbon emissions. The use of BA instead of SF increases the EE and CF values (as evidenced for samples 4, 5 and 6), this is probably due to some pre-treatments necessary before its reuse. In fact, BA was subjected to a thermal treatment, to reduce its moisture, and control the amount of water that was added, to guarantee the sample workability during the synthesis. It will be necessary to try to eliminate these treatments or to provide for alternative treatments to further reduce the environmental impact.

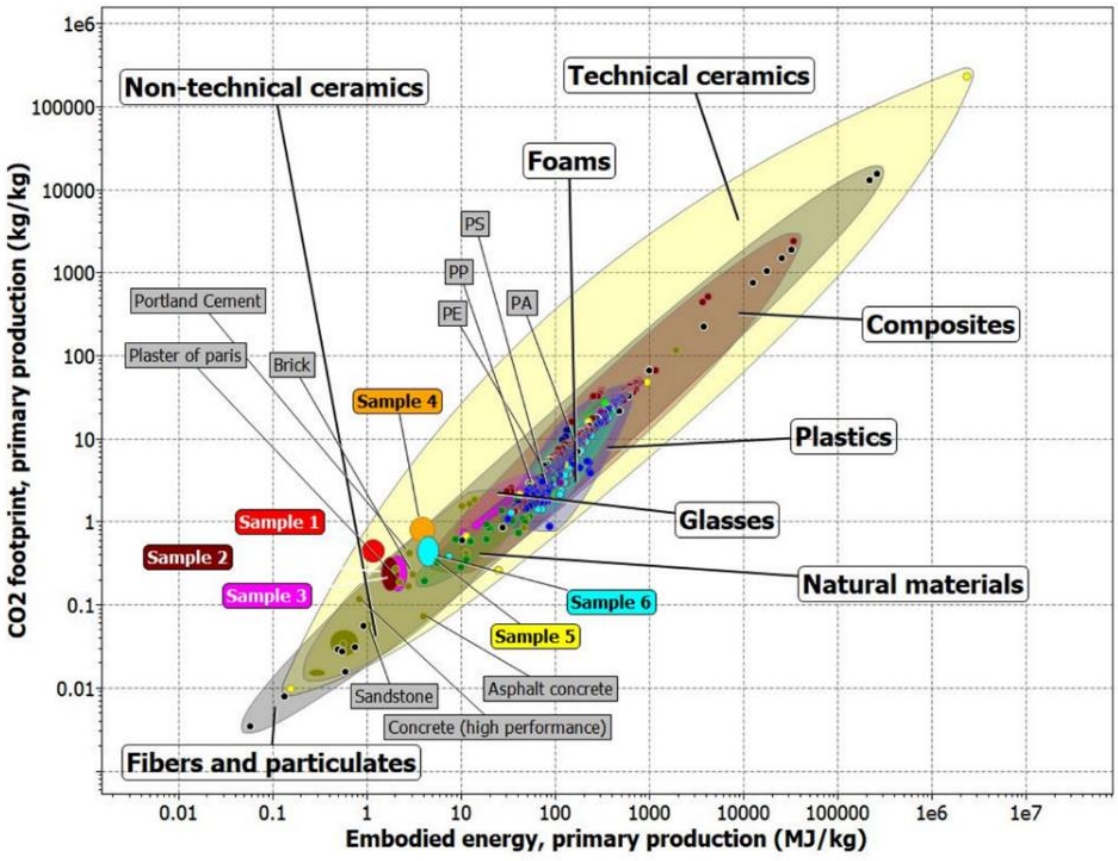

Figure 18. Embodied Energy (EE) versus Carbon Footprint (CF) of six porous samples: samples 1, 2 and 3 were synthetized by silica fume (SF), while samples 4, 5 and 6 by bottom ash (BA). In comparison the environmental impact of plastic materials used in the production of air filters (polypropylene PP, polystyrene PS, polyamide PA, polyethylene PE) and building materials (Portland cement, plaster of Paris, brick or concrete) are reported.

4.4 Adsorption test

As the idea is to use these sustainable porous material to entrap PM, the six samples were subjected to adsorption test.

Experimental tests were carried out, for the first time, by using an aerosol nanoparticle generator (Grimm Particle-generator MODEL 7.811). The instrument is composed of two main elements, the atomizer and the dryer (Figure 19): the atomizer contains the solution to spray while the dryer containing silica gel that allows the dehumidification of the air flow into it. An air flow, taken from the outside, passes through a first filter and then through the silica gel present in the dryer, while a second air flow passes through two other filters and arrives at the atomizer. The two flows then converge at the generator outlet, from which the aerosol is sprayed. Contrary to the previous tests performed on SUNSPACE, the use of the aerosol nanoparticles generator allows to have a control on the airflow which can be controlled by the operator. A titanium dioxide (TiO_2, Hombitan 97% with 300 nm size, kindly supplied by Rifra Masterbatches spa) suspension was used to simulate a PM source. The suspension was prepared by mixing 0.45 g of TiO_2, size dimension 300 nm, with 150 mL of MilliQ water and then sonicated for 15 min, obtaining a concentration of about 3 g/L. Some preliminary tests were conducted to define the experimental setup, settling the following parameters: atomizer pressure about 290 mbar, flow of the dryer 7 L/min, and volume of TiO_2 suspension 7 mL. Both aerosol generator and samples were put in a glove box. As shown in Figure 19, samples, positioned on a fixed support, were exposed in front of the generator outlet, 2 cm away, and at the same height, about 15 cm, to maximize the TiO_2 adsorption. Samples were exposed for 4 min, after 1 min of stabilization. 3 specimens for each material were exposed.

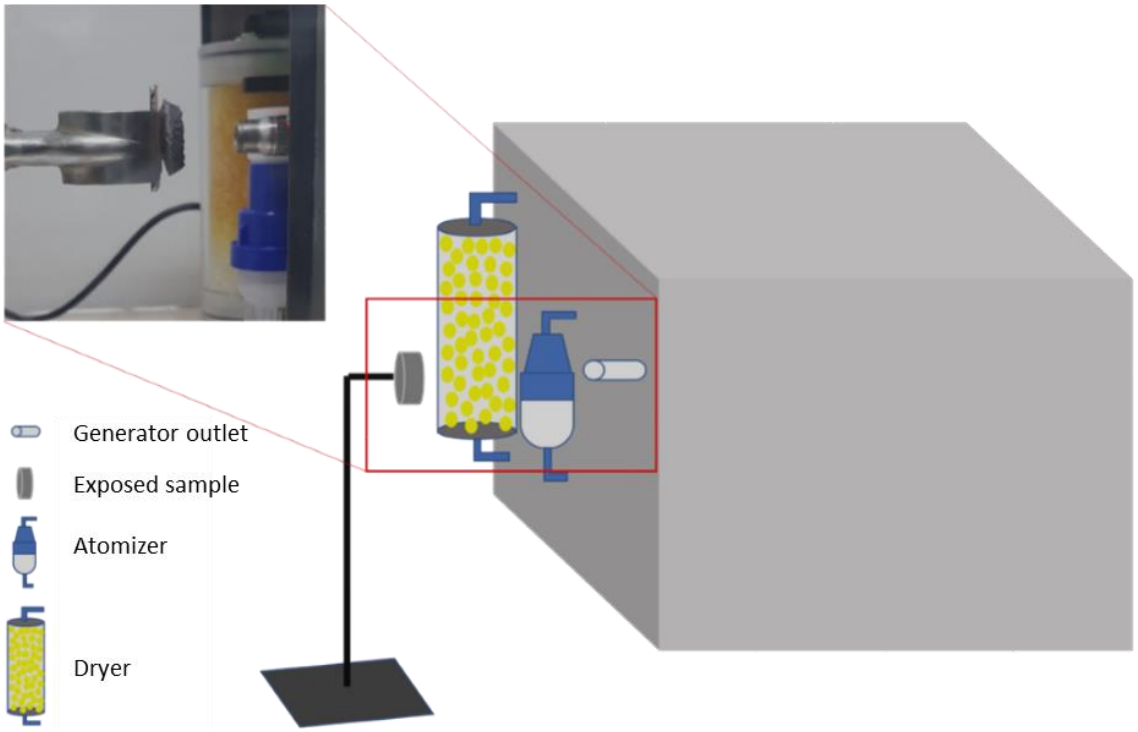

Figure 19. Schematic representation of nanoparticles generator.

The adsorption capacity was evaluated by comparing the pristine and exposed samples. All materials were digested following a standard procedure [90]. Leaf was entirely digested. While for the other samples, exposed samples were first gently shaken 3 times to eliminate any TiO_2 excess, then all samples were superficially scratched to obtain 0.25 g of powder and placed in a teflon vessel with 4 mL of HNO_3 (≥ 65%), 2 mL of HCl (37%), and 2 mL of HF (48%). Each vessel was processed by the CEM SP-D 10/35 microwave digestion system (CEM Corporation, Matthews, United States). Finally, the volume of each digested sample was adjusted to 50 mL with MilliQ water. To evaluate the Ti concentration of each sample, through the TXRF (Total reflection X-Ray Fluorescence) analysis, an internal standard, Ga, in known concentration (1 mg/L), was added to the digested samples. 10 µL of this solution was put in the center of plexiglas support, dried on a heating plate (about 50 °C) and then analyzed. To ensure the repeatability of the measurement, 3 specimens were analyzed for each sample. The spectra obtained were evaluated by the software Picofox (Spectra Plus 5.3, Bruker AXS Microanalysis GmbH, Berlin, Germany) and Ti concentrations were converted to TiO_2 concentrations through simple conversions. Figure 20 reports the results of the adsorption tests. Results show

that sample 2 and sample 4 had the best adsorption capacity. Sample 1 had a modest adsorption capacity probably due to the presence of smaller pores (characterized by ink-bottle shape [17]), according to porosimetric analysis in Paragraph 4.2, than the size of the TiO_2 used (300 nm). Samples 5 and 6, realized with BA and hydrogen peroxide, showed a low adsorption capacity which will be investigated in Chapter 6. *Hedera Helix* leaf showed high TiO_2 concentrations since the TiO_2 suspension was just deposited onto the surface but not adsorbed, because after the test a layer of TiO_2 had formed on the surface of the leaf. Finally, cement had no adsorption capacity.

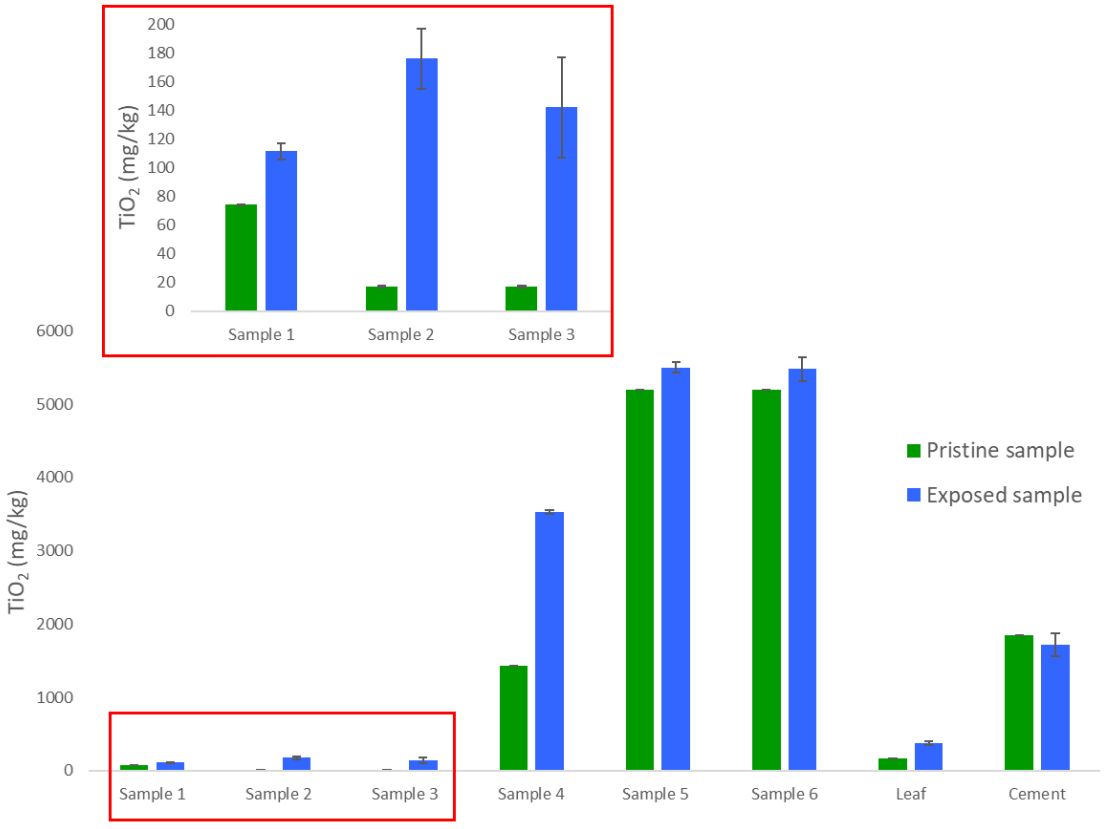

Figure 20. Results of TiO_2 entrapment by porous samples (1, 2, 3, 4, 5 and 6). In comparison also Hedera Helix leaf and cement were reported.

4.5 Conclusions

In this Chapter, SUNSPACE implementations were proposed to obtain a lighter-colored material (using BA) and to eliminate the thermal treatment (substituting the sodium bicarbonate with the hydrogen peroxide) simplifying the synthesis process. Samples

were fully characterized. In particular, porosimetric analysis revealed the presence of pores of smaller dimension in samples realized with SF compared to samples realized with BA. SEM analysis revealed that samples realized with BA are characterized by particles with different forms and irregular morphologies while samples realized with SF presented spherical particles, typical of SF powder. Sustainability analysis, performed with the software Ces Selector revealed that all samples were more sustainable compared to materials commonly used in filters' production, like PP, PE and PS, representing a good starting point for their possible development.

As the main purpose of developing these materials is to reduce PM concentrations in cities, the adsorption capacity of these materials was tested. For the first time, adsorption tests were performed using an aerosol nanoparticles generator (Grimm Particle-generator MODEL 7.811) and a TiO_2 suspension to simulate a PM source. The ability of these materials in particulate matter trap was compared to cement and *Hedera Helix L*. Results showed that sample 2 and sample 4 had the best adsorption capacity. The lower adsorption capacity of samples 5 and 6 will be investigated in Chapter 6.

These works are reported in peer review publications [91][92] and as book chapter in [93].

5. Photodegradation of organic pollutants

There are different ways to remove organic pollutants like photodegradation, biochemical treatment, wet air oxidation, filtration, chemical precipitation and adsorption [94][95]. However, in this Chapter only photodegradation is studied. This process involves reactive species that, when exposed to UV radiation, can photodegrade the organic matter [96]. Organic compounds are responsible for adverse effects on human health and the photodegradation could help in reducing concentrations of these pollutants favoring the environmental remediation process. There are chemical species, called catalysts, which accelerate photo degradation reactions. Many are the existing catalysts, among them one of the most used is titanium dioxide (TiO_2). TiO_2 is presented as a crystalline white powder that finds many applications in different sectors. It is used in paints as white pigment, as opacifying in paper and textile fibers, building materials, wastewater treatment, in the food industry as dye and in the pharmaceutical industry [97][98][99]. Only recently, the European Food Safety Agency (EFSA) recognized that food dye made with TiO_2 may not be safe for health by transposing a 2020 European directive [100]. As catalyst, TiO_2 is a high reactivity semiconductor that can be chemically activated by UV radiation. This strong photocatalytic activity ensures that, exposed at UV radiation, TiO_2 can oxidize organic compounds to H_2O and CO_2 and form oxidizing radicals when present water and oxygen.

In this Chapter, methylene blue (MB) has been used as an organic pollutant to be removed by photodegradation. MB can be degraded using catalysts like Ag doped ZnO, zinc or copper oxide, TiO_2 or TiO_2 in association with other additives like H_2O_2 or UV source [101]. In accordance with literature, TiO_2 was used with an UV source in this work.

5.1 Synthesis of porous materials with titanium dioxide

Thanks to its catalyst qualities, TiO_2 has been used to realize other porous samples. TiO_2 powder (Hombitan 97% with 300 nm size) was used. These new samples were

synthetized to compare their photo degradation ability with the one of the materials described in Paragraph 4.1. To make the comparison, samples that showed the best performance in PM entrapment (Paragraph 4.4), between the different typologies, were chosen to investigate their photo degradation performance. At this purpose, samples 1, 2, 4 and 5 were chosen. New formulations of these 4 samples were proposed by replacing 20% of the powder (SF or BA and calcium hydroxide) with TiO_2.

The synthesis process is the same discussed in 4.1 paragraph. Sample 7 and sample 8 are the same as samples 1 and 2, respectively, but with 14 g of SF and 4 g of TiO_2. Samples 9 and 10 are similar to samples 4 and 5, respectively with 7 g of BA, 7 g calcium hydroxide and 4 g TiO_2. Table 5 shows the quantities of the reagents used in the material synthesis.

Table 5. Quantities of reagents used in samples synthetized with titanium dioxide (TiO_2).

	Silica fume (g)	**Bottom ash (g)**	**TiO_2 (g)**	**Calcium hydroxide (g)**	**Sodium alginate (g)**	**Calcium iodate (g)**	**Sodium bicarbonate (g)**	**Hydrogen peroxide (mL)**	**Thermal treatment**
Sample 7	14		4		0.6	1	5		Yes
Sample 8	14		4		0.6	1		5.4	No
Sample 9		7	4	7	0.6	1	5		Yes
Sample 10		7	4	7				5.4	No

Before photo degradation testing, all samples were washed with approximately 10 mL MilliQ water to release any clogged pores removing unreacted composites.

Figure 21 shows the new samples synthetized with a 20% of substitution of powder with TiO_2.

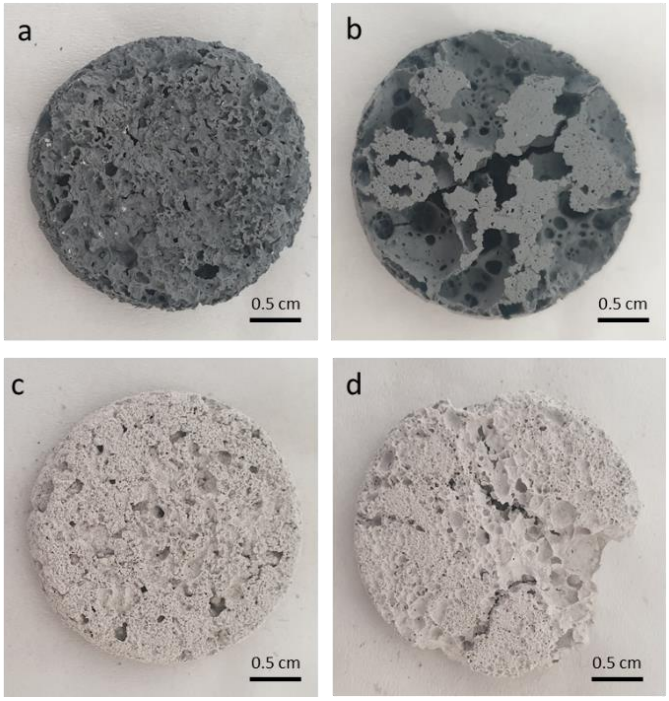

Figure 21. Samples synthetized with titanium dioxide: a) sample 7, b) sample 8, c) sample 9, d) sample 10.

5.2 Samples characterization

Figure 22 reports the optical images of samples. The addition of TiO_2 to samples seems to change the pores size. As reported in Figure 22a, sample 7 (SUNSPACE with TiO_2) presents lower pores' dimension (about 40 - 150 µm), compared to sample 1. Sample 8 presents different morphology and a smoother surface compared to other samples (as reported in Figure 22b and Figure 23a). The detail of internal (Figure 23b) and external (Figure 23c) surfaces was reported. The external surface was mainly characterized by pores with small dimensions (about 40 - 70 µm), and some bigger pores about 150 µm. Instead, internal surface shows pores with variable dimensions (150 µm - 1.3 mm). Sample 9 also presents pores with lower dimension (from 50 µm to 100 µm) and some bigger pores with dimensions in the order of mm. Finally, the presence of TiO_2 influences also sample 10 pores, compare to sample 5, pores are smaller (70 - 200 µm) and with irregular shape.

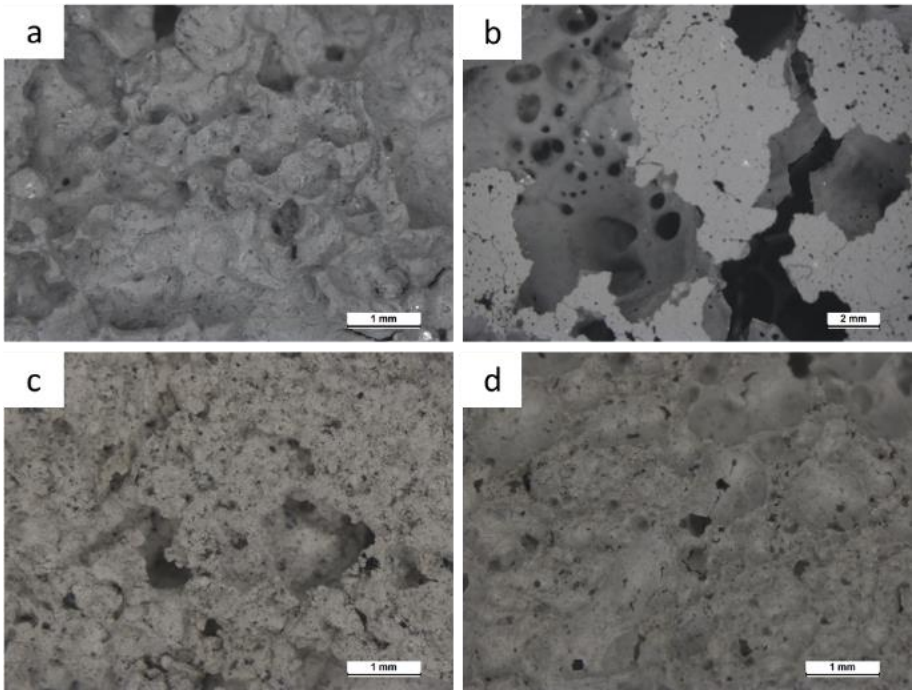

Figure 22. Optical microscopy images of sample 7 (a), sample 8 (b), sample 9 (c) and sample 10 (d).

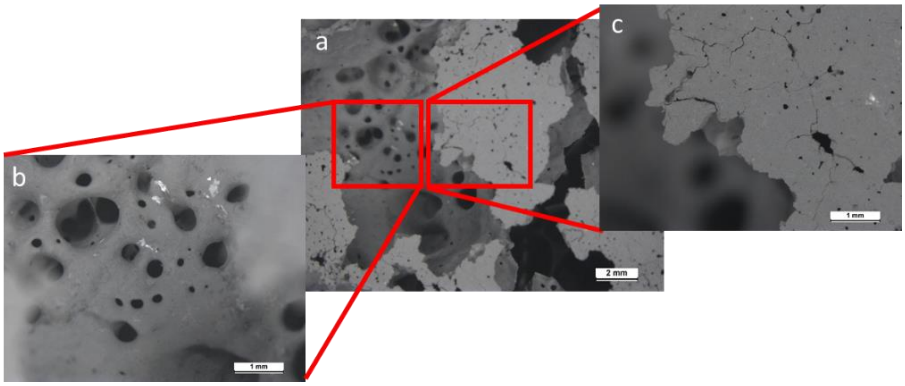

Figure 23. Optical image of sample 8 (a) with detail of internal (b) and external (c) surfaces.

Figure 24 reports the XRD analysis of samples 7, 8, 9, and 10. In comparison also TiO_2 powder pattern is reported. All sample patterns present titanium dioxide peaks (in anatase form). Samples 7 and 8 present a halo in a range between 15° and 30° (2θ) and cristobalite (SiO_2) peaks, due to the presence of amorphous SF powder. Sample 7 is characterized by several diffraction peaks identified as sodium iodate hydrate ($Na(IO_3)!H_2O$), generated during the synthesis of the material. Also, some nahcolite ($NaHCO_3$) peaks are identified, probably due to some incomplete reaction. Sample 8 is mainly characterized by peaks of lautarite ($Ca(IO_3)_2$), used in the sample realization.

Moreover, the lack of sodium iodate hydrate ($Na(IO_3)!H_2O$) phase is probably due to the absence of sodium bicarbonate in the synthesis process. Sample 9 is characterized mainly by sodium iodate hydrate ($Na(IO_3)!H_2O$), generated during the material synthesis, calcium carbonate ($CaCO_3$) and quartz (SiO_2), derived from BA powder. Calcium carbonate is probably also generated during the carbonation process between calcium hydroxide and carbon dioxide. Some peaks of aluminum silicate hydroxide chloride ($Al_3(SiO_4)_5(OH)_{18}Cl$) have been identified. The crystalline phases identified in sample 10 are calcium carbonate ($CaCO_3$), calcium hydroxide ($Ca(OH)_2$), and quartz (SiO_2). Instead, sodium iodate hydrate is not identified, probably due to the absence of sodium bicarbonate in the synthesis process.

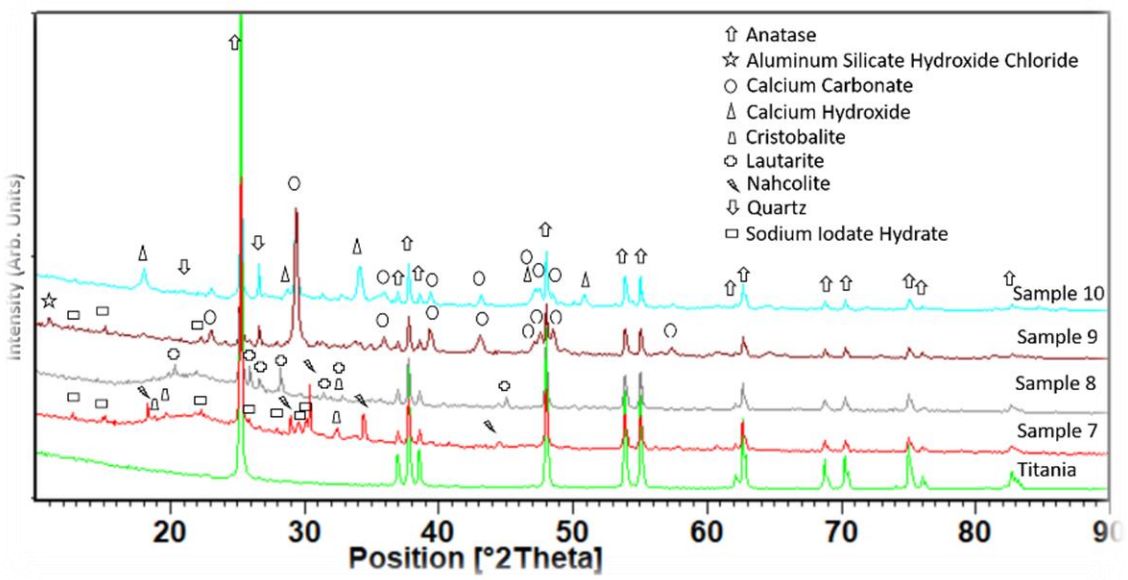

Figure 24. XRD patterns of samples 7, 8, 9, and 10. In comparison also titania (TiO_2) pattern is reported.

5.3 Photo degradation test

MB was used to simulate an organic pollutant that can be removed thanks to these porous materials. First of all, a stock solution of MB (10 mg/L) was prepared. To obtain a calibration curve, other 4 MB solutions at different concentrations (8 mg/L, 5 mg/L, 3 mg/L and 1 mg/L) were prepared and 1 mL of each solution was analyzed at the

spectrophotometer UV-Vis (QE65000, Ocean Optics). To evaluate the reproducibility of data, 3 measurements were performed for each concentration. The maximum absorption wavelength was identified at 663.12 nm. Data were elaborated and reported in Figure 25, obtaining the Equation 1, with R^2 value of 0.9969. The calibration curve obtained allows to calculate the MB concentration x (mg/L), of an unknown solution, once the absorbance value y (-), obtained by analyzing the solution at the spectrophotometer UV-Vis, is known:

$$y = 0.1574x + 0.0538 \qquad \textit{Equation 1}$$

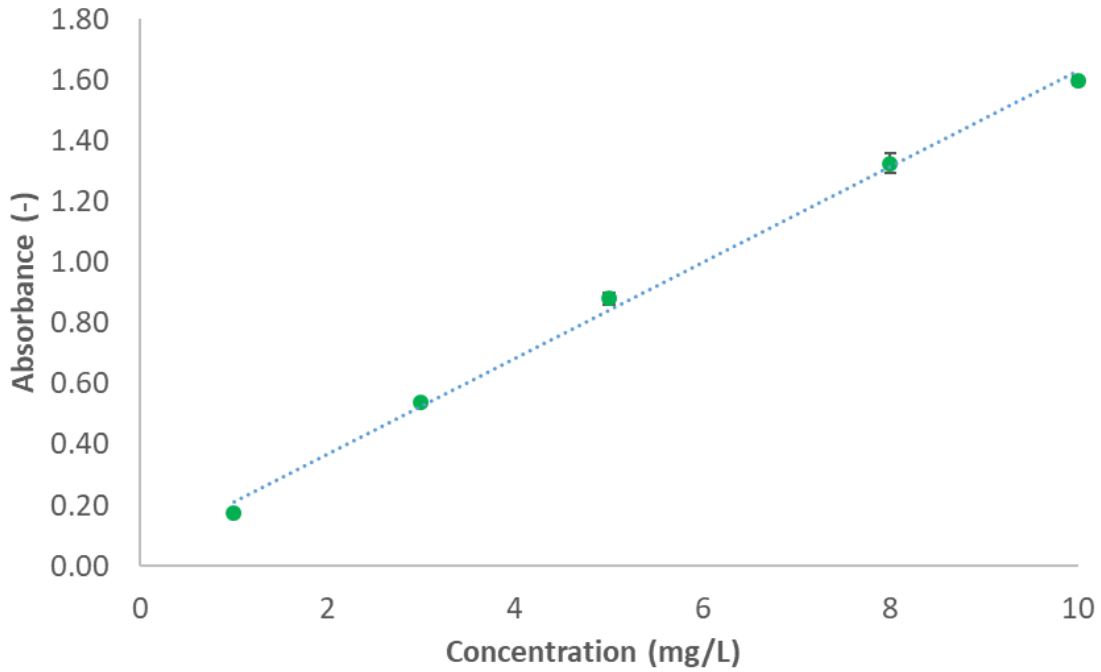

Figure 25. Methylene Blue calibration. Error bars are included within the experimental point size.

According to information obtained from the adsorption test using an aerosol nanoparticles generator (Paragraph 4.4), samples 1, 2, 4 and 5, that showed the best adsorption performance, were chosen for the photo adsorption tests together with samples synthetized in Paragraph 5.1.

For the test, 10 g/L of sample in MB solution was used. 3 specimens for each material were prepared. The experimental setup is reported in Figure 26. In a transparent plastic glass, filled with MilliQ water and a magnetic anchor, was put another smaller plastic glass with the sample, in known concentration, in MB solution (10 mg/ L). This device

was used to avoid direct contact of the sample with the magnetic anchor. The plastic glasses were placed on 3 different magnetic stirrers under the UV lamp.

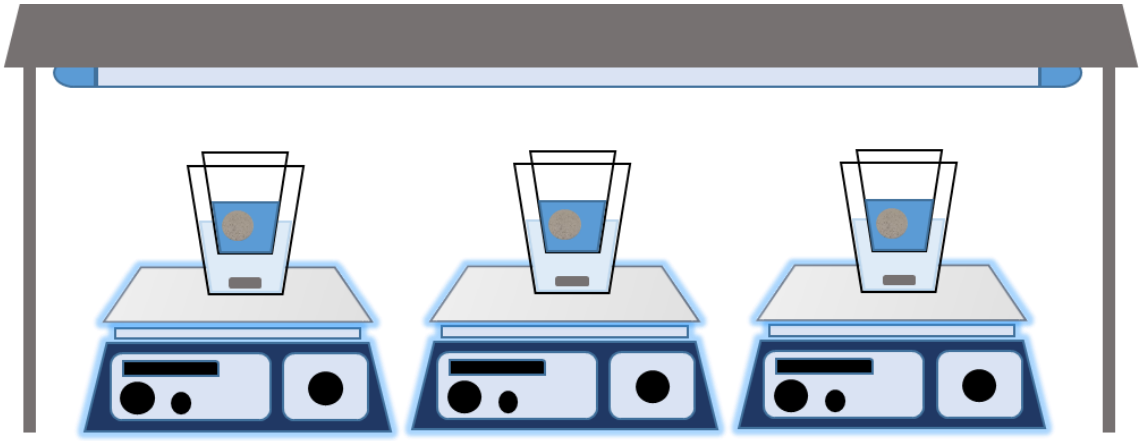

Figure 26. Experimental setup of photo degradation tests. 3 specimens for each material were evaluated.

In the first part of the test, magnetic stirrers were actioned and samples adsorbed MB for 3 hours, in a dark room, assessing MB concentration hourly. This value was chosen because, according to preliminary tests, it was evaluated that after 3 hours there was no more adsorption. In the second part of the test, the UV lamp was switched on and the experiment continued for another 5 hours, continuing to assess the MB concentration every hour. Thanks to Equation 1 it was possible to calculate the MB concentration (x) according to the absorbance value (y) defined hourly through the UV-Vis analysis. Equation 2 allowed to calculate the removal efficiency of adsorption and photo degradation:

$$R\% = \frac{C_0 - C_t}{C_0} * 100 \qquad \textit{Equation 2}$$

Where R is the removal efficiency (%), C_0 is the initial concentration of MB (mg/L) and C_t is the concentration of MB at t time (mg/L).

Figure 27 shows the concentration of MB every hour, starting from the initial concentration of MB (C_0 = 10 mg/L) in green bar chart. In the first 3 hours the UV lamp light is turned off and there is only adsorption, then the lamp is turned on and the test continues for another 5 hours (photodegradation). Samples 1, 2, 4 and 5 are identified by blue bars charts, while samples 7, 8, 9 and 10 are the equivalent of the previous samples but synthetized with the addition of titanium dioxide (pink bars charts).

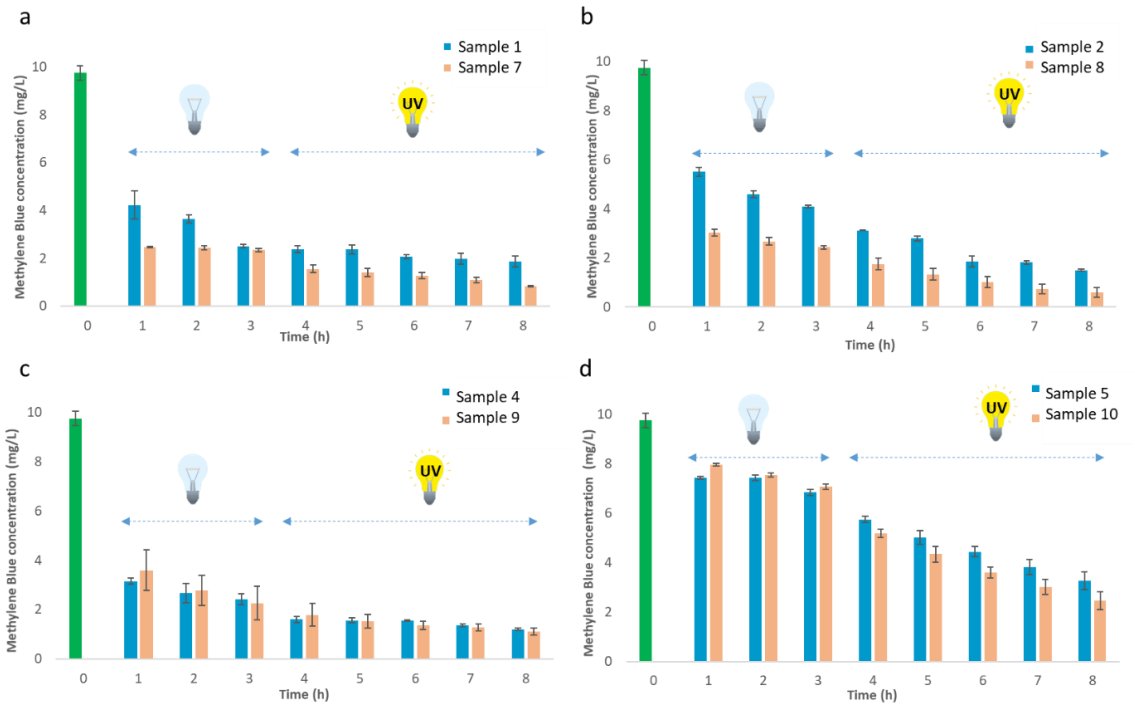

Figure 27. Concentration of methylene blue (C_0=10 mg/L, green bar chart) at different intervals time after adsorption and photodegradation by different porous samples: samples 1 and 7 (a), samples 2 and 8 (b), samples 4 and 9 (c) and samples 5 and 10 (d), identified by blue bars charts, and the respective materials synthetized with the addition of titanium dioxide (pink bars charts).

Figure 28 summarizes the results of MB removal rates after 3 h of adsorption and 5 h of photodegradation by samples synthetized with SF (samples 1, 2, 7 and 8) and BA (4, 5, 9 and 10). All samples with SF show a good adsorption performance of MB (variable from 74% to 76%). Indeed, many papers reported the use of SF as an adsorbent for dye [102][103]. Recently studies demonstrated that mixing SF with other ashes (for example flue gas desulphurization, coal fly ash, and fly ash from MSWI) allows reducing the concentration of heavy metals [80].

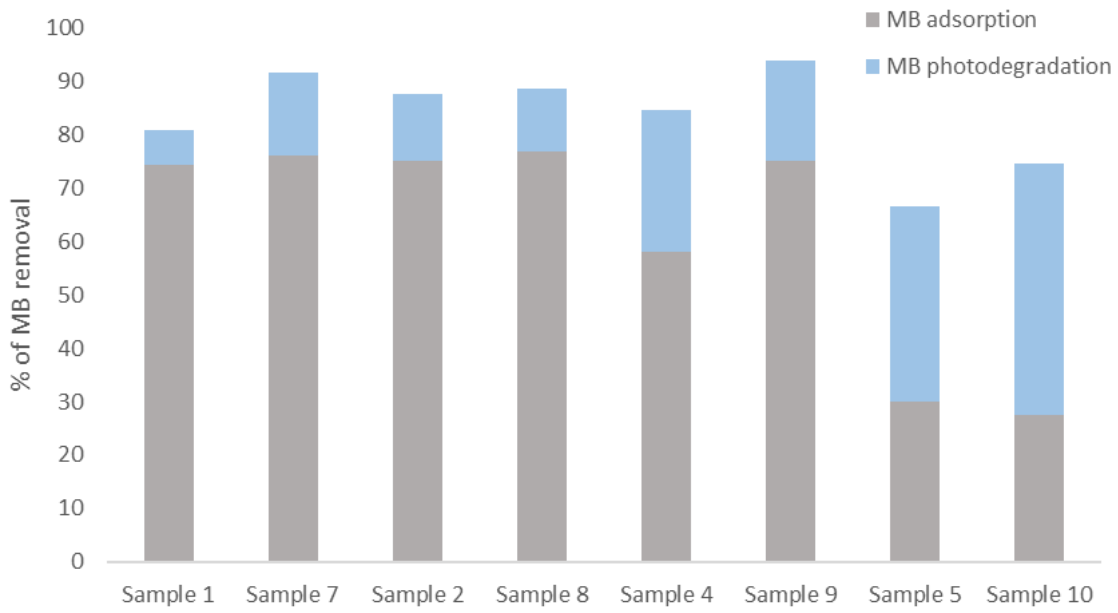

Figure 28. Results of the removal of methylene blue (MB) by adsorption and photodegradation process.

Samples 1 and 7 show a similar adsorption capacity. Sample 7 reaches 15% of photodegradation after 5 h, slightly higher than sample 1. This is due to the presence of TiO_2 powder that increases the photo catalyst reactions. Samples 2 and 8, samples realized with SF without thermal treatment, have the same trends. Sample 9 shows a higher adsorption capacity compared to sample 4, but with lower photodegradation ability (18% compared to 26%). This is probably related to the sample 9 rupture at the beginning of the test. Samples 5 and 10 reveal the lowest percentage of adsorption (30% and 27%, respectively) compared with other samples. Samples realized with BA seem to have water repellent behavior that will be investigated in Chapter 6. However, sample 10 reaches almost 50% of MB photodegradation.

The literature informs of some applications of BA such as pollutant adsorbent, for example for lead [104] dye [105] or phosphate removal from water [106]. Materials realized with BA have a higher percentage of photodegradation compared to samples realized with SF. Literature reveals that BA is characterized by a certain percentage of titanium dioxide [82][107], as also seen from the results of the adsorption tests in Paragraph 4.4. Therefore, to test BA properties, a photodegradation test was conducted only with BA powder. 3 g/L of BA were mixed with MB (10 mg/L) for 3 h in dark condition

and 2 h under UV lamp, reveling a photodegradation capacity of about 10%. This means that, is the material made with BA that has photodegradative abilities and not only the BA itself.

Except samples 10, it seems that the porous materials investigated do not have high photodegradation capacity. This is probably related to the fact that titanium dioxide is inserted in the compound during the material synthesis.

5.4 Conclusions

Nowadays, organic pollutants are more and more widespread in groundwater and watercourses. At this purpose, the porous materials described in Chapter 4 were tested to remove organic pollutants. Samples which shown the best adsorption capacity were chosen and other samples were realized adding a certain percentage of TiO_2, well known for its photocatalytic activity. All samples were fully characterized and tested using a MB solution, in known concentration, to simulate an organic pollutant. Samples, immersed in the MB solution, were put on a magnetic stirrer for 3 h in a dark room and then the experiment continued for other 5 h by turning on the UV lamp. The MB concentration was measured every hour. Results show that sample 10 is the one with the best photodegradation activity probably due to the addition of TiO_2 in the synthesis sample and to the presence of a small percentage of TiO_2 in BA. In fact, compared to samples realized with SF, the ones realized with BA have a higher photodegradation activity. These are preliminary results, an idea to improve their photo degradation ability could be to apply a layer of titanium dioxide on the surface of the samples.

This work is reported as a book chapter in [93].

6. Wettability

Wettability is the preference of a liquid to be in contact with a solid surrounded by another fluid (liquid or gas). Wettability of a solid surface is measured with an optical tensiometer by utilizing the sessile drop method. A water droplet is placed on the surface and the formed contact angle is measured from the three-phase boundary where liquid, gas and solid intersect. Wettability characteristics are fully describable by measuring the contact angle (θ), that is defined as the angle formed by the tangent to the liquid-aeriform interface, and by the tangent to the solid surface, at the contact line between the three phases [108]. In case the liquid perfectly wets the surface the determined angle is zero; while when the drop is perfectly spherical, and therefore θ = 180°, it has a situation of perfect not wettability. In the middle of the two ideal conditions there are intermediate situations for which the angle of contact is 0° < θ < 180°. In such situations a further classification can be made by distinguishing:

- 0° < θ < 90°: hydrophilic surface;
- 90° < θ < 150°: hydrophobic surface;
- 150° < θ < 180°: super hydrophobic surface.

6.1 Synthesis of samples

In Paragraphs 4.4 and 5.3 were presented the results of adsorption and photodegradation tests. Both for nanoparticles capture and photodegradation, samples with BA and hydrogen peroxide were not very performing, showing a water repellent behavior. At this purpose, wettability test was performed on samples 5 and 6, that for convenience from now on will be called samples F and H respectively, and other samples realized varying the volume of hydrogen peroxide added. The synthesis process for all samples is similar to the one described in Paragraph 4.1, excepted for sample A that is synthetized without the addition of hydrogen peroxide. Table 6 reports porous materials composition, while Figure 29 reports the images of all 8 samples.

Table 6. Porous materials composition synthetized with different volume of hydrogen peroxide.

	Bottom ash (g)	Calcium hydroxide (g)	MilliQ water (mL)	Hydrogen peroxide (mL)
Sample A	9	9	18	-
Sample B	9	9	11.3	0.9
Sample C	9	9	9	2.7
Sample D	9	9	9	3.6
Sample E	9	9	9	4.5
Sample F	9	9	9	5.4
Sample G	9	9	9	6.3
Sample H	9	9	9	7.2

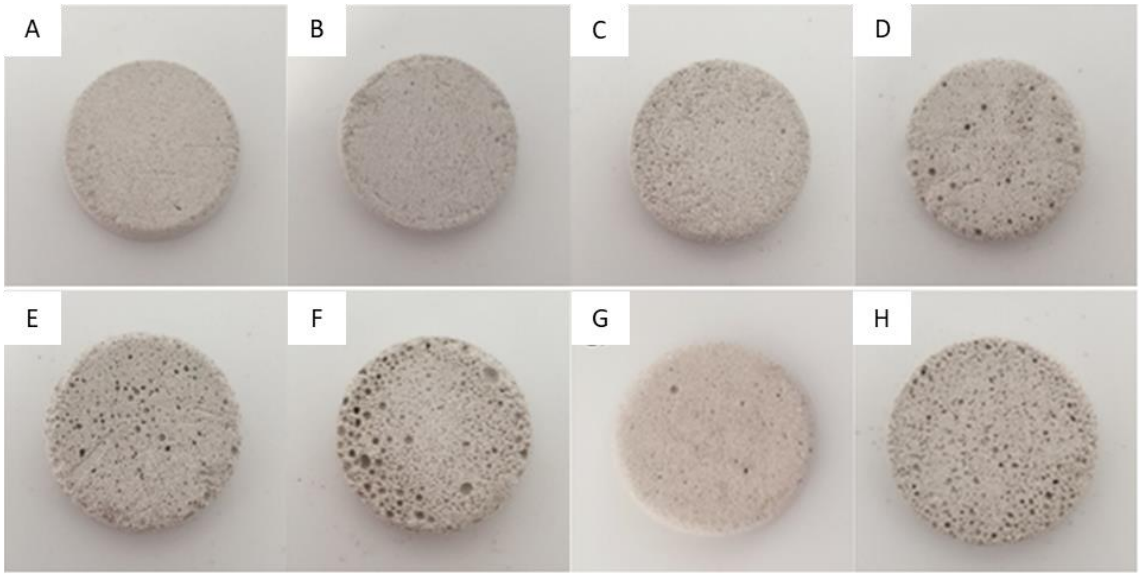

Figure 29. Porous materials synthetized with bottom ash and different volume of hydrogen peroxide.

6.2 Samples characterization

Samples characterization was performed through structural and morphological analysis. XRD patterns of samples are reported in Figure 30. The crystalline phases identified are aluminum silicate ($Al_{13}(SiO_4)_5$), calcium hydroxide ($Ca(OH)_2$) that is used in the samples synthesis, quartz (SiO_2) and calcium carbonate ($CaCO_3$) as vaterite and calcite. $CaCO_3$ was probably generated during the carbonation process between calcium hydroxide and

carbon dioxide. In all samples were identified the same crystalline phases, despite the different volume of hydrogen peroxide used, showing that the amount of hydrogen peroxide does not affect the crystalline structure of the sample.

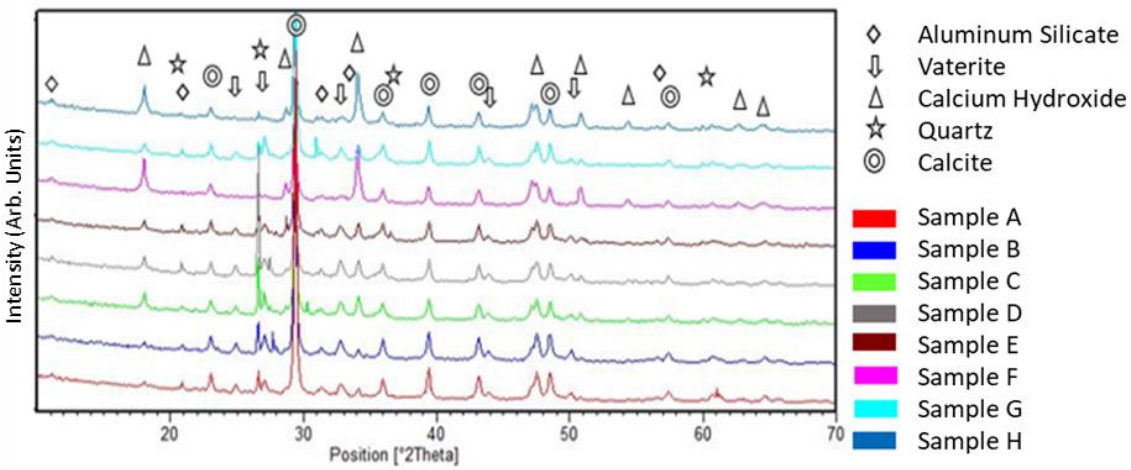

Figure 30. XRD patterns of samples realized with bottom ash and different volume of hydrogen peroxide.

The superficial porosity of samples was investigated using the Leica MZ16 A microscope. Different images were acquired for each sample and then analyzed by the software ImageJ [109]. ImageJ is an open source software, programmed in JAVA, that allows to edit, analyze, process, save and print images; it also offers the possibility to calculate the area and statistics on pixel values relative to regions, called ROI (Region Of Interest), selected by the user. Table 7 shows the surface porosity of the samples calculated from the pore area and sample area.

Table 7. Average surface porosity calculated as average pore area to average sample area ratio.

	Average pore area (μm^2)	**Average sample area (μm^2)**	**Average surface porosity (%)**
Sample A	654,782	9,899,248	6.6
Sample B	908,569	9,857,031	9.2
Sample C	1,327,333	9,850,612	13.5
Sample D	1,166,121	9,812,416	11.9
Sample E	1,616,095	9,787,099	16.5
Sample F	1,015,321	6,875,714	14.8
Sample G	1,150,818	9,856,836	11.7
Sample H	1,529,420	10,065,366	15.3

Although there is a progressive addition of hydrogen peroxide, there is no linear increase in porosity; in particular sample G has a lower surface porosity than sample F, as shown also in Figure 29.

ImageJ allowed to evaluate the diameter of the pores through the analysis of Feret diameter[2]. Results are reported in Figure 31.

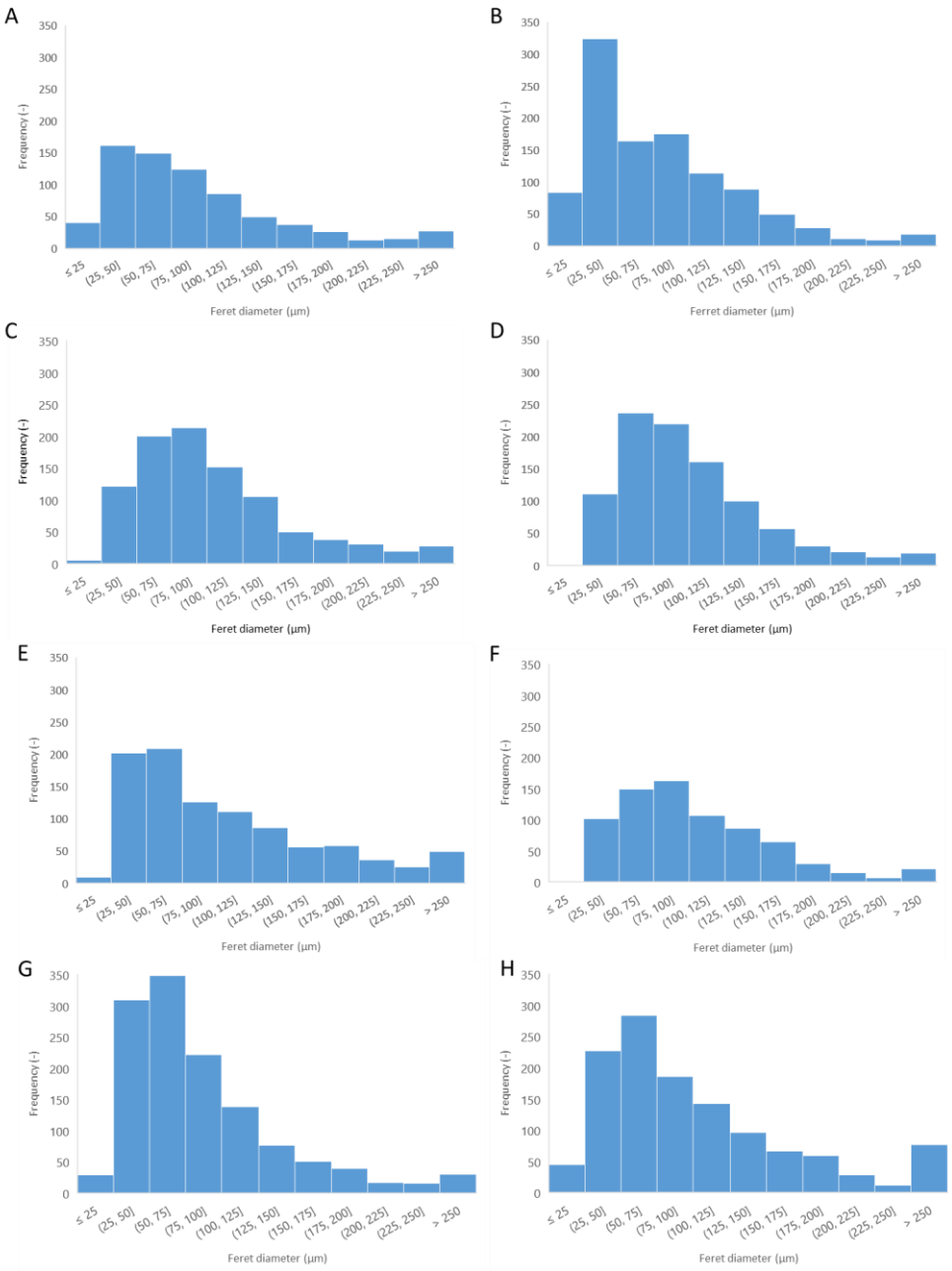

Figure 31. Pore frequency as a function of Feret diameter for each sample.

[2] Feret diameter is the diameter of a hypothetical circle that best approximates the pore considered.

It is observed that all samples are characterized by small pores with a trend of decreasing frequency as the pore size increases. Analyzing sample A, a larger amount of pores can be observed in the range of 25 - 50 µm with a percentage of about 22%, only 3% of the total exceeds the size of 250 µm. Sample B has a high pore value in the range of 25 - 50 µm of 31%; from the next interval there is a sudden decrease in the amount of pores, only 2% exceeds the size of 250 µm. In sample C the largest amount of pores, equal to 22%, develops in the range of 75 - 100 µm, about 3% of the total exceeds the size of 250 µm. In sample D the largest amount of pores, about 24%, is distributed in the range between 50 - 75 µm; while 11% occurs in the initial values between 25 - 50 µm. Pores larger than 250 µm account for 2%. In sample E, 22% of the total pores occur in the range of 50 - 75 µm, an equally significant amount (21%) is that within the range of 25 - 50 µm. There is a greater amount of pores, compared to previous samples, about 5%, for Feret diameter values above 250 µm. In sample F, the greatest pore distribution (22%) is in the range 75 - 100 µm; for values above 250 µm, 3% of the total is obtained. In sample G the largest amount of pores (27%) is between 50 - 75 µm. Only 2% of the total exceeds the size of 250 µm. In sample H, the greatest amount of pores (23%) develops in the range of 50 - 75 µm. Compared to other samples, the frequency of pores with a diameter greater than 250 µm increases to 6%, of the total. In all samples the greatest amount of pores occurs in the range between 25 - 100 µm. For values below 25 µm, the amount of pores is almost restricted and independent of the amount of hydrogen peroxide concentration. By comparing the percentages obtained for values greater than 250 µm, it is possible to see that sample H is the sample with the highest pore rate. This shows that the increase in surface porosity is not strictly related to the increase in pore size: a large amount of small pores prevails over large ones.

6.3 Wettability test

The wettability test was performed using the CAM 200 tensiometer (KSV Instruments, Finland). The instrument is equipped with a calibrated needle to choose the volume to be deposited on the surface of the samples, in this case 3 µL. The drop profile is detected

by a camera and processed by the software to obtain the surface tension and the contact angle. To evaluate the wettability of the samples, the value of the contact angle at t 3 s was considered, a time elapsed from the moment the drop of liquid is deposited on the surface. In this way any interference due to contact between drop and sample is disregarded. To evaluate the behavior of the samples, an observation time of 30 s was set. 5 tests for each sample were performed. The data collected by the instrument were reworked by the software and represented in diagrams with in abscissa time and in ordered angle of contact. Results are reported in Figures 32 for all samples analyzed.

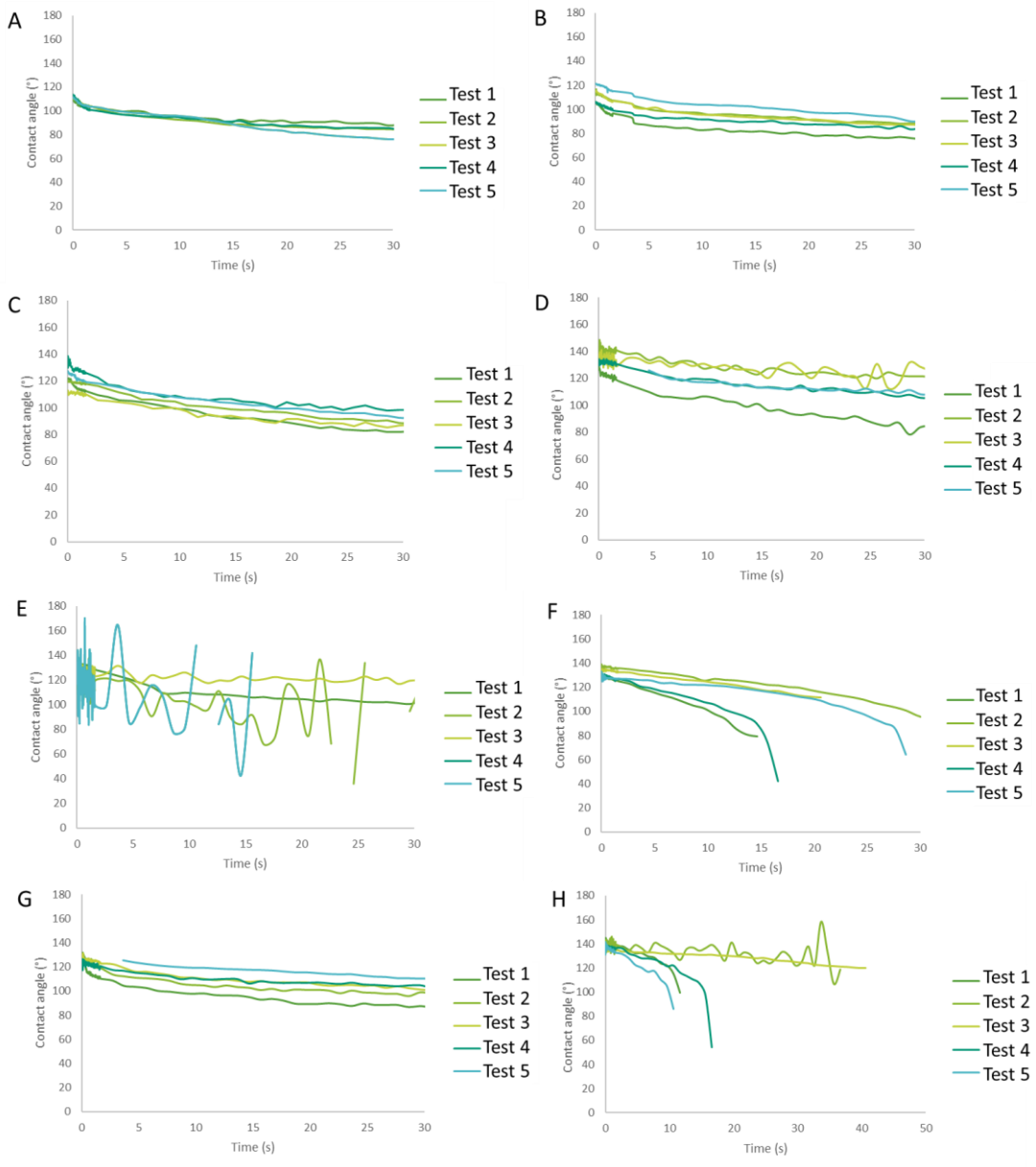

Figure 32. Contact angle versus time for each sample.

Sample A is realized without hydrogen peroxide. Data processing has shown that the average value of contact angle is 100°. In particular, this sample exhibits borderline behavior between the two conditions. The observation time established by the test, 30 s, was not sufficient to evaluate the entire uptake phase. The average contact angle for sample B is 103°. Even in this case, since an observation time of 30 s was imposed, the qualitative trend of the uptake phase could not be detected. For sample C the average value of contact angle is 113°. As can be seen from the graph, the material is characterized by a fairly homogeneous surface with similar trends between the various tests. Average contact angle values for samples D, E and F is about 128°, in particular sample E was interfered with during the measurement while in some sample F tests, drop absorption occurred before 30 s probably due to the presence of pores on the sample surface. The average contact angle for sample G, as can be seen from the graph, is about 117°; the material is characterized by a homogeneous surface with similar trends between the various tests. An ambiguity was found in Test 5 as the instrument did not detect contact angles until time t = 3,64 s. Sample H is characterized by the highest value of contact angle, about 134°, however in some tests, the drop was adsorbed before the end of the test, this is probably due to the presence of pores on sample's surface.

The wettability test was also carried out on a cement sample (Figure 33), described in Paragraph 4.1, to compare it with the samples made with the BA.

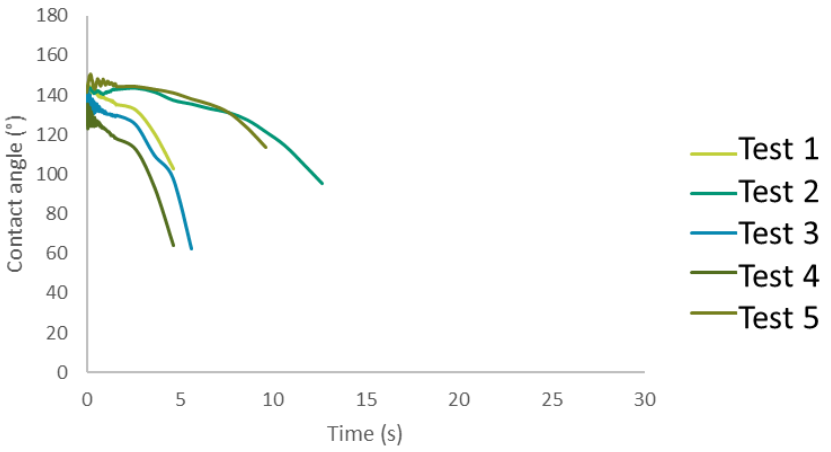

Figure 33. Contact angle versus time for cement sample.

The mean contact angle is about 125°. Although the value is within the range of hydrophobicity, in all the tests it is noted that the drop was completely absorbed before the end of the 30 s with a sudden phase of adsorption due to the physical properties of the cement. These rapid times indicate that cement, as a binder conglomerate to form concrete, is easily subject to phenomena related to the chemical and physical attack of water infiltrations. If uncontrolled, they can lead to corrosion of the elements of the concrete armature, and cycles of frost and thaw. Cement in fact, despite the high contact angle value, does not have waterproof properties and therefore it is necessary to add hydrophobic agents such as fatty acids or crystalline admixtures [110][111].

The mean values of the contact angle for all samples together with cement sample are given in Table 8 and in Figure 34 the comparison of the mean values of contact angle.

Table 8. Average values of contact angle for all samples analyzed.

	Average contact angle (°)
Sample A	100
Sample B	103
Sample C	113
Sample D	128
Sample E	128
Sample F	127
Sample G	117
Sample H	134
Cement	125

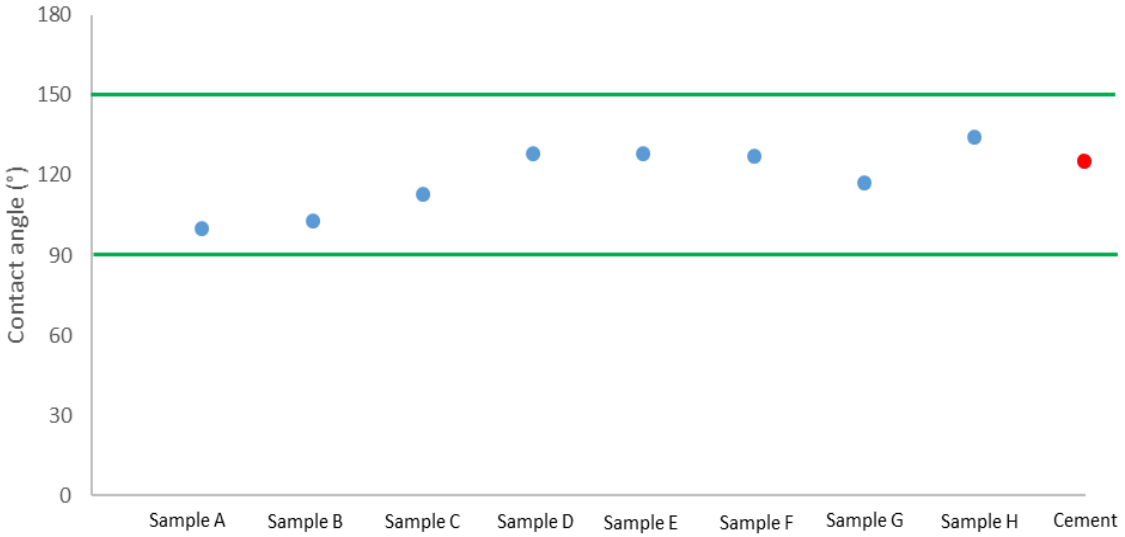

Figure 34. Comparison of the mean values of the contact angle for all samples realized with bottom ash and cement sample.

Results showed that for all samples the mean value of the contact angle is above the hydrophobicity limit, whit increasing values with the added hydrogen peroxide volume except for sample G which showed an anomalous behavior. However, in almost all tests, the set observation time of 30 s was not sufficient to see the adsorption of the drop, which is taken place after about 30 min. The contact angle value for cement is comparable to the values of the other samples, but, as seen from the tests, the drop is immediately adsorbed.

6.4 Conclusions

As discussed in Chapters 4 and 5, samples realized with BA and hydrogen peroxide showed a low adsorption capacity which deserved to be investigated through wettability tests. At this purpose, besides samples already realized for previous tests, other samples were prepared changing the volume of hydrogen peroxide. Samples were characterized by an XRD analysis showing that the change in the volume of hydrogen peroxide does not involve significant changes in the crystalline phases. Moreover, the superficial porosity of samples was investigated thanks to microscopy images reworked with the software ImageJ revealing that the increase in surface porosity is not strictly related to

the increase in pore size: a large amount of small pores prevails over large ones. The wettability test was performed depositing on samples' surface a water drop (volume 3 μL) and evaluating value of the contact angle at 3 s. Also a cement sample was studied as comparison. Results showed that the mean values of the contact angle for all samples is above the hydrophobicity limit. Moreover, the required observation time (30 s) was not sufficient to observe the absorption of the drop that occurred after about 30 min in almost all tests. Based on the results, a possible application of these materials could be as a water-repellent plaster because, as well known, moisture can have devastating effects on walls [38]. A good water-repellent plaster should ensure a good degree of breathability, but also a low level of capillary absorption [112]; consequently, it should be used on walls exposed to meteoric humidity. Some of samples discussed in this Chapter, based on the wettability test performed, seem to reflect some of the characteristics necessary to be defined as such. Many could be the applications of a plaster of this type. For example, in the Italian context, Venice, due to the particular layout of the city and the specific environmental conditions, could be suitable for the use of water-repellent plaster made with the use of BA, which would contrast in part, the historical problem of degradation of the masonry structures.

The wettability measurements were performed at the Biochemistry and Clinical Biology Laboratory, Department of Molecular and Translational Medicine, of the University of Brescia (Head of the Laboratory: prof. Paolo Bergese).

7. Future perspective

In parallel with the wetting tests, another work on SUNSPACE has been carried out to improve the material sustainability. With this purpose and with the idea of making furniture, the thermal treatment on heating plate was substituted with microwave oven treatment because it allows to speed up the thermal process. Moreover, a sustainability analysis comparing the 2 processes was carried out to compare emissions.

7.1 Samples synthesis

The synthesis process is quite similar to SUNSPACE synthesis process described in Paragraph 2.2 but, as it is not possible to insert aluminum molds in microwave oven, graphite and silicone crucibles were used. To define the correct relationship between time and power, several tests were conducted.

7.1.1 Cumulative and not cumulative tests in graphite crucibles

At first cumulative tests in graphite crucibles were carried out at different power of treatment choosing a total duration of treatment of 15 minutes. In all tests, once the slurry is inside the crucible, it is closed with a graphite cap. In Figure 35 about 3 mL of SUNSPACE treated at 300 W with cumulative time intervals of up to 15 min.

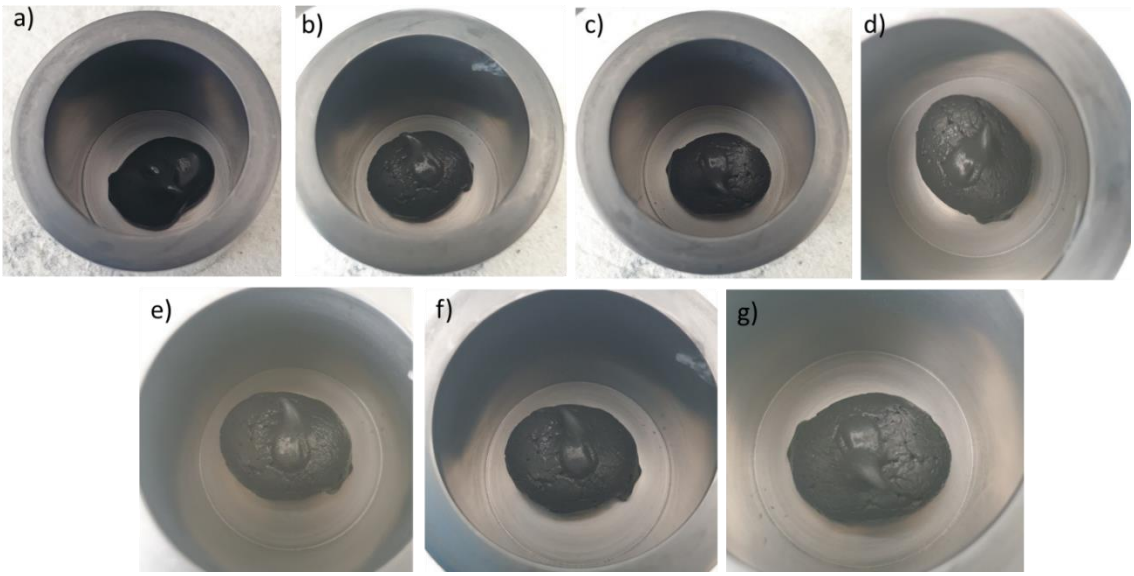

Figure 35. SUNSPACE slurry in microwave at 300 W power: a) sample after 1 min, b) sample after 3 min, c) sample after 5 min, d) sample after 7 min, e) sample after 10 min, f) sample after 12 min, g) sample after 15 min.

In Figure 36 about 3 mL of SUNSPACE treated at 600 W with cumulative time intervals of up to 15 min.

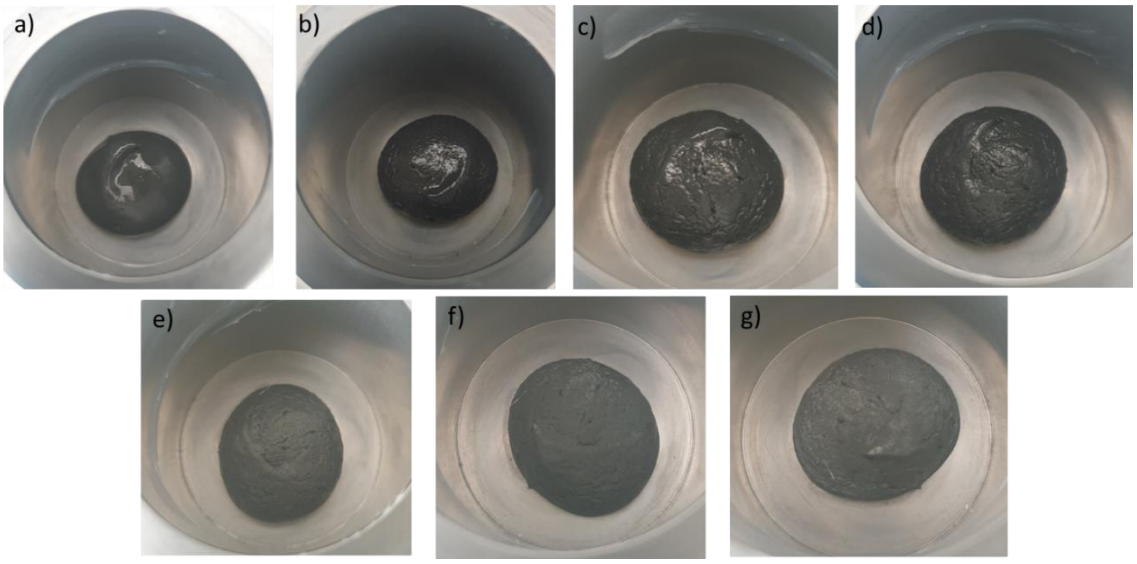

Figure 36. SUNSPACE slurry in microwave at 600 W power: a) sample after 1 min, b) sample after 3 min, c) sample after 5 min, d) sample after 7 min, e) sample after 10 min, f) sample after 12 min, g) sample after 15 min.

In Figure 37 about 3 mL of SUNSPACE treated at 1000 W with cumulative time intervals of up to 15 min.

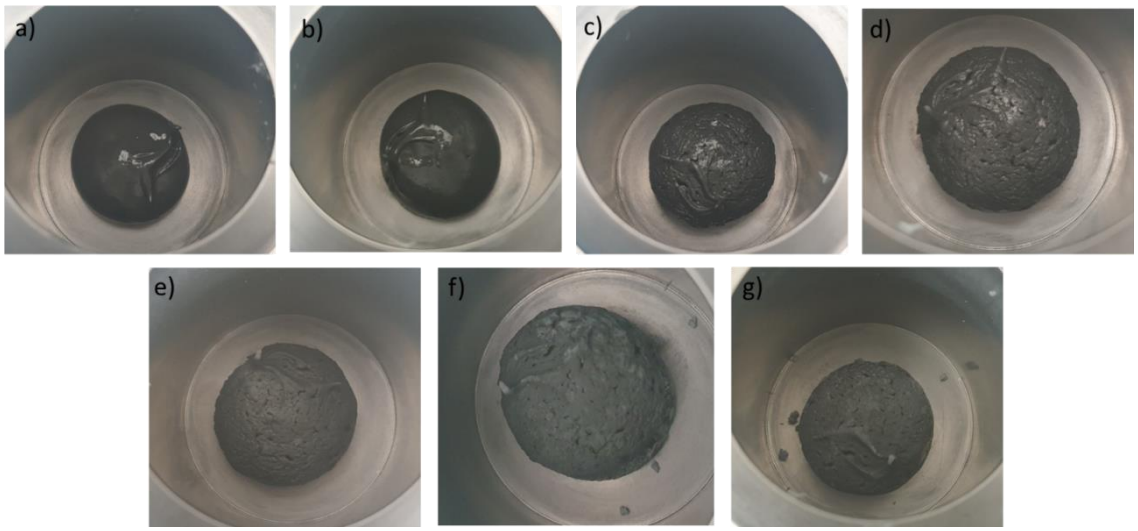

Figure 37. SUNSPACE slurry in microwave at 1000 W power: a) sample after 1 min, b) sample after 3 min, c) sample after 5 min, d) sample after 7 min, e) sample after 10 min, f) sample after 12 min, g) sample after 15 min.

In all tests it is possible to see that the first minutes are not enough to obtain a dry sample, in particular at the end of the test at 300 W the sample is still not dry. Since the cumulative tests took a long time to dry the sample, it was decided to make a single test increasing the treatment time. Tests performed allowed to establish that a single 5 min test is required to obtain a dry sample at 600 W and 1000 W, as shown in Figure 38, while for the sample at 300 W the required time is still insufficient to obtain a dry sample.

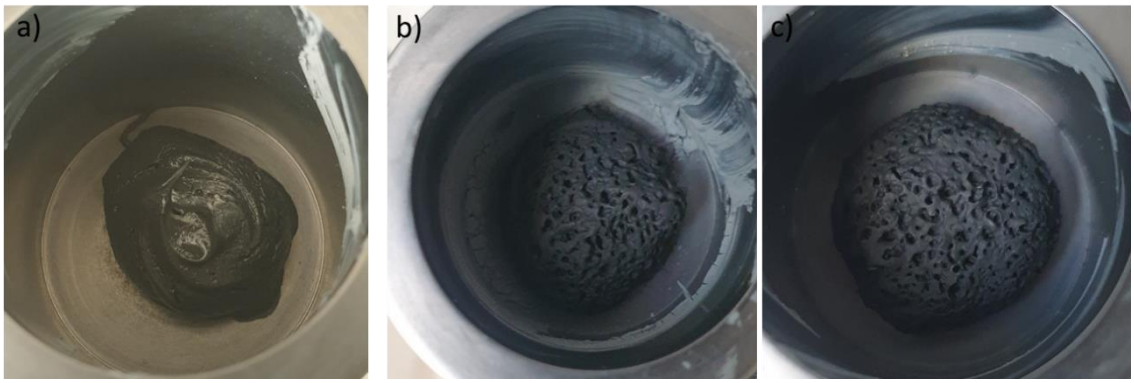

Figure 38. Samples slurry in microwave for 5 min total: a) sample at 300 W, b) sample at 600 W, c) sample at 1000 W.

In carrying out these tests it was found that the graphite crucible caused the test times to be longer and there were also problems with sample extraction. For these reasons, a silicone crucible was used in next tests.

7.1.2 Tests in silicone crucibles

Silicone crucibles allowed to reduce the time treatment. Several tests were performed changing time and power of treatment. Thanks to this type of crucible, it is possible to obtain a dry sample also at 100 W and 1 min and 30 s time of treatment. Figure 39 shows the several samples realized changing time and power. Since test at 600 W and 30 s gives a dry sample, no tests at 1000 W have been carried out.

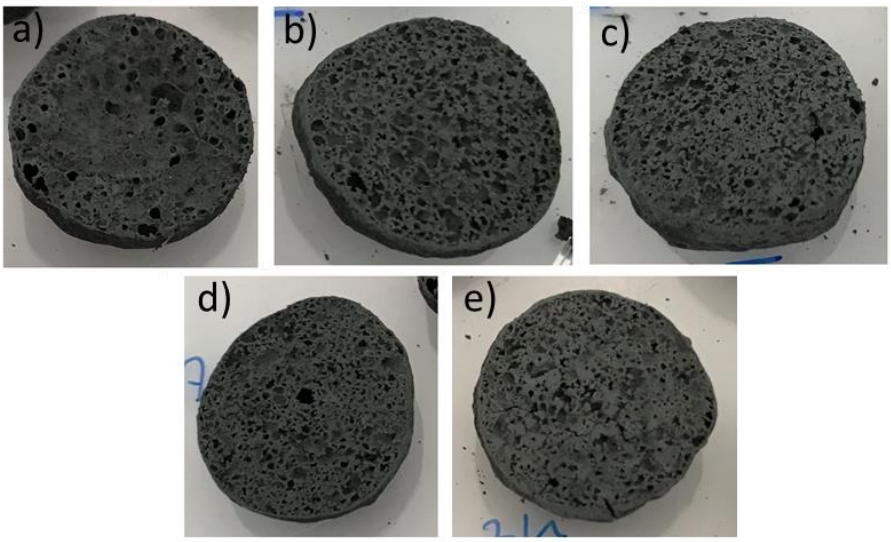

Figure 39. SUNSPACE slurry in microwave: a) 100 W for 1 min and 30 s, b) 100 W for 2 min, c) 300 W for 1 min, sample d) 300 W for 1 min and 30 s, e) 600 W for 30 s.

Of all the samples made, those that seemed to have the best characteristics were those at 100 W for 2 min and 600 W for 30 s, for this reason they were chosen for the characterizations and the adsorption test that will be presented in the Paragraphs 7.2, 7.3 and 7.4.

7.2 Samples characterization

Samples were characterized through structural and morphological analysis. XRD patterns for both samples show a large halo due to the amorphous phase and peaks related to sodium iodate hydrate ($Na(IO_3)!H_2O$), cristobalite (SiO_2) and lautarite

($Ca(IO_3)_2$), as shown in Figure 40. It seems that there are no differences between the 2 samples, also the patterns are the same as the SUNSPACE shown in Figure 3.

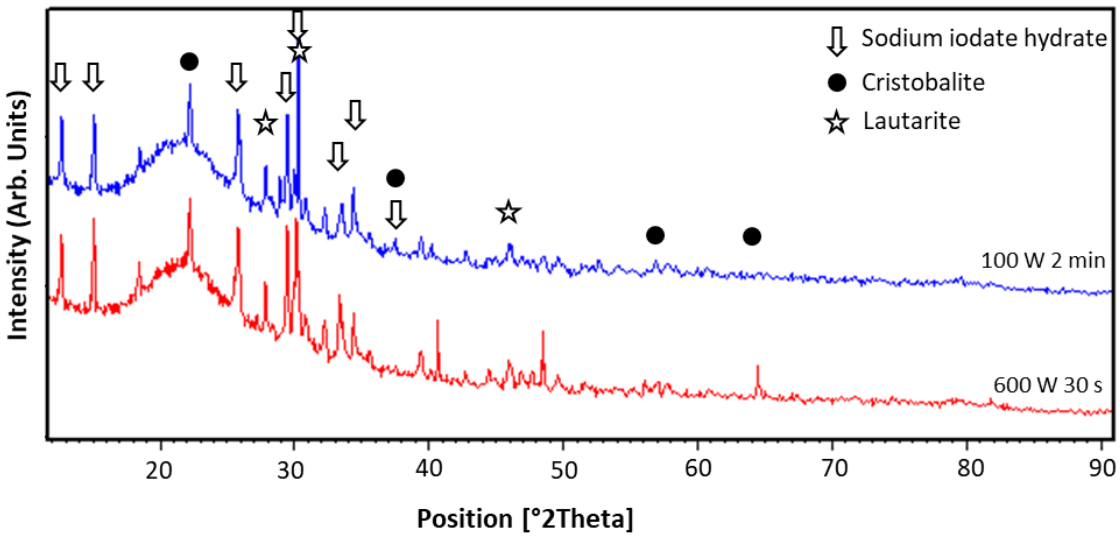

Figure 40. XRD patterns for SUNSPACE samples with microwave thermal treatment: red line) 100 W 2 min, blue line) 600 W 30 s.

SEM analysis (Figure 41) shows that samples are characterized by spherical particles of silica (ranging in size from 20 to 500 nm, as also reported in [16]) agglomerated together. It is also clearly identified the presence of micro and macro pores on the surface of the SUNSPACE mainly due to the action of sodium bicarbonate in the phase of synthesis of the material itself. The characteristic pore size is between 200 nm and 400 nm. No substantial differences were found between the 2 samples.

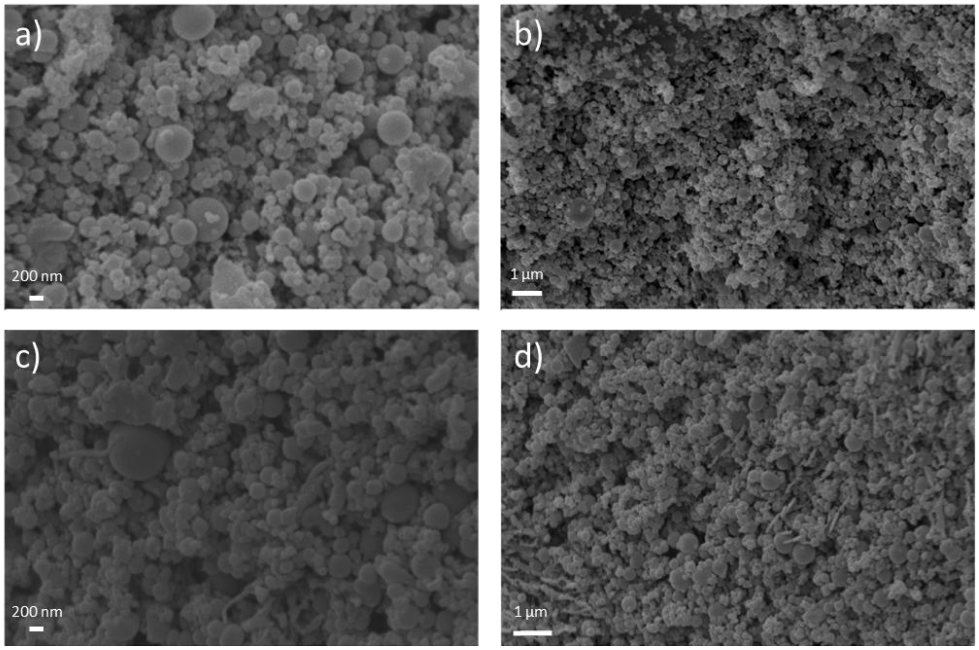

Figure 41. SEM images of SUNSPACE samples at different magnification: a) and b) 100 W 2 min; c) and d) 600 W 30 s.

7.3 Sustainability analysis

Microwave treatment, instead of heating plate, is intended to reduce the emissions associated with the process. In this regard, the values of EE and CF were calculated with Equations 3 and 4:

$$EE = I_{EE} * t * P \qquad \textit{Equation 3}$$

$$CF = I_{CF} * t * P \qquad \textit{Equation 4}$$

Where I_{EE} and I_{CF} are the energy indices reported in [113] expressed in MJ/kgmat and $kgCO_{2eq}$/kgmat respectively, *t* is the time associated with the duration of the process expressed in min and *P* the power associated to the process expressed in W. The power associated to the heating plate is 114 W. This value is obtained by making a simple proportion between the maximum power and the maximum temperature of the heating plate and the power at the temperature of 80 °C (temperature used for the heat treatment of SUNSPACE). Results of EE and CF, multiplied for the weight of each component, values are reported in Figure 42.

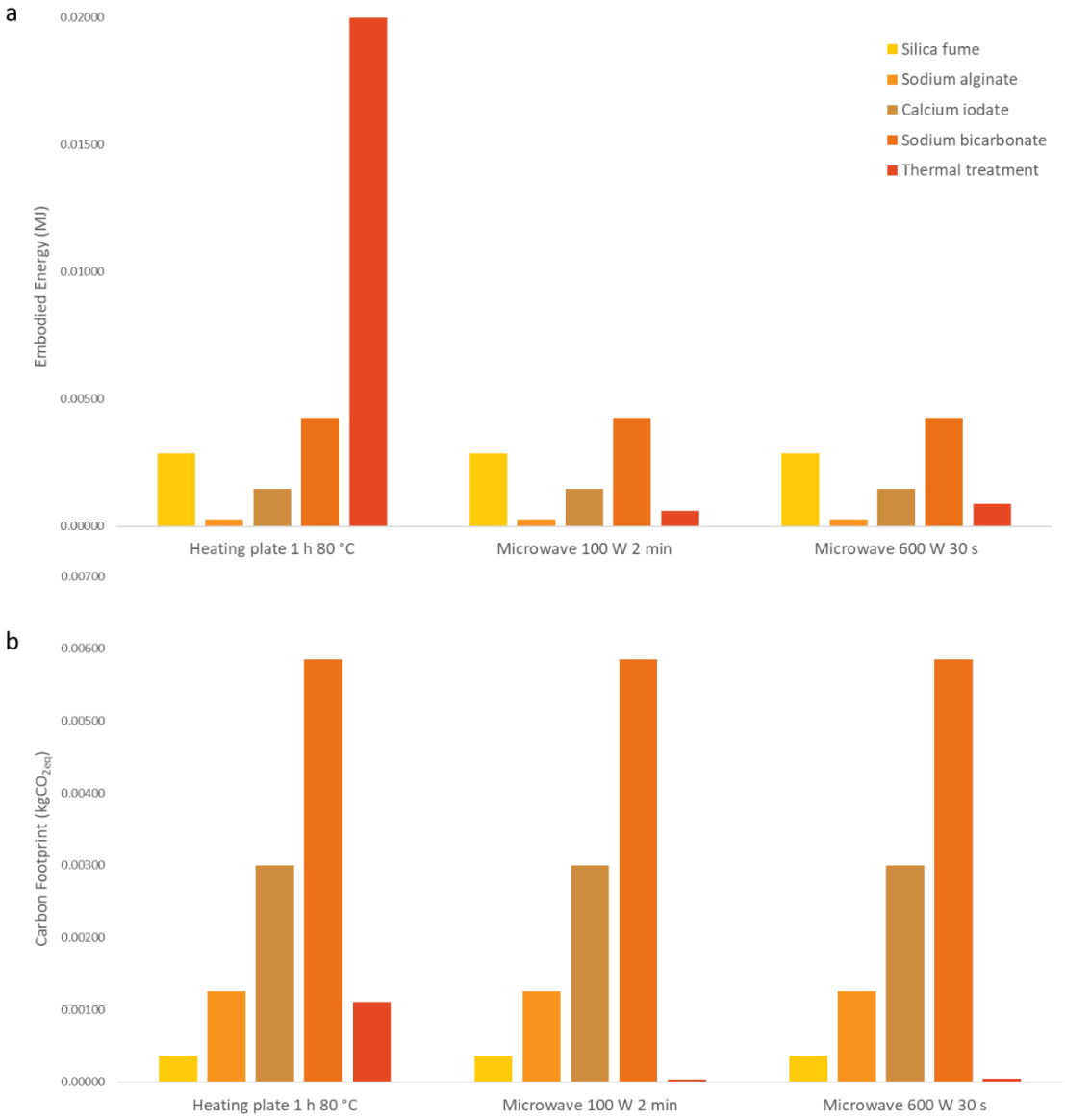

Figure 42. Embodied energy and Carbon Footprint values for SUNSPACE samples in microwave (100 W for 2 min and 600 W for 30 s) and on heating plate.

For microwave treated samples, the greater percentage of the impact is given by the chemical reagents used while the thermal treatment influences in very little way. As for the sample made on heating plate, the thermal treatment greatly affects the value of EE, while for CF, it is the sodium bicarbonate to affect more than thermal treatment

As it is possible to see, the EE and CF values associated to microwave samples are much lower than those associated with the sample on heating plate. Microwave treatment

could be a valid substitute of the one on heating plate drastically reducing the emissions related to the thermal process.

Moreover, a CES analysis was performed to compare samples realized with microwave treatment and heating plate, shown in Figure 43.

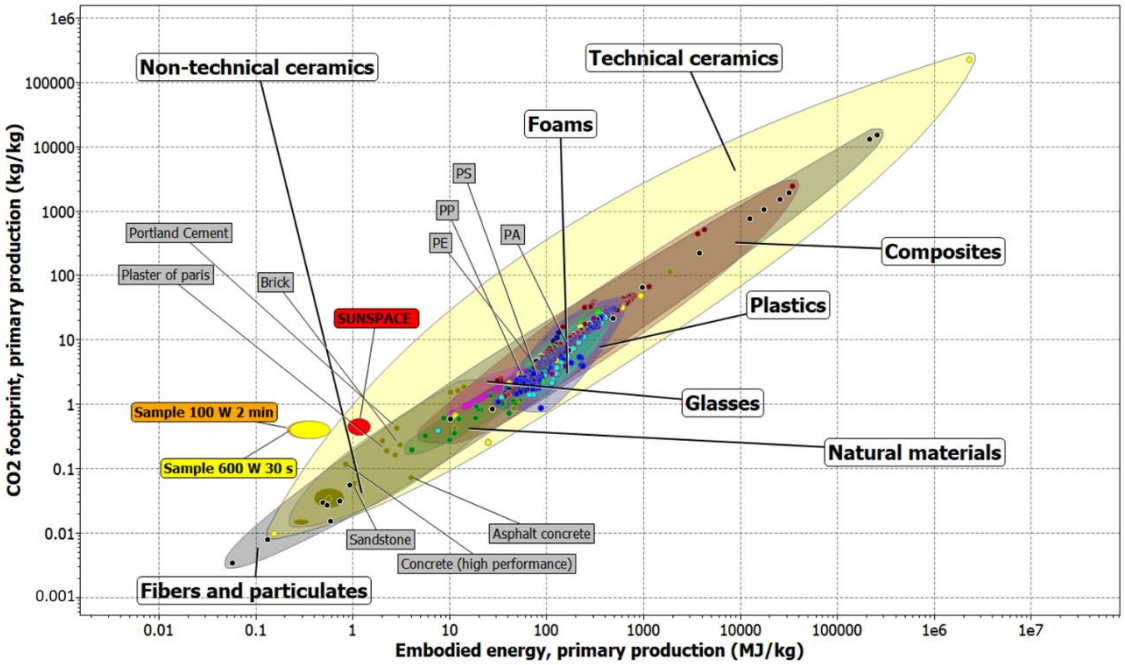

Figure 43. Embodied Energy (EE) versus Carbon Footprint (CF) of SUNSPACE and samples with microwave treatment (orange and yellow dots) and on heating plate (red dot). In comparison the environmental impact of plastic materials used in the production of air filters (polypropylene PP, polystyrene PS, polyamide PA, polyethylene PE) and building materials (Portland cement, plaster of Paris, brick or concrete) are reported.

The values of the microwave treated samples are very similar. Like SUNSPACE, these samples have much lower EE and CF values than the materials commonly used in the production of particulate filters. The idea of replacing the heating plate thermal treatment with the microwave treatment certainly decreases the emissions related to the synthesis of the sample as well as the time required for the process.

7.4 Adsorption test

According to the adsorption capability of SUNSPACE, adsorption test with the nanoparticles generator (Grimm Particle-generator MODEL 7.811) was performed. The experimental set-up is the same explained in Paragraph 4.4. A TiO_2 suspension was used

to simulate PM particles. After the exposition, samples were digested following the EPA procedure [90] and then analyzed by TXRF. Figure 44 shows the results.

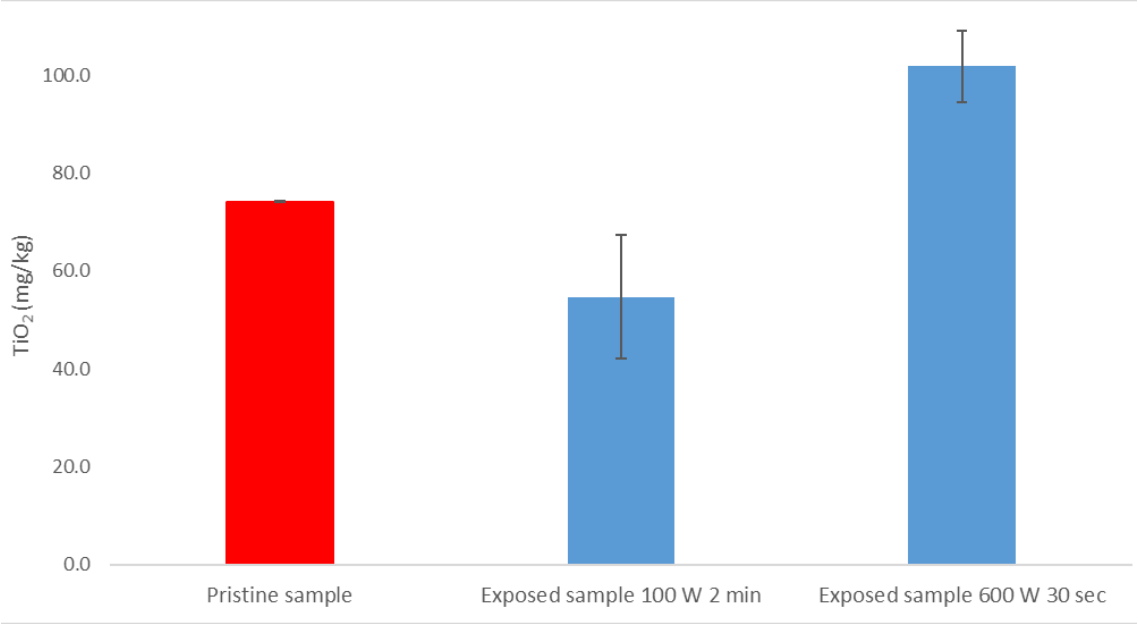

Figure 44. Results of TiO_2 entrapment by porous samples comparing pristine sample with samples microwave treated.

The sample at 100 W 2 min seems to have no absorption capacity while the sample at 600 W 30 s shows a minimum absorption capacity, slightly lower than that found in SUNSPACE, as seen in Paragraph 4.4. This is an interesting result that will be further investigated. The idea of making furniture with this method, such as outdoor vases, could help to reduce PM concentrations in cities and improve air quality. However, further studies and tests will be necessary to evaluate the different application modes, as well as other analyses to understand the different degree of adsorption of the various samples.

7.5 Conclusions

In this Chapter a new treatment for SUNSPACE was proposed in order to speed up the thermal treatment and to reduce the emissions related to the drying process. Several tests were carried out to define power and time of treatment. At first cumulative tests

were carried out putting the slurry in graphite crucible. However, using this procedure the drying times lengthened much so no cumulative tests were conducted using a crucible of silicone and changing the power and the time of treatment. After several tests, 2 typologies of samples were chosen, 100 W for 2 min and 600 W for 30 s. Samples were characterized. SEM images revealed that samples showed very similar morphological characteristics, comparable to original SUNSPACE sample. They are characterized by spherical particles of silica, with size dimensions from 20 to 700 nm, agglomerated together. Moreover, the XRD analysis reported, comparing these samples with the original SUNSPACE, showed that no significant differences in crystalline phases of samples are visible. A sustainability analysis was performed through the software Ces selector. For microwave treated samples, the greater percentage of the impact is given by the chemical reagents used while the thermal treatment influences in very little way. By the results it is possible to assess that the EE and CF values associated to microwave samples are much lower than those associated with the sample on heating plate. Microwave treatment could be a valid substitute of the one on heating plate drastically reducing the emissions related to the thermal process. As the idea was to create furniture items that could help trap the PM, adsorption tests were carried out following the experimental set up shown in Paragraph 4.4 using an aerosol nanoparticles generator and exposing 3 specimens for each sample. Results showed that the sample at 100 W 2 min seems to have no absorption capacity while the sample at 600 W 30 s shows a minimum absorption capacity, slightly lower than that found in SUNSPACE. However, these preliminary results are very interesting and deserve to be further investigated. Next steps will be porosimetric analysis to define the shape and size of the pores, so as to better understand the abnormal result of the sample at 100 W 2 min, and resistance tests.

8. SDGs activity and PM

In my first year as a PhD student, the COVID-19 epidemic spread around the world. This caused a disruption of all activities, including the inability to go to the laboratory. During these months, not being able to do laboratory research, I focused on other topics regarding the impact of COVID-19 on: extraction of raw materials, use of face masks and concentrations of pollutants in the city of Brescia, Italy.

8.1 Raw materials extraction and COVID-19

The COVID-19 spread led to a drastic change of all human habits. The forced confinement of people has led to rediscovering some household activities and stressed the importance of technology and the internet to study and work. The great importance of electronic devices was never so evident than during lockdown, when it was necessary to reduce to a minimum or just avoid human interactions [114]. The increase of digital connectivity is also one of the European Commission (EC) ambition for the next future, coupled with the aims to construct a green and resilient society [115]. In this context, it is fundamental to highlight that green and digital technologies are based on the use of several raw materials (RMs). Moreover, many of the electrical and electronic equipment become unavoidable during lockdown contain essential elements, with limited and/or restricted supply, that are defined critical raw materials (CRMs). They play a fundamental role mainly for industrialized regions in the world because several of these CRMs have contributed to revolutionary development of some recent technologies and are necessary for energy efficiency. Their economic importance is connected to their applications that are expected will be ulterior developed in green, defense, and high-tech sectors [116]. Considering some CRMs necessity in technological applications also for green energies and ecological transition, 30 metals are currently inserted in the list of critical raw materials [117]. EC has the aspiration to reach 2050 climate neutrality and recognizes that the access to resources is strategic to fulfil this ambition. As a consequence, CRMs that have been already considered crucial for society, are now even

defined super-critical [118]. It results evident that it is mandatory to invest efforts in developing sustainable ways to recycle CRMs from waste, considering that some available natural resources are inappropriate to support the raw materials need of the next future. Global annual production of electronic waste was estimated to be approximatively 50 million tons [119], and is expected to grow continuously due to the increased use of electronics, as it was also demonstrated during pandemic (for example forced people to adopt smart-working). By 2030, more than 1 million of batteries is expected to reach the end of their first-life [120]. Lots of precious materials constituting these devices, like gold, cooper, silver, lithium and cobalt, often go into landfilling, despite their value, with a waste of resources that can also cause soil and water pollution [120]. It is evident that the generated electronic wastes offer an opportunity for recycling precious [119].

Due to the total blocking of activities due to COVID-19 in almost all the World, it is possible to assess that the pandemic affected critical raw materials extraction causing losses of billions of € especially in South America countries where most of the mines have been closed due to numerous infections. Figure 45 shows the position of the most important mining sites in the world and the losses suffered by countries due to the closure of activities.

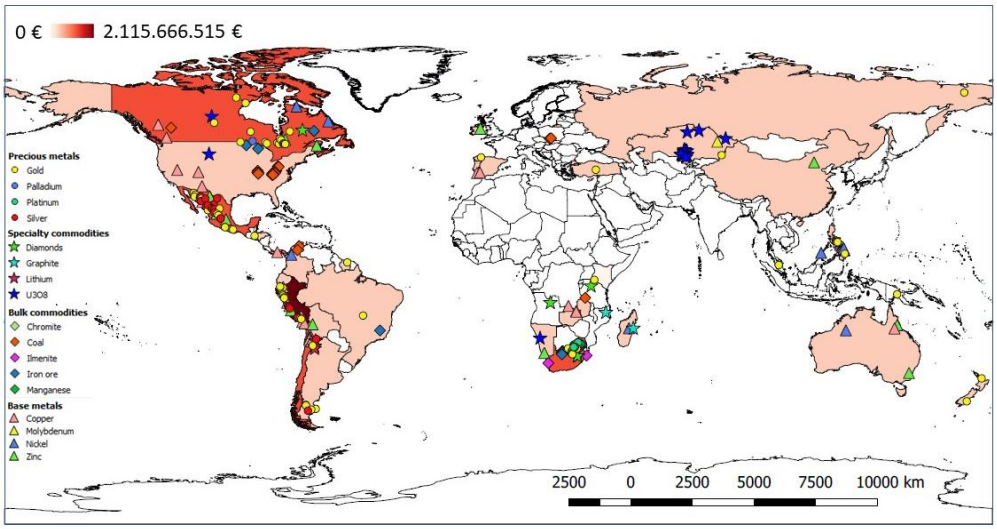

Figure 45. Representation of the most endangered mining sites (divided into precious metals, specialty commodities, bulk commodities, and base metals) and the countries that have suffered the greatest losses. Data analysis was performed by Qgis software [121].

Critical commodity prices fell during Wuhan's lockdown and then rose due to the high demand for electronic devices for smart working (Figure 46).

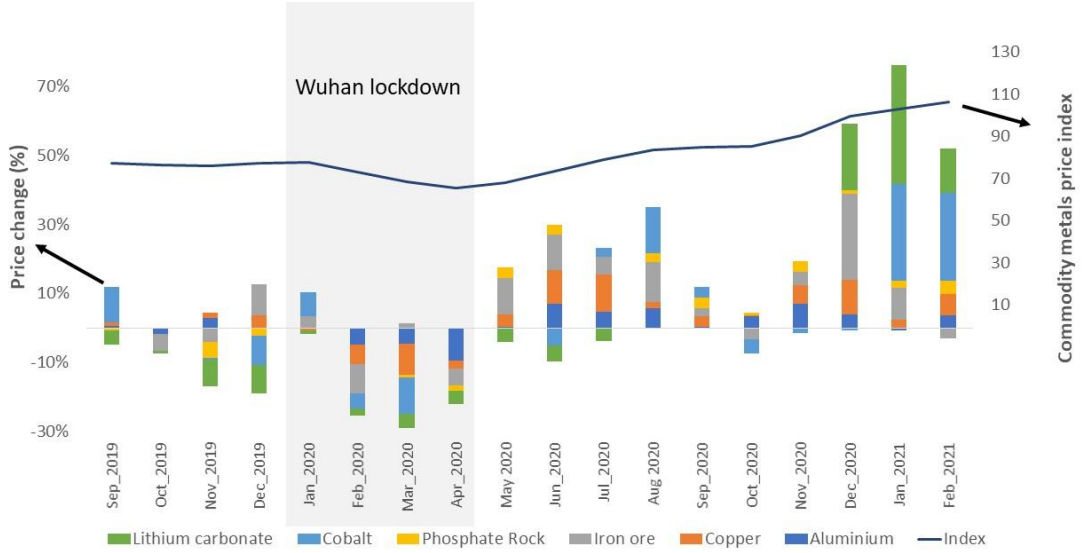

Figure 46. Monthly price change (%) of lithium carbonate, cobalt, rock phosphate, iron ore, copper and aluminum and Commodity Metals Price Index (2005 = 100, includes Cu, Al, iron ore, Sn, Ni, Zn, Pb, and U Price Indices) from January 2019 to February 2021. The Wuhan lockdown period was from 23 January to April 8, 2020. Data source: World Bank and Trading Economics.

CRMs play a key role for the progress of the industrialized regions in the world. They have contributed to recent technological development and energy efficiency improvement. They serve as essential RM for high-technology, sustainable, and green applications. COVID-19 disease has contributed to reduce the availability of several of these materials. However, the pandemic has also demonstrated the need of structured and global efforts to face crisis, because individual actions are pointless. Moreover, global crisis due to pandemic may have severe consequences on the achievement of SGDs. The post-pandemic recovery period could be an opportunity to develop new prosperity models, based on green principles needs and priorities: a more resilient economy, able to catch the new opportunities of digitization, and meet the environment and climate targets. The materials production and consumption must be secured in a sustainable way, that probably will need a revision of giant ore deposits management strategies. Technology will be a fundamental player of this innovation, but also mining code and practices need strict revisions and improvements. Finally, increased materials recycle will help to fulfil some of the circular economy aims, by reducing reliance on

finite resources and mitigating permanent waste disposal. The expected post-pandemic scenario will contribute to SDGs 5, 7, 8, 9, 10, 11, 12, 13, 14, 15, 16 and 17 fulfil among others.

This work is reported in [122].

8.2 Environmental impact of face masks

Due to COVID-19 spread, the use of face masks became mandatory. To cope with the high demand for masks and other protective devices, such as gloves, many industries converted their production. In particular, the WHO estimated that in 2020 the global production of masks and gloves was 129 and 69 billion per month, respectively [123]. Most of face masks are produced from plastic polymers such as PP, PE and PU, therefore relying on fossil sources for production. Moreover, not only the use of personal protective equipment (PPE) but also disposable products such as plastic products (like cutlery and plates) and packaging was encouraged to limit the spread of virus contagion [124]. This highlights the essential role of plastic in daily life. For instance, the use of plastic packaging increased by 31% for Italy and 78% for the US [125].

Surgical masks are made of plastic polymers with very low biodegradability. Indeed, they take hundreds of years to degrade and during this process they fragment in micro plastics due to different factors such as temperature, UV radiation, and mechanical processes, as reported in recent studies [126][127][128]. In particular, Saliu et al. [129] reveal that a surgical mask can release in the marine environment thousands of microscopic fibers that are potentially dangerous both for marine flora and fauna and for humans. On the contrary, fabric masks are generally made with cotton, which is more biodegradable and can be reused several times. An alternative to the use of surgical masks may be the use of fabric masks, cheaper, more easily producible and more sustainable. At this purpose an evaluation of the environmental impact of surgical and fabric masks was proposed through the evaluation of CO_2 emissions assessing the quantity of masks needed to meet the needs of the Italian population. 3 different types of surgical masks and 2 types of fabric masks were analyzed. Masks were cut and each

was weighed in order to assess the impact associated with the individual material forming the template. Data on the Italian population, divided by region, were found on the Istat (National Institute of Statistics) website, considering data on 1 January 2020 [130]. The Italian population was divided according to working conditions, distinguishing between workers, older than 15 years, and non-workers, recalling that in accordance with the law, children under 6 years do not have the obligation to wear the mask [45]. In accordance with these considerations it was possible to define the impact of the masks for each Italian region, Figure 47. The data was processed with Qgis software [121].

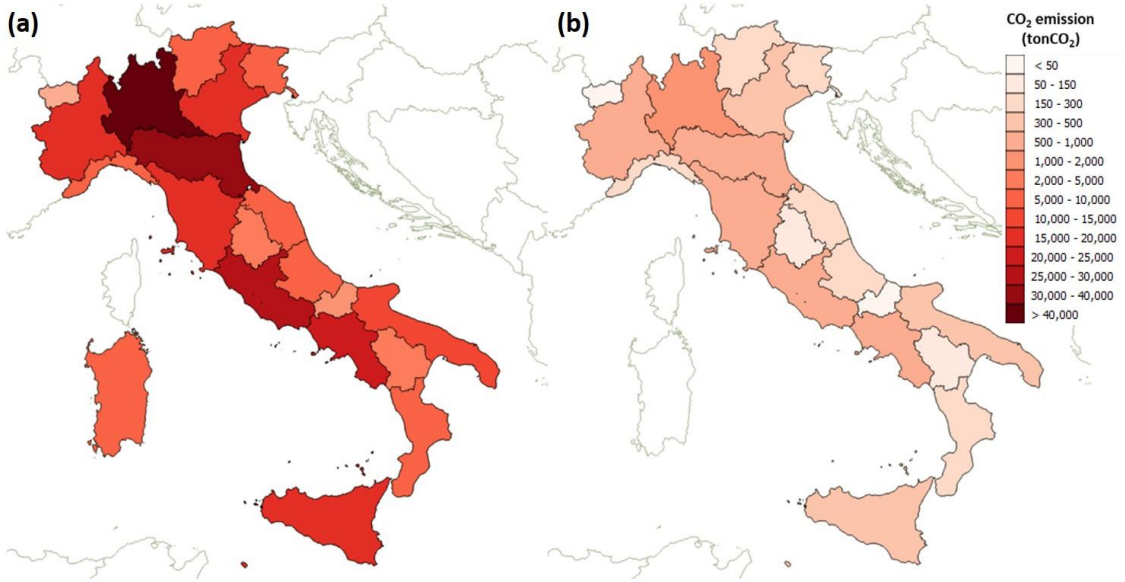

Figure 47. Qgis geographical visualization of CO2 emissions associated with: (a) surgical masks consumption; (b) fabric masks consumption. Data were calculated considering the period from March 2020 to December 2021. These data were evaluated only considering the materials used.

The high emissions of surgical masks are also due to the high number of masks required daily, unlike fabric masks, which in addition to being made of cotton, are reusable more than a day. The total CO_2 emissions associated with the use of surgical masks for all Italian regions from March 2020 to December 2021 corresponds to 240 kton. The highest value is in Lombardy (followed by Lazio and Emilia-Romagna) as it is the most populated region in Italy and with a higher level of employment compared to the other regions. While the CO_2 emissions value embodied in fabric masks is about 7 kton, almost 35 times less than the value related to surgical masks.

Although the approach used in this work is simplified compared to LCA analysis, it allows us to obtain a preliminary evaluation of the environmental impact. It is evident that surgical masks have a higher environmental impact due to the increased number of masks needed to meet the demand and use of poorly degradable materials. Moreover, surgical masks are specially imported from abroad, increasing CO_2 emissions due to their use and transport. While, fabric masks are made of cotton, more degradable and reusable. Moreover, they are often produced locally reducing the transport component.

This work is reported in [131].

8.3 COVID-19 and PM emissions

The introduction in 2015 of the SDGs had as objective the achievement of the goals by 2030. The COVID-19 epidemic, due to the serious consequences worldwide, has unfortunately caused a delay in their achievement. Reducing air pollution remains one of the most important problems to be addressed. The COVID-19 spread gave to researchers the unique opportunity to evaluate the impact of emission control strategies (even if related to a limited range of activities) on air quality. Different studies tried to evaluate the pollutants concentrations before and during COVID-19 pandemic [132][133]. In these studies, the approach consisted in comparing pollutants concentrations before and during the pandemic not taking into account other factors such as air quality improvement trends, seasonality, the weather conditions, and the local characteristic of the investigated area. The aim of the work was to evaluate the effect of the lockdown limitations on PM_{10} and NO_2 concentration in the Brescia (Italy) urban area, considering possible contributions of confounding factors, like meteorological parameters. The area under exam was selected because: Brescia is characterized by very high PM_{10} and NO_2 concentrations [24]; the area was among the most affected by the epidemic, leading to very active participation of the population to the lockdown limitations [134]; this area was never still investigated in terms of lockdown connected air change, and the results of this study may be interesting also in the frame of the discussion about a possible role of PM in COVID-19 transmission [135].

For this aim, models able to distinguish the air quality changes due to confounding factors from the ones obtained because of the lockdown restriction measures are used. Indeed, some works have highlighted that incomplete correction for meteorological factors may lead to biased results [136]. The work is based on both data monitored by a portion of the Regional Authority network and modelling systems results. The results show that, considering the estimated pollutants concentration reduction trends due to the implementation of the air quality policies in the area and in the whole Po Valley, the lockdown impact on NO_2 reduction is extremely clear and results considerable. Nevertheless, a meteorology analysis shows that it is higher in strong accumulation conditions (low wind speed and no rain period). On the contrary, the measured PM_{10} concentrations result almost in accord with the values reported on the same period for the last 4 years (2016 – 2020). Finally, the causes of the detected differences between NO_2 and PM_{10} behavior have been investigated through a source-apportionment modelling technique. The results of this analysis showed that emissions due to road transport are responsible to the formation of more than the 50% of the NO_2 concentration, while the formation of PM_{10} in atmosphere depends on a larger number of emission sources like road transport, residential heating, agriculture, and industrial processes. Then, it is possible to conclude that lockdown restrictions, that essentially affect the urban mobility, have a limited effect on PM_{10} reduction.

This work is reported in [137], in collaboration with “Integrated Assessment Modeling for Environmental Systems” group.

9. Conclusions

PM is the most present pollutant in urban areas due to traffic and domestic heating. In many cities worldwide the limits imposed by legislation are often exceeded, with serious consequences for human health due to the PM capacity to penetrate the respiratory system. It becomes therefore necessary to define methods that allow to reduce the concentrations of PM and at this purpose several solutions have been proposed, like filters. Unfortunately, these filters are petroleum based and have a high environmental impact. Eco-friendlier solutions are leaves as it has been demonstrated that they have a good adsorption capacity to entrap PM, unfortunately alone they cannot significantly reduce the PM concentrations. It is therefore necessary to adopt sustainable solutions that help to improve air quality. SUNSPACE was the first sustainable, porous material, realized with industrial by-product (SF) and low energy process, able to entrap PM. However, its dark color represents a limit to its application, the aim of my Ph.D. was to implement SUNSPACE characteristics.

In this Ph.D. thesis some SUNSPACE modification were proposed. First of all, the color change was achieved by the substitution of SF with BA, solid residue of waste combustion provided by the A2A waste incineration plant of Brescia. Thanks to its composition, BA can react with calcium hydroxide, favoring the pozzolanic reaction. Moreover, other modifications were proposed by the elimination of the thermal treatment. As the idea is to use these sustainable materials as plaster, the thermal treatment is a limitation to its application. In SUNSPACE and SUNSPACE BA samples, sodium bicarbonate was used to generate CO_2 by thermal decomposition at low temperatures and to produce the pores. To avoid the thermal treatment and to obtain the pore formation the hydrogen peroxide, in different concentration, was used instead of sodium bicarbonate. Samples were fully characterized by different techniques. The colorimetric analysis allowed to define the clear change of color from dark to light grey (as demonstrated by the change of L value from about 44 to 81). By the XRD analysis the main crystalline peaks were identified showing that, changing the volume of hydrogen peroxide used in sample synthesis, there were not significant structural change in the

materials. Morphological analysis, performed by SEM, showed that samples realized with SF are characterized by spherical particles of silica agglomerated together with size dimension from 20 nm to 700 nm. SUNSPACE BA presented a fibrillary matrix typical of the C-S-H formation that was not so visible in samples realized with BA and hydrogen peroxide probably due to the fact that not all the calcium hydroxide reacted with BA, as confirmed by XRD analysis. The porosimetric analysis revealed that samples realized with SF were characterized by a unimodal pore size distribution while samples realized with BA were characterized by a bimodal pore size distribution with pores of greater dimension. The sustainability analysis performed using the software Ces Selector demonstrated that these materials are more sustainable than materials commonly used for air filters, like PP, PE and PS. Samples realized with BA have higher values of EE and CF due to the pretreatments necessary to obtain the power for the sample synthesis. However, the elimination of the thermal treatment allowed to reduce the values associated with CF. As the idea is to use this material to entrap PM, an adsorption test was performed using an aerosol nanoparticles generator (Grimm Particle-generator MODEL 7.811). Once defined the experimental set-up parameters, a TiO_2 suspension was used to simulate the PM source. 3 specimens for each samples were exposed and a cement and a *Hedera Helix* leaf samples were used as reference. After the exposure, samples were digested and analyzed by TXRF. The results highlights that samples realized with SF had a good adsorption capacity as well as SUNSPACE BA, unlike samples realized with BA and hydrogen peroxide. During the test it was evident that the TiO_2 suspension was just deposited on the leaf surface without actually be adsorbed instead cement sample did not have any adsorption capacity.

Moreover, the samples described were tested to evaluate the photodegradation of organic pollutants. MB was used to simulate an organic pollutant. As TiO_2 is a well-known catalyst, it was used to realize other porous samples replacing 20% of the powder (SF or BA and calcium hydroxide) with TiO_2. The set-up of the experiment was defined. 3 specimens for each material were prepared. Materials were immersed in a MB solution, in known concentration, and after 3 hours of adsorption in a dark room, the UV lamp was switched on and the experiment continued for another 5 hours assessing

MB concentration every hour. Results showed that samples realized with SF had a good adsorption capacity but low photodegradation activity, on the contrary, sample with BA, hydrogen peroxide and TiO_2 had the best performance: about 50% of MB photo degradation.

Some samples realized with BA and hydrogen peroxide showed a water repellent behavior that was investigated by wettability test for the measure of contact angle. At this purpose, other samples were synthetized changing the volume of hydrogen peroxide. Samples were characterized through XRD analysis that allowed to define the same crystalline phases in all samples, showing that the amount of hydrogen peroxide did not affect the structure of the sample. Moreover, a morphological analysis was performed using the Leica MZ16 A microscope to investigate the superficial porosity of samples. Different images were acquired for each sample and then analyzed by the software ImageJ. Results showed that although there is a progressive addition of hydrogen peroxide, there is no linear increase in porosity. Thanks to the software ImageJ, it was possible to evaluate the Feret's diameter of pores, showing that, for all samples, the greatest amount of pores occurs in the range between 25 - 100 µm. The wettability test was performed using the CAM 200 tensiometer (KSV Instruments, Finland). The instrument was equipped with a calibrated needle to define the volume to be deposited on the surface of the samples, in this case 3 µL. The drop profile was detected by a camera and processed by the software to obtain the surface tension and the contact angle. To evaluate the wettability of the samples, the value of the contact angle at time 3 s was considered. To evaluate the behavior of the samples, an observation time of 30 s was set. 5 tests for each sample were performed. Also a cement sample was analyzed. The rated contact angle for each sample was above the hydrophobicity value ($\theta > 90°$), ranging from 100° to a maximum of 134°. The cement sample had a contact angle of about 125°. Unlike samples with hydrogen peroxide, on which the drop was not absorbed and remained on the surface for much longer than the duration of the test (about 30 min), the drop deposited on the cement sample was absorbed before the end of the test. Based on the results, a possible application of these materials could be as a water-repellent plaster.

In parallel with the wetting tests, another work on SUNSPACE was carried out to improve the material sustainability and to speed up the synthesis process. The thermal treatment for SUNSPACE was changed: the heating plate was substituted by microwave oven. The use of microwaves reduced the drying time of samples. Several tests were conducted changing the time and power of the microwave treatment to define the most performing samples. Of all the samples synthetized, those that seemed to have the best characteristics were chosen for the characterizations and the adsorption test. XRD and SEM analyses did not showed significant differences between samples and in comparison with original SUNSPACE. A sustainability analysis was performed. Results showed that replacing the heating plate treatment with the microwave treatment the EE value decreased, as the greatest percentage of the impact was related to the thermal treatment. On the contrary, for CF, the greater percentage of the impact was given by the chemical reagents used while the thermal treatment influenced minimally. As the idea was to make objects such as outdoor to entrap PM, adsorption tests were carried out using the aerosol nanoparticles generator with the parameters already settled. One of the analyzed sample (600 W 30 s) had a better adsorption capacity than the other.

Finally, in these 3 years, due to COVID-19 spread and the impossibility of going to the laboratory, the attention was focused on others topics regarding the impact of COVID-19 on: extraction of raw materials, use of face masks and concentrations of pollutants in the city of Brescia.

References

[1] E.B. Weiss, The Evolution of International Environmental Law. The Contribution of International Environmental Law to International Law: Past Achievements and Future Expectation, Japanese Yearb. Int. Law. 54 (2011) 1–27.

[2] European Union, Environment and climate change, (2023). https://eur-lex.europa.eu/content/summaries/summary-20-expanded-content.html (accessed March 16, 2023).

[3] United Nations, Transforming our world: the 2030 Agenda for Sustainable Development, (2015). https://sdgs.un.org/2030agenda (accessed December 31, 2022).

[4] Z. Wei, Q. Su, J. Yang, G. Zhang, S. Long, X. Wang, High-performance filter membrane composed of oxidized Poly (arylene sulfide sulfone) nanofibers for the high-efficiency air filtration, J. Hazard. Mater. 417 (2021) 126033. https://doi.org/10.1016/j.jhazmat.2021.126033.

[5] E.E. Agency, Environmental pollution, (2010) 1–28.

[6] B. Hoffmann, S. Moebus, N. Dragano, A. Stang, S. Möhlenkamp, A. Schmermund, M. Memmesheimer, M. Bröcker-Preuss, K. Mann, R. Erbel, K.H. Jöckel, Chronic residential exposure to particulate matter air pollution and systemic inflammatory markers, Environ. Health Perspect. 117 (2009) 1302–1308. https://doi.org/10.1289/ehp.0800362.

[7] A. Nemmar, M.F. Hoylaerts, P.H.M. Hoet, J. Vermylen, B. Nemery, Size effect of intratracheally instilled particles on pulmonary inflammation and vascular thrombosis, Toxicol. Appl. Pharmacol. 186 (2003) 38–45. https://doi.org/10.1016/S0041-008X(02)00024-8.

[8] A. Zanoletti, F. Bilo, L.E. Depero, D. Zappa, E. Bontempi, The first sustainable material designed for air particulate matter capture: An introduction to Azure Chemistry., J. Environ. Manage. 218 (2018) 355–362. https://doi.org/10.1016/j.jenvman.2018.04.081.

[9] B. Gandu, A.G. Rao, R. Cahan, Air pollution control by using different types of techniques and sorbents, in: A.N. Delgado (Ed.), Sorbent Mater. Control. Environ. Pollut., Elsevier, 2021: pp. 575–594.

[10] EPA, Air pollution control equipment, in: MACT EEE Train. Work., 2008.

[11] C. Woodford, Electrostatic smoke precipitators, (2020). https://www.explainthatstuff.com/electrostaticsmokeprecipitators.html.

[12] K. Dzierzanowski, R. Popek, H. Gawrońska, A. Saebø, S.W. Gawroński, Deposition of particulate matter of different size fractions on leaf surfaces and in waxes of urban forest species, Int. J. Phytoremediation. 13 (2011) 1037–1046. https://doi.org/10.1080/15226514.2011.552929.

[13] C. Liu, P.C. Hsu, H.W. Lee, M. Ye, G. Zheng, N. Liu, W. Li, Y. Cui, Transparent air filter for high-efficiency PM 2.5 capture, Nat. Commun. 6 (2015). https://doi.org/10.1038/ncomms7205.

[14] B. Khalid, X. Bai, H. Wei, Y. Huang, H. Wu, Y. Cui, Direct Blow-Spinning of Nanofibers on

a Window Screen for Highly Efficient PM2.5 Removal, Nano Lett. 17 (2017) 1140–1148. https://doi.org/10.1021/acs.nanolett.6b04771.

[15] A. Zanoletti, I. Vassura, E. Venturini, M. Monai, T. Montini, S. Federici, A. Zacco, L. Treccani, E. Bontempi, A New Porous Hybrid Material Derived From Silica Fume and Alginate for Sustainable Pollutants Reduction, Front. Chem. 6 (2018) 60. https://doi.org/10.3389/fchem.2018.00060.

[16] A. Zanoletti, F. Bilo, L. Borgese, L.E. Depero, A. Fahimi, J. Ponti, A. Valsesia, R. La Spina, T. Montini, E. Bontempi, SUNSPACE, A Porous Material to Reduce Air Particulate Matter (PM)., Front. Chem. 6 (2018) 534. https://doi.org/10.3389/fchem.2018.00534.

[17] A. Zanoletti, F. Bilo, S. Federici, L. Borgese, L.E. Depero, J. Ponti, A. Valsesia, R. La, M. Segata, T. Montini, E. Bontempi, The first material made for air pollution control able to sequestrate fine and ultra fine air particulate matter, Sustain. Cities Soc. 53 (2020) 101961. https://doi.org/10.1016/j.scs.2019.101961.

[18] F. Bilo, A. Zanoletti, L. Borgese, L.E. Depero, E. Bontempi, Chemical Analysis of Air Particulate Matter Trapped by a Porous Material , Synthesized from Silica Fume and Sodium Alginate, 2019 (2019).

[19] a2a, Il Termovalorizzatore di Brescia, (2022). https://www.gruppoa2a.it/it/chi-siamo/nostri-impianti/termovalorizzatore-brescia (accessed January 5, 2023).

[20] J. Longhurst, J. Barnes, T. Chatterton, L. De Vito, M. Everard, E. Hayes, E. Prestwood, B. William, ANALYSING AIR POLLUTION AND ITS MANAGEMENT THROUGH THE LENS OF THE UN SUSTAINABLE DEVELOPMENT GOALS: A REVIEW AND ASSESSMENT, WIT Trans. Ecol. Environ. 230 (2018). https://doi.org/10.2495/AIR180011.

[21] World Health Organization, The global health observatory, (2021). https://www.who.int/data/gho/data/themes/topics/topic-details/GHO/ambient-air-pollution (accessed April 4, 2023).

[22] European Commission, Climate negotiations, (2022). https://climate.ec.europa.eu/eu-action/international-action-climate-change/climate-negotiations_it (accessed December 9, 2022).

[23] C. Carnevale, E. Pisoni, M. Volta, A non-linear analysis to detect the origin of PM10 concentrations in Northern Italy, Sci. Total Environ. 409 (2010) 182–191. https://doi.org/10.1016/j.scitotenv.2010.09.038.

[24] C. Carnevale, E. De Angelis, F.L. Tagliani, E. Turrini, M. Volta, A short-term air quality control for pm10 levels, Electron. 9 (2020) 1–17. https://doi.org/10.3390/electronics9091409.

[25] World Health Organization, Ambient (outdoor) air pollution, (2021). https://www.who.int/news-room/fact-sheets/detail/ambient-(outdoor)-air-quality-and-health (accessed December 9, 2022).

[26] A. Thorpe, R.M. Harrison, Sources and properties of non-exhaust particulate matter from road traffic: A review, Sci. Total Environ. 400 (2008) 270–282. https://doi.org/10.1016/j.scitotenv.2008.06.007.

[27] C. Perrino, M. Catrambone, S. Canepari, Chemical composition of PM10 in 16 Urban, industrial and background sites in Italy, Atmosphere (Basel). 11 (2020) 1–22.

https://doi.org/10.3390/ATMOS11050479.

[28] F. Zhang, Y. Chen, M. Cui, Y. Feng, X. Yang, J. Chen, Y. Zhang, H. Gao, C. Tian, V. Matthias, H. Liu, Emission factors and environmental implication of organic pollutants in PM emitted from various vessels in China, Atmos. Environ. 200 (2019) 302–311. https://doi.org/10.1016/j.atmosenv.2018.12.006.

[29] J. Wang, S. Ogawa, Effects of Meteorological Conditions on PM 2 . 5 Concentrations in, (2015) 9089–9101. https://doi.org/10.3390/ijerph120809089.

[30] N. Galindo, M. Varea, J. Gil-moltó, E. Yubero, J. Nicolás, The Influence of Meteorology on Particulate Matter Concentrations at an Urban Mediterranean Location, (2011) 365–372. https://doi.org/10.1007/s11270-010-0484-z.

[31] B.R. Larsen, S. Gilardoni, K. Stenström, J. Niedzialek, J. Jimenez, C.A. Belis, Sources for PM air pollution in the Po Plain , Italy : II . Probabilistic uncertainty characterization and sensitivity analysis of secondary and primary sources, AEA. 50 (2012) 203–213. https://doi.org/10.1016/j.atmosenv.2011.12.038.

[32] Q. Yang, Q. Yuan, The Relationships between PM 2 . 5 and Meteorological Factors in China : Seasonal and Regional Variations, 5 (2017). https://doi.org/10.3390/ijerph14121510.

[33] S. Vardoulakis, B.E.A. Fisher, K. Pericleous, N. Gonzalez-flesca, MODELLING AIR QUALITY IN STREET CANYONS : A REVIEW, (n.d.).

[34] F. Murena, Sustainable Development of the Historic Centre of Naples : The Impact of Vehicular Tra ffi c and Food Service Business on Air Quality, (2020).

[35] Medical Facts, L'impatto sulla salute dell'inquinamento atmosferico da particolato: dati ed evidenze scientifiche, 2020. (n.d.). https://www.medicalfacts.it/2020/02/12/inquinamento-atmosferico-particolato/ (accessed December 9, 2022).

[36] M.T. Cheng, W.C. Chou, C.P. Chio, S.C. Hsu, Y.R. Su, P.H. Kuo, B.J. Tsuang, S.H. Lin, C.C.K. Chou, Compositions and source apportionments of atmospheric aerosol during Asian dust storm and local pollution in central Taiwan, J. Atmos. Chem. 61 (2008) 155–173. https://doi.org/10.1007/s10874-009-9131-8.

[37] Y.F. Xing, Y.H. Xu, M.H. Shi, Y.X. Lian, The impact of PM2.5 on the human respiratory system, J. Thorac. Dis. 8 (2016) E69–E74. https://doi.org/10.3978/j.issn.2072-1439.2016.01.19.

[38] I.M. Peters, S. Karthik, H. Liu, T. Buonassisi, A. Nobre, Urban haze and photovoltaics, Energy Environ. Sci. 11 (2018) 3043–3054. https://doi.org/10.1039/c8ee01100a.

[39] G. Fattoruso, M. Nocerino, G. Sorrentino, V. Manna, M. Fabbricino, G. Di Francia, Estimating Air Pollution Related Solar Insolation Reduction in the Assessment of the Commercial and Industrial Rooftop Solar PV Potential, Lect. Notes Comput. Sci. (Including Subser. Lect. Notes Artif. Intell. Lect. Notes Bioinformatics). 12250 LNCS (2020) 665–677. https://doi.org/10.1007/978-3-030-58802-1_48.

[40] L. Zhou, D.B. Schwede, K. Wyat Appel, M.J. Mangiante, D.C. Wong, S.L. Napelenok, P.Y. Whung, B. Zhang, The impact of air pollutant deposition on solar energy system efficiency: An approach to estimate PV soiling effects with the Community Multiscale

Air Quality (CMAQ) model, Sci. Total Environ. 651 (2019) 456–465. https://doi.org/10.1016/j.scitotenv.2018.09.194.

[41] M.H. Bergin, C. Ghoroi, D. Dixit, J.J. Schauer, D.T. Shindell, Large Reductions in Solar Energy Production Due to Dust and Particulate Air Pollution, Environ. Sci. Technol. Lett. 4 (2017) 339–344. https://doi.org/10.1021/acs.estlett.7b00197.

[42] IQAir, Air quality and pollution city ranking, (2022). https://www.iqair.com/world-air-quality-ranking (accessed December 29, 2022).

[43] European Environment Agency (EEA), Air quality in Europe — 2019 report, 2019.

[44] A. Lombardia, QUALITÀ DELL ' ARIA UN PRIMO BILANCIO DEL 2021 ARPA Lombardia, (2022).

[45] Gazzetta Ufficiale della Repubblica Italinana, Decreto del presidente del consiglio dei ministri 26 aprile 2020, (n.d.). https://www.gazzettaufficiale.it/eli/id/2020/04/27/20A02352/sg (accessed January 13, 2023).

[46] World Health Organization, WHO global air quality guidelines, 2021.

[47] Z. Wang, Energy and Air Pollution, 2018. https://doi.org/10.1016/B978-0-12-809597-3.00127-9.

[48] Tecnosida, Electrostatic Precipitator, (2021). https://www.tecnosida.com/electrostatic-precipitator.

[49] Energy Education, Electrostatic precipitator, (2018). https://energyeducation.ca/encyclopedia/Electrostatic_precipitator.

[50] J.A. Cross, R. Helstroom, R. Beck, Method for Continuously the Weight and Tension in a Fabric Filter, Filtr. Sep. 32 (1995) 443–447. https://doi.org/https://doi.org/10.1016/S0015-1882(97)84082-7.

[51] B. Guan, R. Zhan, H. Lin, Z. Huang, Review of the state-of-the-art of exhaust particulate filter technology in internal combustion engines, J. Environ. Manage. 154 (2015) 225–258. https://doi.org/10.1016/j.jenvman.2015.02.027.

[52] W. Xia, Y. Zheng, X. He, D. Yang, H. Shao, J. Remias, J. Roos, Y. Wang, Catalyzed Gasoline Particulate Filter (GPF) Performance: Effect of Driving Cycle, Fuel, Catalyst Coating, SAE Tech. Pap. 2017–Octob (2017). https://doi.org/10.4271/2017-01-2366.

[53] EPA, What is a HEPA filter?, (2022). https://www.epa.gov/indoor-air-quality-iaq/what-hepa-filter (accessed January 16, 2023).

[54] A.G. McDonald, W.J. Bealey, D. Fowler, U. Dragosits, U. Skiba, R.I. Smith, R.G. Donovan, H.E. Brett, C.N. Hewitt, E. Nemitz, Quantifying the effect of urban tree planting on concentrations and depositions of PM10 in two UK conurbations, Atmos. Environ. 41 (2007) 8455–8467. https://doi.org/10.1016/j.atmosenv.2007.07.025.

[55] A. Petroff, A. Mailliat, M. Amielh, F. Anselmet, Aerosol dry deposition on vegetative canopies. Part I: Review of present knowledge, Atmos. Environ. 42 (2008) 3625–3653. https://doi.org/10.1016/j.atmosenv.2007.09.043.

[56] A. Ikeda, A. Takemura, H. Ono, Preparation of low-molecular weight alginic acid by acid

hydrolysis, 42 (2000) 421–425.

[57] GRANTA Selector, Ces Selector, 2022. (n.d.). https://www.grantadesign.com/it/industry/products/ces-selector/ (accessed December 31, 2022).

[58] A. Zanoletti, C. Carnevale, E. Bontempi, A porous hybrid material for air particulate matter reduction, in: A. Nunez-Delgado (Ed.), Sorbent Mater. Control. Encironmental Pollut., Elsevier, 2021: pp. 595–622.

[59] United Nations, Our Common Future, 1987.

[60] H.E. Daly, Sustainable Development : From Concept and Theory to Operational Principles, Popul. Dev. Rev. 16 (1990) 25–43.

[61] United Nations, Make the SDGs a reality, (2015). https://sdgs.un.org/ (accessed December 31, 2022).

[62] World Health Organization, Air pollution, 2022. (n.d.). https://www.who.int/health-topics/air-pollution#tab=tab_2 (accessed January 1, 2023).

[63] World Health Organization, SDG Target 3.9 Mortality from environmental pollution, (2022). https://www.who.int/data/gho/data/themes/topics/sdg-target-3_9-mortality-from-environmental-pollution (accessed January 1, 2023).

[64] United Nation Procurement Division, Goal 11 Sustainable cities and communities, (2022). https://www.undp.org/sustainable-development-goals?utm_source=EN&utm_medium=GSR&utm_content=US_UNDP_PaidSearch_Brand_English&utm_campaign=CENTRAL&c_src=CENTRAL&c_src2=GSR&gclid=CjwKCAiA-8SdBhBGEiwAWdgtcPYmbAvJrqfjKvi-YMnPg1x-ZmEmIlXfjoe8KmgJAgMl2MAiez97wx (accessed January 1, 2023).

[65] United Nations, SDG 13 Take urgent action to combat climate change and its impact, (2022). https://sdgs.un.org/goals/goal13 (accessed January 1, 2023).

[66] Tecno B, MICROSILICATI: APPUNTI D'USO, (2016). https://www.tecnob-srl.it/news/microsilicati-appunti-duso/ (accessed January 20, 2023).

[67] E. Güneyisi, M. Gesoğlu, S. Karaoğlu, K. Mermerdaş, Strength, permeability and shrinkage cracking of silica fume and metakaolin concretes, Constr. Build. Mater. 34 (2012) 120–130. https://doi.org/10.1016/j.conbuildmat.2012.02.017.

[68] S. Haruehansapong, T. Pulngern, S. Chucheepsakul, Effect of the particle size of nanosilica on the compressive strength and the optimum replacement content of cement mortar containing nano-SiO2, Constr. Build. Mater. 50 (2014) 471–477. https://doi.org/10.1016/j.conbuildmat.2013.10.002.

[69] V. Lilkov, I. Rostovsky, O. Petrov, Y. Tzvetanova, P. Savov, Long term study of hardened cement pastes containing silica fume and fly ash, Constr. Build. Mater. 60 (2014) 48–56. https://doi.org/10.1016/j.conbuildmat.2014.02.045.

[70] A. Mardani-Aghabaglou, G. Inan Sezer, K. Ramyar, Comparison of fly ash, silica fume and metakaolin from mechanical properties and durability performance of mortar mixtures view point, Constr. Build. Mater. 70 (2014) 17–25. https://doi.org/10.1016/j.conbuildmat.2014.07.089.

[71] A. C1240-15, Standard Specification for Silica Fume Used in Cementitious Mixtures, West Conshohocken, Pa. (2015) 1–7. https://doi.org/10.1520/C1240-14.2.

[72] R. Siddique, Kunal, Utilization of industrial by-products and natural ashes in mortar and concrete, Elsevier, 2016. https://doi.org/10.1016/b978-0-08-100038-0.00007-x.

[73] D.K. Panesar, Supplementary cementing materials, Elsevier LTD, 2019. https://doi.org/10.1016/B978-0-08-102616-8.00003-4.

[74] L. Black, Low clinker cement as a sustainable construction material, in: Sustain. Constr. Mater., Elsevier, 2016: pp. 415–457. https://doi.org/10.1016/B978-0-08-100370-1.00017-2.

[75] P. Fidjestol, R. Lewis, Microsilica as an Addition, Lea's Chem. Cem. Concr. (2003) 679–712. https://doi.org/10.1016/B978-075066256-7/50024-2.

[76] ISPRA, Localizzazione degli impianti di trattamento dei rifiuti urbani - Impianti di incenerimento, anno 2021, (2021). https://www.catasto-rifiuti.isprambiente.it/index.php?pg=gestnazione&aa=2021&regid=&mappa=6#p (accessed January 5, 2023).

[77] European Parliament and European Union Council, Directive 2010/75/EU on industrial emissions (integrated pollution prevention and control), Off. J. Eur. Union. (2010).

[78] D.R. Italiana, Attuazione della direttiva 2010/75/UE relativa alle emissioni industriali (prevenzione e riduzione integrate dell'inquinamento)., Gazz. Uff. (2014).

[79] M.J. Quina, E. Bontempi, A. Bogush, S. Schlumberger, G. Weibel, R. Braga, V. Funari, J. Hyks, E. Rasmussen, J. Lederer, Science of the Total Environment Technologies for the management of MSW incineration ashes from gas cleaning : New perspectives on recovery of secondary raw materials and circular economy, Sci. Total Environ. 635 (2018) 526–542. https://doi.org/10.1016/j.scitotenv.2018.04.150.

[80] A. Assi, F. Bilo, A. Zanoletti, J. Ponti, A. Valsesia, R. La Spina, L.E. Depero, E. Bontempi, Review of the reuse possibilities concerning ash residues from thermal process in a medium-sized urban system in Northern Italy, Sustain. 12 (2020). https://doi.org/10.3390/su12104193.

[81] A. Assi, F. Bilo, A. Zanoletti, J. Ponti, A. Valsesia, R. La Spina, A. Zacco, E. Bontempi, Zero-waste approach in municipal solid waste incineration: Reuse of bottom ash to stabilize fly ash, J. Clean. Prod. 245 (2020) 118779. https://doi.org/10.1016/j.jclepro.2019.118779.

[82] A. Assi, F. Bilo, S. Federici, A. Zacco, L.E. Depero, E. Bontempi, Bottom ash derived from municipal solid waste and sewage sludge co-incineration: First results about characterization and reuse, Waste Manag. 116 (2020) 147–156. https://doi.org/10.1016/j.wasman.2020.07.031.

[83] A. Riva, L. Biganzoli, M. Grosso, P. Milano, I. Civile, Gestione delle scorie da incenerimento di rifiuti solidi urbani : sistemi di estrazione e layout impiantistici di trattamento, 2016.

[84] U.S. Food & Drug Administration, Food Additive Status List, (2022). https://www.fda.gov/food/food-additives-petitions/food-additive-status-list (accessed January 18, 2023).

[85] Samrat Pharmachem Limited, Calcium iodate, (n.d.). https://www.samratpharmachem.com/product/calcium-iodate/ (accessed January 18, 2023).

[86] B. Casini, F. Aquino, M. Totaro, M. Miccoli, I. Galli, L. Manfredini, C. Giustarini, A.L. Costa, B. Tuvo, P. Valentini, G. Privitera, A. Baggiani, Application of Hydrogen Peroxide as an Innovative Method of Treatment for Legionella Control in a Hospital Water Network, Pathogens. 6 (2017) 1–12. https://doi.org/10.3390/pathogens6020015.

[87] A.A. Ramezanianpour, M. Nikravan, R. Maknoon, Characterization of Bottom Ash from Petrochemical, (2011).

[88] M.F. Ashby, Materials and Environment, Elsevier, New York, 2012.

[89] E. Bontempi, A new approach for evaluating the sustainability of raw materials substitution based on embodied energy and the CO2 footprint, J. Clean. Prod. 162 (2017) 162–169. https://doi.org/10.1016/j.jclepro.2017.06.028.

[90] US-EPA, Method 3052-microwave assisted acid digestion of siliceous and organically based matrices, (1996).

[91] A. Cornelio, A. Zanoletti, S. Federici, L.E. Depero, E. Bontempi, Porous materials derived from industrial by-products for titanium dioxide nanoparticles capture, Appl. Sci. 10 (2020) 1–11. https://doi.org/10.3390/app10228086.

[92] A. Cornelio, A. Zanoletti, R. Braga, L.E. Depero, E. Bontempi, The reuse of industrial by-products for the synthesis of innovative porous materials, with the aim to improve urban air quality, Appl. Sci. 11 (2021). https://doi.org/10.3390/app11156798.

[93] A. Cornelio, A. Zanoletti, L.E. Depero, E. Bontempi, Hybrid materials to reduce pollution involving photocatalysis and particulate matter entrapment, in: A. Assadi, A. Amrane, T.A. Nguyen (Eds.), Hybrid Comb. Process. Air Pollut. Control Methodol. Mech. Eff. Key Parameters, Elsevier, 2022: pp. 201–229. https://doi.org/10.1016/C2020-0-02279-6.

[94] A.K. Prodjosantoso, S. Kamilia, M.P. Utomo, K.S. Budiasih, Silica supported copper-nickel oxide catalyst for photodegradation of methylene blue, Asian J. Chem. 31 (2019) 2891–2896. https://doi.org/10.14233/ajchem.2019.22284.

[95] S. Zhao, S. Li, Y. Long, X. Shen, Z. Zhao, Q. Wei, S. Wang, Z. Zhang, X. Zhang, Z. Zhang, Ce-based heterogeneous catalysts by partial thermal decomposition of Ce-MOFs in activation of peroxymonosulfate for the removal of organic pollutants under visible light, Chemosphere. 280 (2021) 130637. https://doi.org/10.1016/j.chemosphere.2021.130637.

[96] J.L. Lopes, M.J. Martins, H.I.S. Nogueira, A.C. Estrada, T. Trindade, Carbon-based heterogeneous photocatalysts for water cleaning technologies: a review, Environ. Chem. Lett. 19 (2021) 643–668. https://doi.org/10.1007/s10311-020-01092-9.

[97] J. Wang, Y. Liu, F. Jiao, F. Lao, W. Li, Y. Gu, Y. Li, C. Ge, G. Zhou, B. Li, Y. Zhao, Z. Chai, C. Chen, Time-dependent translocation and potential impairment on central nervous system by intranasally instilled TiO2 nanoparticles, Toxicology. 254 (2008) 82–90. https://doi.org/10.1016/j.tox.2008.09.014.

[98] W. Wilczyńska-Michalik, K. Rzeźnikiewicz, B. Pietras, M. Michalik, Fine and ultrafine TiO2 particles in aerosol in Kraków (Poland), Mineralogia. 45 (2014) 65–77.

https://doi.org/10.1515/mipo-2015-0005.

[99] R. Meena, S. Kumar, R. Paulraj, Titanium oxide (TiO2) nanoparticles in induction of apoptosis and inflammatory response in brain, J. Nanoparticle Res. 17 (2015). https://doi.org/10.1007/s11051-015-2868-x.

[100] Autorità Europea per la Sicurezza Alimentare (EFSA), Biossido di titanio: l'E171 non è più considerato sicuro se usato come additivo alimentare, (2022). https://www.efsa.europa.eu/it/news/titanium-dioxide-e171-no-longer-considered-safe-when-used-food-additive (accessed January 19, 2023).

[101] M. Rani, U. Shanker, Sun-light driven rapid photocatalytic degradation of methylene blue by poly(methyl methacrylate)/metal oxide nanocomposites, Colloids Surfaces A Physicochem. Eng. Asp. 559 (2018) 136–147. https://doi.org/10.1016/j.colsurfa.2018.09.040.

[102] E. Kalkan, H. Nadaroglu, Adsorptive removal of acid fuchsin dye using by-product silica fume and laccase-modified silica fume, Iran. J. Chem. Chem. Eng. 40 (2021) 551–564. https://doi.org/10.30492/ijcce.2019.37339.

[103] E. Kalkan, H. Nadaroğlu, N. Celebi, G. Tozsin, Removal of textile dye Reactive Black 5 from aqueous solution by adsorption on laccase-modified silica fume, Desalin. Water Treat. 52 (2014) 6122–6134. https://doi.org/10.1080/19443994.2013.811114.

[104] J.B. Gorme, M.C. Maniquiz, S.-S. Kim, Y.-G. Son, Y.-T. Kim, L.-H. Kim, Characterization of Bottom Ash as an Adsorbent of Lead from Aqueous Solutions, Environ. Eng. Res. 15 (2010) 207–213. https://doi.org/10.4491/eer.2010.15.4.207.

[105] C. Jarusiripot, Removal of Reactive Dye by Adsorption over Chemical Pretreatment Coal based Bottom Ash, Procedia Chem. 9 (2014) 121–130. https://doi.org/10.1016/j.proche.2014.05.015.

[106] K.S. Hashim, H.M. Ewadh, A.A. Muhsin, S.L. Zubaidi, P. Kot, M. Muradov, M. Aljefery, R. Al-Khaddar, Phosphate removal from water using bottom ash: Adsorption performance, coexisting anions and modelling studies, Water Sci. Technol. 83 (2021) 77–89. https://doi.org/10.2166/wst.2020.561.

[107] K.A. Clavier, J.M. Paris, C.C. Ferraro, E.T. Bueno, C.M. Tibbetts, T.G. Townsend, Washed waste incineration bottom ash as a raw ingredient in cement production: Implications for lab-scale clinker behavior, Resour. Conserv. Recycl. 169 (2021) 105513. https://doi.org/10.1016/j.resconrec.2021.105513.

[108] B.M. Law, S.P. Mcbride, J.Y. Wang, Line tension and its influence on droplets and particles at surfaces, 92 (2017) 1–39.

[109] N.I. of Health, ImageJ, (2022). https://imagej.net/ij/ (accessed January 19, 2023).

[110] C. Wang, Y. Bu, Effect of hydrophobic agent in cement and concrete : A Review Effect of hydrophobic agent in cement and concrete : A Review, (2021). https://doi.org/10.1088/1757-899X/1116/1/012175.

[111] M.M. Rahman, D.A. Chamberlain, Development of hydrophobic concrete by adding dual-crystalline admixture at mixing stage, (2018) 1504–1511. https://doi.org/10.1002/suco.201700254.

[112] A. Vidales-barriguete, E. Atanes-sánchez, M. Río-merino, C. Piña-ramírez, Analysis of the improved water-resistant properties of plaster compounds with the addition of plastic waste, Constr. Build. Mater. 230 (2020) 116956. https://doi.org/10.1016/j.conbuildmat.2019.116956.

[113] S. Ducoli, A. Fahimi, E. Mousa, G. Ye, S. Federici, P. Frontera, E. Bontempi, ESCAPE approach for the sustainability evaluation of spent lithium-ion batteries recovery: Dataset of 33 available technologies, Data Br. 42 (2022) 108018. https://doi.org/10.1016/j.dib.2022.108018.

[114] J. Sarkis, M.J. Cohen, P. Dewick, P. Schröder, A brave new world: Lessons from the COVID-19 pandemic for transitioning to sustainable supply and production, Resour. Conserv. Recycl. 159 (2020). https://doi.org/10.1016/j.resconrec.2020.104894.

[115] European Commission, Towards a green, digital and resilient economy, Eur. Comm. Website | Press Release. (2022) 1–3. https://ec.europa.eu/commission/presscorner/detail/en/IP_22_1467.

[116] S. Althaf, C.W. Babbitt, Disruption risks to material supply chains in the electronics sector, Resour. Conserv. Recycl. 167 (2021) 105248. https://doi.org/10.1016/j.resconrec.2020.105248.

[117] A. Akcil, Z. Sun, S. Panda, COVID-19 disruptions to tech-metals supply are a wake-up call, Nature. 587 (2020) 365–367. https://doi.org/10.1038/d41586-020-03190-8.

[118] R.J. Heffron, The role of justice in developing critical minerals, Extr. Ind. Soc. 7 (2020) 855–863. https://doi.org/10.1016/j.exis.2020.06.018.

[119] B. Larmer, E-Waste Offers an Economic Opportunity as Well as Toxicity, (2018). https://www.nytimes.com/2018/07/05/magazine/e-waste-offers-an-economic-opportunity-as-well-as-toxicity.html.

[120] H. Ribeiro, D. Kinch, X. Zhang, A. Franke, M. Goldenberg, Recycling to be key for future battery raw materials supply, 2018.

[121] Qgis, QGIS A Free and Open Source Geographic Information System, (n.d.). https://www.qgis.org/en/site/ (accessed January 13, 2023).

[122] A. Zanoletti, A. Cornelio, E. Bontempi, A post-pandemic sustainable scenario: What actions can be pursued to increase the raw materials availability?, Environ. Res. 202 (2021) 111681. https://doi.org/10.1016/j.envres.2021.111681.

[123] T.P. Bondaroff, S. Cooke, Masks on the Beach, 2020.

[124] J.J. Klemeš, Y. Van Fan, R.R. Tan, P. Jiang, Minimising the present and future plastic waste, energy and environmental footprints related to COVID-19, Renew. Sustain. Energy Rev. 127 (2020). https://doi.org/10.1016/j.rser.2020.109883.

[125] J.S. Smith, H. Hanseler, J. Welle, R. Rattray, M. Campbell, T. Brotherton, T. Moudgil, T.F. Pack, K. Wegmann, S. Jensen, J. Jin, C.B. Bifulco, S.A. Prahl, B.A. Fox, N.L. Stucky, Effect of various decontamination procedures on disposable N95 mask integrity and SARS-CoV-2 infectivity, J. Clin. Transl. Sci. 5 (2021). https://doi.org/10.1017/cts.2020.494.

[126] M. Bansal, J.G. Sharma, Plastic pollution by COVID-19 pandemic: An urge for sustainable approaches to protect the environment, J. Pure Appl. Microbiol. 15 (2021) 1083–1093.

https://doi.org/10.22207/JPAM.15.3.36.

[127] M. Shen, Z. Zeng, B. Song, H. Yi, T. Hu, Y. Zhang, G. Zeng, R. Xiao, Neglected microplastics pollution in global COVID-19: Disposable surgical masks, Sci. Total Environ. 790 (2021). https://doi.org/10.1016/j.scitotenv.2021.148130.

[128] A.L. Patrício Silva, J.C. Prata, T.R. Walker, D. Campos, A.C. Duarte, A.M.V.M. Soares, D. Barcelò, T. Rocha-Santos, Rethinking and optimising plastic waste management under COVID-19 pandemic: Policy solutions based on redesign and reduction of single-use plastics and personal protective equipment, Sci. Total Environ. 742 (2020) 140565. https://doi.org/10.1016/j.scitotenv.2020.140565.

[129] F. Saliu, M. Veronelli, C. Raguso, D. Barana, P. Galli, M. Lasagni, The release process of microfibers: from surgical face masks into the marine environment, Environ. Adv. 4 (2021) 100042. https://doi.org/10.1016/j.envadv.2021.100042.

[130] Istat, Istat Banca dati completa, (2022). http://dati.istat.it/ (accessed January 13, 2023).

[131] A. Cornelio, A. Zanoletti, S. Federici, L. Ciacci, L.E. Depero, E. Bontempi, Environmental Impact of Surgical Masks Consumption in Italy Due to COVID-19 Pandemic, Materials (Basel). 15 (2022). https://doi.org/10.3390/ma15062046.

[132] F. Dutheil, J.S. Baker, V. Navel, COVID-19 as a factor influencing air pollution?, Environ. Pollut. 263 (2020) 2019–2021. https://doi.org/10.1016/j.envpol.2020.114466.

[133] F. Liu, A. Page, S.A. Strode, Y. Yoshida, S. Choi, B. Zheng, L.N. Lamsal, C. Li, N.A. Krotkov, H. Eskes, R. Van der A, P. Veefkind, P.F. Levelt, O.P. Hauser, J. Joiner, Abrupt decline in tropospheric nitrogen dioxide over China after the outbreak of COVID-19, Sci. Adv. 28 (2020). https://doi.org/10.1126/sciadv.abc2992.

[134] E. De Angelis, S. Renzetti, M. Volta, F. Donato, S. Calza, D. Placidi, R.G. Lucchini, M. Rota, COVID-19 incidence and mortality in Lombardy, Italy: An ecological study on the role of air pollution, meteorological factors, demographic and socioeconomic variables, Environ. Res. 195 (2021) 110777. https://doi.org/10.1016/j.envres.2021.110777.

[135] E. Bontempi, M. Coccia, International trade as critical parameter of COVID-19 spread that outclasses demographic, economic, environmental, and pollution factors, Environ. Res. 201 (2021) 111514. https://doi.org/10.1016/j.envres.2021.111514.

[136] L. Menut, B. Bessagnet, G. Siour, S. Mailler, R. Pennel, A. Cholakian, Impact of lockdown measures to combat Covid-19 on air quality over western Europe, Sci. Total Environ. 741 (2020) 140426. https://doi.org/10.1016/j.scitotenv.2020.140426.

[137] E. Bontempi, C. Carnevale, A. Cornelio, M. Volta, A. Zanoletti, Analysis of the lockdown effects due to the COVID-19 on air pollution in Brescia (Lombardy), Environ. Res. 212 (2022) 113193. https://doi.org/10.1016/j.envres.2022.113193.

Publications

Mousa E, Hu X, Ånnhagen L, Ye G, **Cornelio A**, Fahimi A, Bontempi E, Frontera P, Badenhorst C, Santos AC, Moreira K, Guedes A, Valentim B. Characterization and Thermal Treatment of the Black Mass from Spent Lithium-Ion Batteries. Sustainability. 2023; 15(1):15. https://doi.org/10.3390/su15010015

Fahimi A, Zanoletti A, **Cornelio A**, Mousa E, Ye G, Frontera P, Depero LE, Bontempi E. Sustainability Analysis of Processes to Recycle Discharged Lithium-Ion Batteries, Based on the ESCAPE Approach. Materials. 2022; 15(23):8527. https://doi.org/10.3390/ma15238527

Ciniglia D, Cirelli P, Bilo F, Zanoletti A, **Cornelio A**, De Iuliis S, Depero LE, Bontempi E, Perrone MG, Lopinto P, Zonca M, Borgese L, Characterization of nebulization generated aerosol particles dispersion and deposition by total reflection X-ray fluorescence, Aerosol Sci. Technol. 0 (2022) 1–10. https://doi.org/10.1080/02786826.2022.2155104.

Fattoruso G, Toscano D, **Cornelio A**, De Vito S, Murena F, Fabbricino M, Di Francia G. Using Mobile Monitoring and Atmospheric Dispersion Modeling for Capturing High Spatial Air Pollutant Variability in Cities. Atmosphere. 2022; 13(11):1933. https://doi.org/10.3390/atmos13111933

Fiameni L, Fahimi A, Federici S, **Cornelio A**, Depero LE, Bontempi E, A new breakthrough in the P recovery from sewage sludge ash by thermochemical processes, Green Chem., 2022, 24, 6836-6839, DOI: 10.1039/D2GC02328H.

Bontempi E, Carnevale C, **Cornelio A**, Volta M, Zanoletti A, Analysis of the lockdown effects due to the COVID-19 on air pollution in Brescia (Lombardy), Environmental Research, Volume 212, Part A, 2022, 113193, ISSN 0013-9351, https://doi.org/10.1016/j.envres.2022.113193.

Cornelio A, Zanoletti A, Federici S, Ciacci L, Depero LE, Bontempi E. Environmental Impact of Surgical Masks Consumption in Italy Due to COVID-19 Pandemic. Materials. 2022; 15(6):2046. https://doi.org/10.3390/ma15062046

Cornelio A, Zanoletti A, Depero LE, Bontempi E, Chapter 8 - Hybrid materials to reduce pollution involving photocatalysis and particulate matter entrapment, Editor(s): Aymen Assadi, Abdeltif Amrane, Tuan Anh Nguyen, Hybrid and Combined Processes for Air Pollution Control, Elsevier, 2022, Pages 201-229, ISBN 9780323884495, https://doi.org/10.1016/B978-0-323-88449-5.00010-3.

Cornelio, A.; Zanoletti, A.; Federici, S.; Depero, L.E.; Bontempi, E. Porous Materials Derived from Industrial By-Products for Titanium Dioxide Nanoparticles Capture. Appl. Sci. 2020, 10, 8086

Zanoletti A, **Cornelio A**, Bontempi E. A post-pandemic sustainable scenario: What actions can be pursued to increase the raw materials availability? Environ Res. 2021 Jul 15; 202:111681. doi: 10.1016/j.envres.2021.111681. Epub ahead of print. PMID: 34273363.

Cornelio, A.; Zanoletti, A.; Braga, R.; Depero, L.E.; Bontempi, E. The Reuse of Industrial By-Products for the Synthesis of Innovative Porous Materials, with the Aim to Improve Urban Air Quality. Appl. Sci. 2021, 11, 6798. https://doi.org/10.3390/app11156798

Ringraziamenti

Il giorno della mia partenza per Brescia, circa 3 anni fa, mio fratello mi inviò un'immagine su *whatsapp* raffigurante un seme che veniva piantato nella terra e innaffiato con la scritta *"you will grow"*. Da allora spesso penso a questa frase, chiedendomi a che punto sia arrivata. In questi 3 anni ho avuto la possibilità di fare tante nuove esperienze, di crescere, di imparare, di scoprire e di mettermi alla prova e per questo ci tengo a ringraziarvi perché, ognuno di voi, in tanti modi diversi, l'ha reso possibile.

GRAZIE:

Prof.ssa Elza Bontempi, per aver creduto in me quel giorno di settembre 2019, per l'immensa disponibilità, per il supporto in questi anni e per le grandi possibilità che mi ha dato.

Prof.ssa Laura Eleonora Depero, per la disponibilità, per la fiducia e per tutti i dolci rifornimenti.

Dott.ssa Alessandra Zanoletti, pilastro di tutto il mio percorso di dottorato. Grazie per essere stata sempre presente, per l'aiuto, per il supporto costante, per l'incoraggiamento e per tutti i caffè presi insieme in via telematica durante il COVID.

Chem4Tech, grazie a tutto il gruppo. Ai *senior*, per il costante incoraggiamento, per la disponibilità e per i discorsi più o meno seri della pausa caffè e dell'ora di pranzo. Ai dottorandi, più o meno da smaltire, per aver trovato non solo dei colleghi (anche di bevute) ma degli amici.

Ai **miei genitori,** per aver creduto nei miei sogni, sostenendomi nelle mie scelte. Mamma, sempre presente, anche in silenzio ma sempre pronta a darmi un consiglio e ad ascoltarmi. Papà, più rumoroso, ma anche lui sempre pronto a venirmi incontro (e a prendere ovunque in giro per l'Italia e probabilmente anche nel resto del mondo).

Antonio, per avermi insegnato la differenza fra puntone e tirante che non dimenticherò più (era d'obbligo ricordarlo anche in quest'occasione). Per essere sempre presente, anche da lontano, per essere sempre pronto a consigliarmi e spronarmi. Senza di te tante cose sarebbero state molto più difficili. Il cordone ombelicale che non taglierò mai.

Maurizio, la mia persona *favorita*. Grazie per farmi vedere sempre il lato più leggero e ironico delle cose. Per essere sempre presente, per l'elevata capacità di sopportare i miei momenti no, per ascoltarmi, per farmi ridere e per farmi vincere ad *exploding kittens*.

Ai **miei zii**, per essere stati sempre presenti in tutti i miei traguardi più importanti. Sono stata fortunata ad avervi e vi ringrazio per tutti i momenti passati insieme, per avermi insegnato tanto, per le risate, per i viaggi, per gli scherzi, per i momenti creativi e per avermi sempre assecondato (soprattutto nei giri dentro Alife).

Zio Lolo, un grazie speciale a te, che mi hai insegnato a non arrendermi mai, che è importante lottare mantenendo sempre quella dose di ironia. So che saresti orgoglioso di me in questo momento, mi manchi tanto.

Renata, cugina giovane, con le *open when letters* hai reso più divertenti tanti momenti e più facile da sopportare la lontananza. Ti voglio bene nonostante mi ricordi sempre quanto sia vecchia.

Francesco, per tutti i discorsi telepatici che valgono più di mille parole.

Dott.ssa Grazia Fattoruso, mio grande esempio. Senza di te tutto questo non sarebbe stato possibile. Grazie per aver sempre creduto in me e per avermi spronato a seguire questo percorso.

Marina, coinquilina e amica. Grazie per il supporto in questi anni, per le cene in terrazza (ma anche sul mini tavolo), per gli aperitivi a casa e dal nostro amico, per le risate, per le lunghe chiacchierate e per le serate sul divano cercando di convincermi a vedere *Harry Potter*.

Zaira, non semplicemente un'amica ma una sorella. Grazie per aver sempre creduto in me e nelle mie capacità, anche quando ero la prima a dubitarne, grazie per tutti i

consigli e le lunghe sessioni telefoniche, per i concerti insieme in giro per l'Italia. Anche se ultimamente sta diventando più difficile vederci, so che ci sei sempre.

Luigi, per avermi sempre ascoltato e consigliato, per le lunghe discussioni e confronti non sempre pacifici ma che si sono sempre risolti con un ti voglio bene. Grazie soprattutto per avermi convinto che la mia fossetta non è poi così male.

Giampiero e Giammarco, con la *m* mi raccomando, **Giada**, **Claudio**, **Laura** e **Ario** per aver reso divertenti tante giornate in ufficio e fuori (con battute più o meno improponibili), per tutti i momenti di confronto e di supporto. Siete stati fondamentali in questi anni.

Concludo questi ringraziamenti con un pezzo di una delle mie canzoni preferite, che mi ha accompagnato in questi anni:

"E per quanta strada ancora c'è da fare

amerai il finale."